TIC

NUREG/CR-0506
ORNL/NUREG-52

Stresses in Reinforced Nozzle-Cylinder Attachments under External Moment Loadings Analyzed by the Finite-Element Method—A Parameter Study

J. W. Bryson
W. G. Johnson
B. R. Bass

Prepared for the U.S. Nuclear Regulatory Commission
Office of Nuclear Regulatory Research
Under Interagency Agreements DOE 40-551-75 and 40-552-75

OAK RIDGE NATIONAL LABORATORY
OPERATED BY UNION CARBIDE CORPORATION · FOR THE DEPARTMENT OF ENERGY

Printed in the United States of America. Available from
National Technical Information Service
U.S. Department of Commerce
5285 Port Royal Road, Springfield, Virginia 22161

TO: Recipients of This Report:

In keeping with ORNL's continued efforts to eliminate the production of excess paper, the distribution of this report has been reduced to the bare minimum required to meet our obligations. After a report has been issued, however, we often get requests for a copy from individuals who have specific interest but who are not on our regular distribution list.

If you decide not to keep this copy, would you please return it to the author.

J. W. Bryson
Oak Ridge National Laboratory
P. O. Box Y
Oak Ridge, TN 37830

NUREG/CR-0506
ORNL/NUREG-52
Dist. Category R5

Contract No. W-7405-eng-26

Engineering Technology Division

STRESSES IN REINFORCED NOZZLE-CYLINDER ATTACHMENTS UNDER EXTERNAL MOMENT LOADINGS ANALYZED BY THE FINITE-ELEMENT METHOD – A PARAMETER STUDY

J. W. Bryson W. G. Johnson
B. R. Bass

Manuscript Completed – July 9, 1979
Date Published – August 1979

Prepared for the
U.S. Nuclear Regulatory Commission
Office of Nuclear Regulatory Research
Under Interagency Agreements DOE 40-551-75 and 40-552-75

NRC FIN No. B0123

Prepared by the
OAK RIDGE NATIONAL LABORATORY
Oak Ridge, Tennessee 37830
operated by
UNION CARBIDE CORPORATION
for the
DEPARTMENT OF ENERGY

CONTENTS

FOREWORD

The work reported here was performed at the Oak Ridge National Laboratory (ORNL) in support of the ORNL Design Criteria for Piping and Nozzle Program being conducted for the U.S. Nuclear Regulatory Commission (USNRC), Office of Nuclear Regulatory Research. P. Albrecht of the Metallurgy and Materials Branch, Division of Reactor Safety Research, USNRC, is the cognizant RSR engineer, and S. E. Moore of ORNL, Engineering Technology Division, is the program manager.

The objectives of the ORNL program are to conduct integrated experimental and analytical stress analysis studies of piping system components and pressure vessel nozzles in order to confirm and/or improve the adequacy of structural design criteria and analytical methods used to ensure the safe design of nuclear power plants. Activities under the program are coordinated with other safety-related piping and pressure vessel research through the Design Division, Pressure Vessel Research Committee of the Welding Research Council, and the ASME Boiler and Pressure Vessel Code Committees. Results from the ORNL program are used by appropriate Codes and Standards groups in drafting new or improved design rules and criteria.

The following reports have been issued under NRC sponsorship:

J. W. Bryson, J. P. Callahan, and R. C. Gwaltney, *Stress Analyses of Flat Plates with Attached Nozzles, Vol. 1. Comparison of Stresses in a One-Nozzle-to-Flat-Plate Configuration and in a Two-Nozzle Configuration with Theoretical Predictions*, ORNL-5044, Vol. 1 (July 1975).

R. L. Battiste et al., *Stress Analysis of Flat Plates with Attached Nozzles, Vol. 2. Experimental Stress Analyses of a Flat Plate with One Nozzle Attached*, ORNL-5044, Vol. 2 (July 1975).

E. C. Rodabaugh and S. E. Moore, *Stress Indices for ANSI Standard B16.11 Socket-Welding Fittings*, ORNL/TM-4929 (August 1975).

R. C. Gwaltney, J. W. Bryson, and S. E. Bolt, *Theoretical and Experimental Stress Analyses of ORNL Thin-Shell Cylinder-to-Cylinder Model 2*, ORNL-5021 (October 1975).

S. E. Moore, "Contributions of the ORNL Piping Program to Nuclear Piping Design Codes and Standards," *Proceedings of the Technology Information Meeting on Methods for Analyzing Piping Integrity, Nov. 11–12, 1975*, ERDA 76-50; also in *J. Pressure Vessel Technol., Trans. ASME* 99, 224-30 (February 1977).

W. L. Greenstreet, "Summary and Accomplishments of the ORNL Program for Nuclear Piping Design Criteria," *Proceedings of the Technology Information Meeting on Methods for Analyzing Piping Integrity, Nov. 11–12, 1975*, ERDA 76-50.

J. W. Bryson and W. F. Swinson, *Stress Analyses of Flat Plates with Attached Nozzles, Vol. 3. Experimental Stress Analyses of a Flat Plate with Two Closely Spaced Nozzles of Equal Diameter Attached*, ORNL-5044, Vol. 3 (December 1975).

E. C. Rodabaugh, F. M. O'Hara, Jr., and S. E. Moore, *FLANGE: A Computer Program for the Analysis of Flanged Joints with Ring-Type Gaskets*, ORNL-5035 (January 1976).

R. E. Textor, *User's Guide for SHFA: Steady-State Heat Flow Analysis of Tee Joints by the Finite-Element Method*, UCCND/CSD/INF-60, Oak Ridge Gaseous Diffusion Plant (January 1976).

E. C. Rodabaugh and S. E. Moore, *Flanged Joints with Contact Outside the Bolt Circle — ASME Part B Design Rules*, ORNL/SUB/2913-1, Battelle-Columbus Laboratories (May 1976).

E. C. Rodabaugh, *Appropriate Nominal Stresses for Use with ASME Code Pressure-Loading Stress Indices for Nozzles*, ORNL/SUB/2913-1, Battelle-Columbus Laboratories (June 1976).

S. E. Moore and J. W. Bryson, *Progress Report for the Design Criteria for Piping and Nozzles Program for the Two Quarterly Periods July 1 to Sept. 30 and Oct. 1 to Dec. 31, 1975*, ORNL/NUREG/TM-18 (June 1976).

R. L. Maxwell and R. W. Holland, *Experimental Stress Analysis of the Attachment Region of a Hemispherical Shell with a Radially Attached Nozzle, Zero Penetration*, ORNL/SUB/2203-4, University of Tennessee (July 1976).

J. P. Callahan and J. W. Bryson, *Stress Analyses of Perforated Flat Plates under In-Plane Loadings*, ORNL/NUREG-2 (August 1976).

E. C. Rodabaugh and S. E. Moore, *Evaluation of the Bolting and Flanges of ANSI B16.5 Flanged Joints — ASME Part A Flanges*, ORNL/SUB/2913-3, Battelle-Columbus Laboratories (September 1976).

E. C. Rodabaugh and R. C. Gwaltney, *Elastic Stresses at Reinforced Nozzles in Spherical Shells with Pressure and Moment Loading*, ORNL/SUB/2913-4 (October 1976).

E. C. Rodabaugh, S. E. Moore, and J. N. Robinson, *Dimensional Control of Buttwelding Pipe Fittings for Nuclear Power Plant Class 1 Piping Systems*, ORNL/SUB/2913-5 (December 1976).

S. E. Moore and J. W. Bryson, *Design Criteria for Piping and Nozzle Program Quarterly Progress Report for April–June 1976*, ORNL/NUREG/TM-107 (April 1977).

E. C. Rodabaugh and S. E. Moore, *Flexibility Factors for Small (d/D < 1/3) Branch Connections with External Loadings*, ORNL/SUB/2913-6 (March 1977).

S. E. Moore and J. W. Bryson, *Design Criteria for Piping and Nozzles Program Quarterly Progress Report for July–September 1976*, ORNL/NUREG/TM-91 (February 1977).

P. G. Fowler and J. W. Bryson, *User's Manual for the CORTES Graphics Package GRFPAK*, ORNL/NUREG/TM-127 (August 1977).

B. R. Bass, J. W. Bryson, and S. E. Moore, "Validation of the Finite-Element Stress Analysis Computer Program CORTES-SA for Analyzing Piping Tees and Pressure Vessel Nozzles," *Pressure Vessels and Piping Computer Program Evaluation and Qualification*, PVP-PB-024, pp. 9–25, ASME (1977).

J. K. Hayes and S. E. Moore, "Experimental Stress Analysis for Four 24-in. ANSI Standard B16.9 Tees," Paper 77-PVP-4, presented at the ASME Energy Technology Conference and Exhibition, Houston, Texas, Sept. 18–23, 1977.

S. E. Moore and J. W. Bryson, *Design Criteria for Piping and Nozzles Program Quarterly Progress Report for October–December 1976*, ORNL/NUREG/TM-144 (September 1977).

J. W. Bryson, W. G. Johnson, and B. R. Bass, *Stresses in Reinforced Nozzle-Cylinder Attachments under Internal Pressure Loading Analyzed by the Finite-Element Method — A Parameter Study*, ORNL/NUREG-4 (October 1977).

F. K. W. Tso et al., *Stress Analysis of Cylindrical Pressure Vessels with Closely Spaced Nozzles by the Finite-Element Method, Vol. 1. Stress Analysis of Vessels with Two Closely Spaced Nozzles Under Internal Pressure*, ORNL/NUREG-18/V1 (November 1977).

W. L. Greenstreet, *Experimental Study of Plastic Responses of Pipe Elbows*, ORNL/NUREG-24 (February 1978).

E. C. Rodabaugh, S. K. Iskander, and S. E. Moore, *End Effects on Elbows Subjected to Moment Loadings*, ORNL/SUB-2913/7 (March 1978).

E. C. Rodabaugh and S. E. Moore, *Evaluation of the Plastic Characteristics of Piping Products in Relation to ASME Code Criteria*, NUREG/CR-0261, ORNL/SUB-2913/8 (July 1978).

F. K. W. Tso and R. A. Weed, *Stress Analysis of Cylindrical Pressure Vessels with Closely Spaced Nozzles by the Finite-Element Method, Vol. 2. Vessels with Two Nozzles Under External Force and Moment Loadings*, NUREG/CR-0132, ORNL/NUREG-18/V2 (August 1978).

E. C. Rodabaugh and S. E. Moore, *Stress Indices for Girth Welded Joints, Including Radial Weld Shrinkage, Mismatch and Tapered-Wall Transitions*, NUREG/CR-0371, ORNL/SUB-2913/9 (September 1978).

F. K. W. Tso and R. A. Weed, *Stress Analysis of Cylindrical Pressure Vessels with Closely-Spaced Nozzles by the Finite-Element Method, Vol. 3. Vessels with Three Nozzles Under Internal Pressure and External Loadings*, NUREG/CR-0507, ORNL/NUREG-18/V3 (May 1979).

STRESSES IN REINFORCED NOZZLE-CYLINDER ATTACHMENTS UNDER EXTERNAL MOMENT LOADINGS ANALYZED BY THE FINITE-ELEMENT METHOD — A PARAMETER STUDY

J. W. Bryson W. G. Johnson*
B. R. Bass*

ABSTRACT

A parameter study was conducted on stresses in reinforced nozzle-to-cylinder attachments under external moment loadings as analyzed by the finite-element method. Twenty-five models with nozzle-to-cylinder diameter ratios $0.08 \leq d/D \leq 0.50$ and cylinder diameter-to-thickness ratios $10 \leq D/T \leq 100$ were investigated. A three-dimensional finite-element program, CORTES-SA, developed specifically for analyzing tee-joint configurations, was used in the study. Each of the 25 models was analyzed for 6 individually applied external moment loadings, with 3 mutually orthogonal moment loadings on the nozzle end and 3 on the cylinder.

Two of the recommended nozzle reinforcement designs given in Subsection NB-3338.2, Section III, of the ASME Boiler and Pressure Vessel Code were examined: nozzle thickening or "standard" reinforcement (S1 models) and 30° triangular pad reinforcement (P30 models). Essentially unreinforced models (U models) were also included for comparison. Although these design configurations have been recommended by the Code for many years, very little specific stress analysis information exists by which the adequacy or relative safety margins of the Code design rules can be judged. Results from the parameter studies reported here provide some of the needed information.

It was concluded from the study that both of the reinforcement designs investigated significantly reduce maximum stresses relative to configurations having little or no reinforcement. Out-of-plane bending moment loading on the nozzle gave high maximum stress values for both unreinforced and reinforced configurations having relatively large, thin ($d/D = 0.50$, $D/T \geq 20$) nozzle attachments.

1. INTRODUCTION

Nozzles attached to cylindrical shells are common configurations in the pressure vessel and piping industry. Nozzle-to-cylinder diameter

*Computer Sciences Division.

ratios (d/D) up to 0.5 cover almost all pressure vessel designs; however, for piping, d/D ratios up to 1.0 are fairly common. Cylindrical shell diameter-to-thickness ratios (D/T) may be as high as 1000 for steel containment vessels (e.g., large oil storage tanks) but are generally less than 100 for nuclear vessels. Most of the stress analysis data available in the literature for nozzle-to-cylinder attachments are limited to either flush unreinforced connections or models having very small fillet radius reinforcements. Very few of such data, either experimental or analytical, are available in the open literature on reinforced connections, particularly for nozzle-to-cylinder attachments having the reinforcement designs given in Subsections NB-3330 through NB-3339, Section III, of the ASME Boiler and Pressure Vessel Code.* Also, much of the available stress analysis data is limited to internal pressure loading.

Additional data are needed in order to confirm and/or improve the design rules and safety criteria specified in the Code for the qualification of reinforced nozzle designs. The stress analysis parameter study for 25 isolated nozzle-to-cylinder attachments under external moment loadings described in this report was conducted to provide some of the needed information. This work is an extension of that reported in Ref. 1, where results for the same 25 isolated nozzle-to-cylinder attachments under internal pressure loading are given. A three-dimensional finite-element computer program[2] developed under subcontract at the University of California, Berkeley, specifically for analyzing tee-joint configurations, was used in the study. The program (CORTES-SA) features an automatic mesh-generation package with a number of input-variable options that enable the user to model a wide variety of nozzle-attachment designs using a minimal amount of input data. The same program was used in the study in Ref. 1, and in fact, the identical finite-element representations (meshes) used in that study were also used in the present study.

The parameter study consisted of 25 models with dimensionless parameter ratios within the ranges $10 \leq D/T \leq 100$ and $0.08 \leq d/D \leq 0.50$. Two types of nozzle reinforcement were examined: nozzle thickening, or the so-called "standard" reinforcement (S1 models), and 30° triangular pad

*Henceforth, Code refers to the ASME Boiler and Pressure Vessel Code, Section III, Subsections NB-3330 through NB-3339.

reinforcement (P30 models). These reinforcement designs are given in Subsection NB-3338.2, Section III, of the Code. Of the 25 models analyzed, 19 had one of these two types of reinforcement, and 6 were essentially unreinforced, except for the minimum fillet radius at the junction as required by the Code.

...sic nozzle-to-cylindrical shell configuration and the external moment loadings considered in this report are shown in Fig. 1. Six separate loading cases were analyzed for each model, three mutually perpendicular moment loadings individually applied at the end of the nozzle and three at the free end of ...e cylinder. In the finite-element idealization for all the models in the study, the ends of the nozzle and cylinder were capped with stiff end diaphragms. These diaphragms were represented by finite elements with an artificially large elastic modulus.

For bending moment loadings, a finite-element analysis of the "cantilever" tee depicted in Fig. 1 requires that one-half of the configuration be modeled ($Z \geq 0$) to specify the appropriate boundary conditions. However, as will be shown in Chapter 2, one can analyze a "simply supported" tee such that the applied moment loading on the nozzle or right end of the

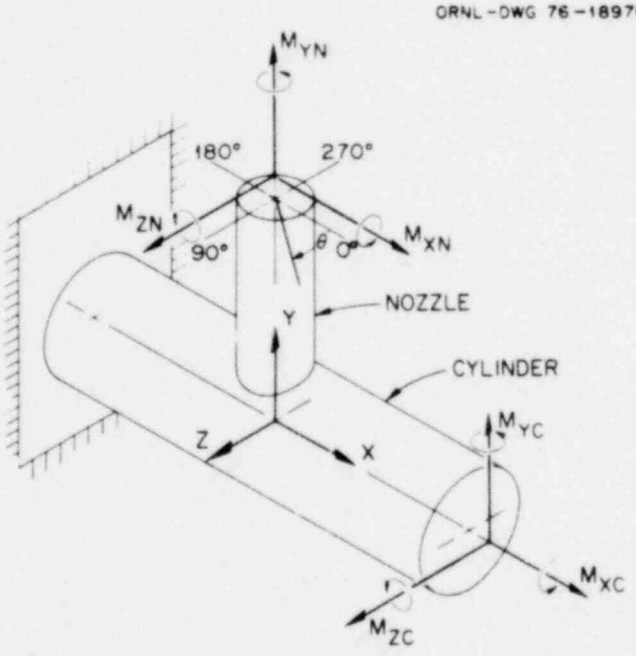

Fig. 1. Nozzle-to-cylindrical shell configuration and basic load cases.

cylinder (Y > 0) is always resisted by an equal and opposite moment acting on the left end of the cylinder (X < 0). This analysis requires that only one-quarter of the tee be modeled, thus representing a significant savings in both computer time and operating costs. This latter approach was taken in the parameter study reported here.

The objective of this report is to summarize and present the more important and relevant results of the parameter study. No attempt is made here to relate these results to the design rules of Subsections NB-3330 through NB-3339, Section III, of the Code. We plan to address this subject in a follow-up document that will include recommendations for improved design rules for nozzles and branch connections. The results of this study are presented in a tabular format that gives the normal principal stresses and their direction cosines and the stress intensity for each nodal point on the outside and inside surfaces. Because of the very large amount of data obtained, the tables are printed on microfiche and included in the envelope on the back cover. Summary tables of the largest and smallest principal stresses obtained and their locations, as well as the maximum stress intensities for each model, are provided in Chapter 5 for each of the six loadings.

Data relating to the relative displacements of nodes on the end caps are given in Appendix A for in-plane and out-of-plane moment loadings applied to the nozzle. This information should prove useful in the preparation of a follow-up document that will examine and evaluate the current flexibility factors for small branch connections listed in Section NB-3687.5 of the Code.

Isometric views of the finite-element meshes for each of the models are provided in Appendix B. These figures are helpful in defining the locations of the stress values given in the summary tables of Chapter 5. Cross-sectional views of the meshes have been omitted to minimize the size and cost of the report; however, they may be found in the companion report (Ref. 1) for internal pressure loading. For each model, the same finite-element mesh was used for all six moment loadings.

The following chapters discuss the finite-element computer program used in the study, the checkout and verification of the program, the parameter study itself, and results and conclusions.

2. THE COMPUTER PROGRAM

The finite-element computer program CORTES-SA (California, Oak Ridge, TEeS – Stress Analysis) used in the study was developed earlier at the University of California, Berkeley.[2] It is the first in a four-program package designed specifically for analyzing tee joints subjected to a variety of mechanical and thermal loadings. The other programs in the package include CORTES-THFA (Transient Heat Flow Analysis), -TSE (Thermal Stress Analysis), and -EPA (Elastic-Plastic Analysis). These programs, identified as NESC 759 CORTES, are available on request from the National Energy Software Center, Argonne National Laboratory (ANL). They were originally developed for the analysis of ANSI B16.9 Standard tee but are also applicable to a wide range of tee-joint geometries, including the reinforcement configurations discussed here. Some of the more prominent features of CORTES-SA include the use of a relatively economical finite element and automatic mesh generation, and the convenience of using only a quarter section of the model by utilizing superposition of component load cases that are either symmetric or skew-symmetric about the X-Y and Y-Z planes to obtain a solution for an arbitrary loading. These features are discussed below.

2.1 The Finite Element

The finite element used in CORTES-SA is the ZIB8R9 element originated by Irons and Zienkiewicz.[3] It is an eight-node isoparametric brick element with additional deformation modes and is the same element that is used in the general purpose computer program SAP.[4] The added deformation modes allow the element edges to deform quadratically rather than linearly; however, as a consequence, displacement compatibility along the element edges is violated. The element is more flexible than a linear isoparametric brick element, and thus behaves much better in bending; however, certain problems with regard to convergence and bounding of the solution are introduced.

The displacement expansions for the ZIB8R9 element are given by

$$u = \sum_{i=1}^{8} N_i u_i + \alpha_1(1 - r^2) + \alpha_2(1 - s^2) + \alpha_3(1 - t^2) ,$$

$$v = \sum_{i=1}^{8} N_i v_i + \beta_1(1 - r^2) + \beta_2(1 - s^2) + \beta_3(1 - t^2) ,$$

$$w = \sum_{i=1}^{8} N_i w_i + \gamma_1(1 - r^2) + \gamma_2(1 - s^2) + \gamma_3(1 - t^2) ,$$

where u_i, v_i, and w_i are nodal displacements; α, β, and γ represent generalized displacements associated with the added modes; and N_i represents the shape functions defined as

$$N_i = \frac{1}{8}(1 + rr_i)(1 + ss_i)(1 + tt_i) .$$

Figure 2 shows the local and global coordinates for the element. When the strain energy within the element is minimized with respect to α, β, and

ORNL-DWG 76-10347

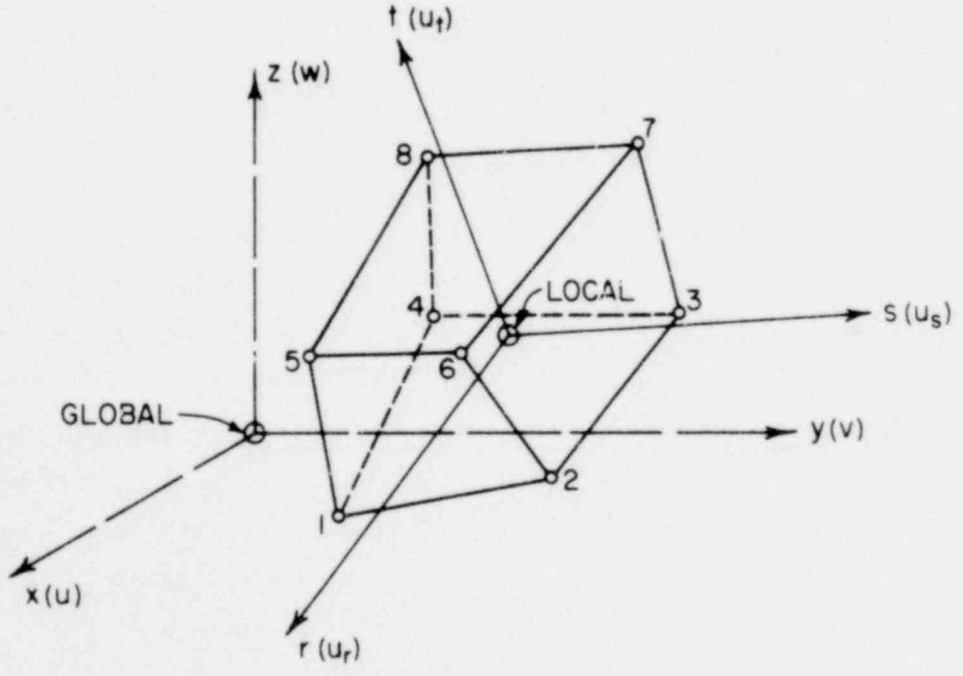

Fig. 2. Local and global coordinates for Z1B8R9 element.

γ, nine additional equations are obtained that permit these terms to be eliminated. The resulting (condensed) stiffness matrix is therefore 24 × 24. A more detailed discussion of the element and the finite-element method in general may be found in Ref. 2.

The modified 8-node brick element has given results comparable to the 20-node element for plates and shells with moderately fine element subdivisions.[2] Its inherent simplicity makes it more economical than the 20-node element, because it requires less computational effort.

2.2 Mesh-Generation Capability

The input for most finite-element computer programs without mesh-generation capability usually consists of a rather large number of cards describing the element connectivity and giving the global (or local) coordinates of the nodes. In contrast, CORTES-SA can require as few as ten cards to generate a mesh for a tee connection. This is a great advantage to the user, particularly if many problems requiring different meshes (such as for a parameter study) are to be solved.

The program uses a "pentagonal" scheme for mesh generation; that is, a quarter section of a tee is divided into five main parts or "quadrilaterals" that are joined at a common "control node." These quadrilaterals are further subdivided into "quadrilateral elements." The five quadrilaterals, or parts, connect with each other along five axes that emanate from the control node (see Figs. 3 and 4). The user specifies the number of elements or divisions along each axis for each quadrilateral, the lengths of the nozzle and cylinder, and fillet radii in the X-Y and Y-Z planes. Additional input data define the material properties and any machining of the tee region.

Because it is necessary to define corresponding meshes on both the outer and inner surfaces of the joint, two options for outer and inner surface mesh generation are provided. The first option generates both surfaces using specified lengths, fillet radii, and other necessary dimensions. The second option generates the inside surface by projecting from the outer surface using thicknesses at specified nodes supplied by

ORNL-DWG 76-10349

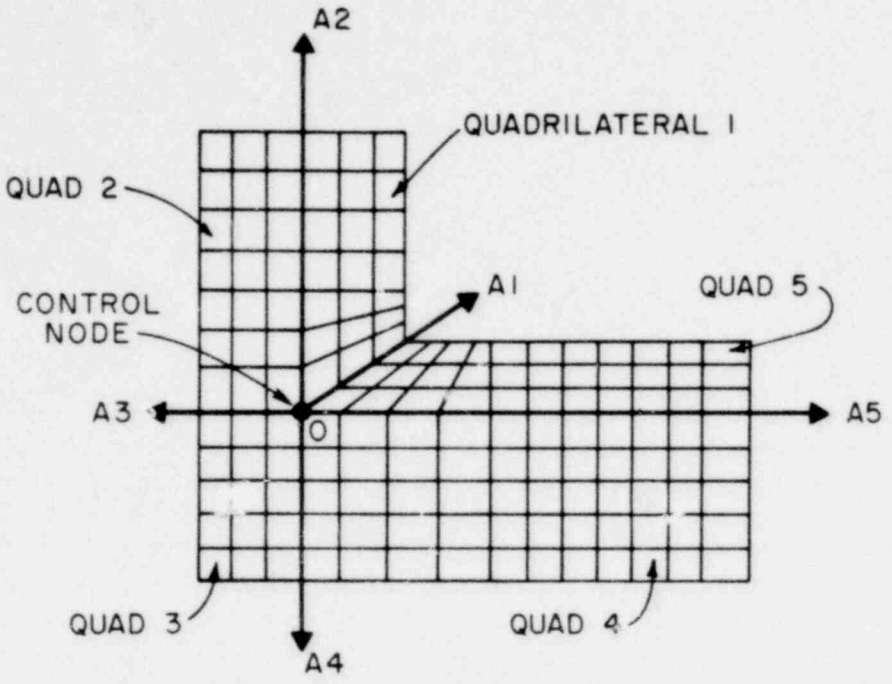

Fig. 3. Pentagonal system.

the user. As many as five layers of elements can be specified through the wall thickness.

Other features of the program, such as the mathematical relationships that describe the fillet and junction region of the nozzle-cylinder connection and the manner in which the external loads are applied, are discussed in detail in Ref. 2. Bending moment loadings are represented by statically equivalent sets of linearly varying nodal forces at the ends of the branch and run; torsional moment loadings are represented by statically equivalent sets of equal nodal forces. Decomposition of the basic load cases shown in Fig. 1 into component load cases that are symmetric and skew-symmetric about the X-Y and Y-Z planes, the analyses of these component loadings, and their subsequent combination to give the desired basic loading are discussed below.

ORNL-DWG 76-10350

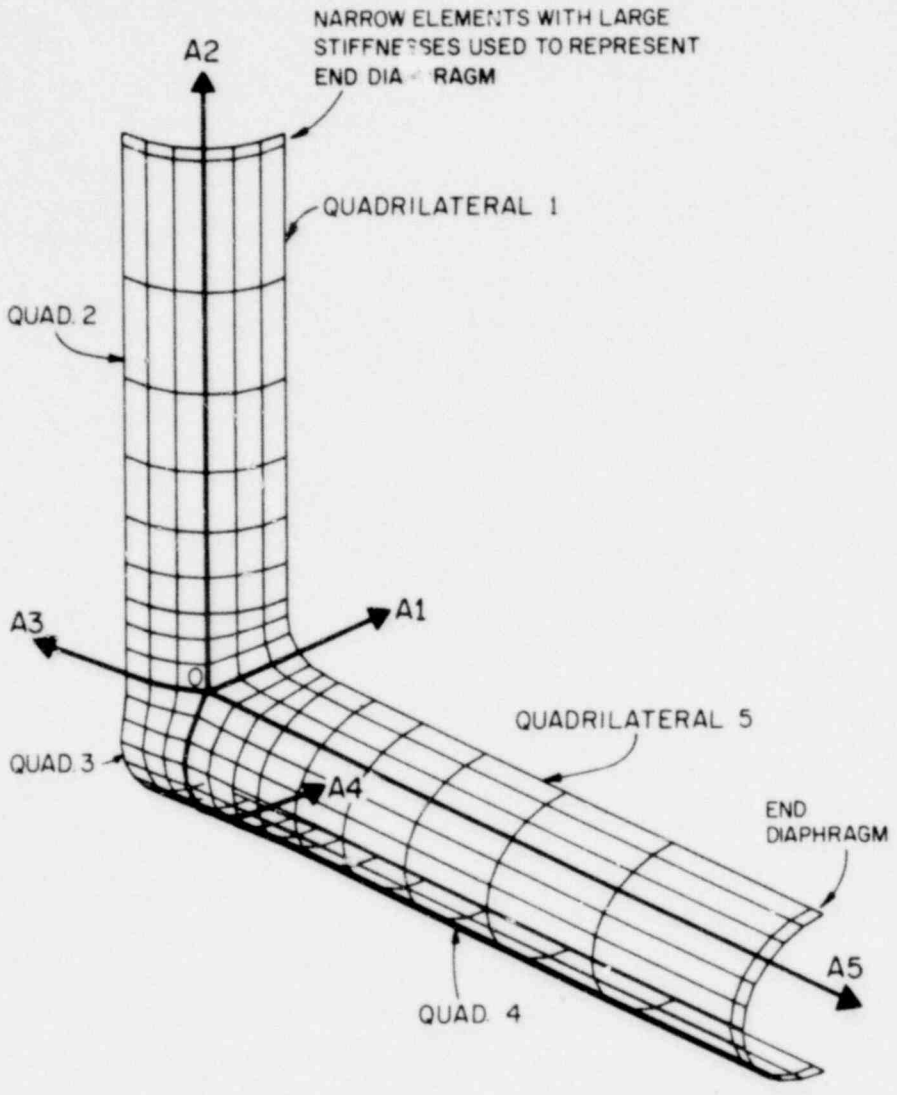

Fig. 4. Finite-element mesh.

2.3 Basic and Component Load Cases

CORTES-SA takes advantage of geometric, material, and loading symmetry by subdividing an arbitrary loading into component load cases that are either symmetric or skew-symmetric about the X-Y and Y-Z planes, obtaining stress solutions for these component cases, and then superposing the results to obtain a solution for the original loading. This, of course, implies that the program is restricted to small-displacement elastic problems.

For each component load case, CORTES-SA generates a mesh for a quarter section of the nozzle-cylinder configuration, writes appropriate boundary conditions for nodes in the X-Y and Y-Z planes, and applies the proper statically equivalent sets of nodal forces at the nozzle and/or cylinder end caps to simulate the desired external moment loadings(s). Stresses and displacements in the other quadrants are obtained by the following symmetry and/or skew-symmetry arguments. With reference to the global X-Y-Z coordinate system, loadings that are symmetric about a plane give identical normal stresses on mirror-image elements and shear stresses of the same magnitude but opposite sign. Skew-symmetric loadings give normal stresses of the same magnitude but opposite sign and identical shear stress on mirror-image elements. Also, loadings that are symmetric about a plane give mirror-image displacements on mirror-image nodes. Loadings that are skew-symmetric about a plane give displacements with the same magnitude and line of action as symmetric loadings, but in the opposite direction on mirror-image nodes. CORTES-SA writes displacement boundary conditions on the X-Y and Y-Z planes as follows: for symmetric loadings, points in a plane of symmetry cannot displace normal to that plane, while for skew-symmetric loadings, nodal points in the plane of symmetry can only move normal to that plane.

The "cantilever" tee depicted in Fig. 1 poses a problem for "bending" moment loadings when only a quarter section of the structure is modeled, because the boundary conditions are neither symmetric nor skew-symmetric (fixed at the left end of the cylinder and free on the right end). The best that can be done using CORTES-SA is to analyze a "simply supported" tee so that the moment restraining the applied loading always acts at the left end of the cylinder. A true cantilever problem can be worked, however, for the "torsional" moment loadings by adding a constant rigid body rotation to the appropriate component load case.

Figures 5 and 6 and Tables 1 and 2 summarize the above statements and show the basic load cases, their component load cases, and the boundary conditions used in the moment-loading parameter study. Note that two of the basic load cases, M_{ZC} and M_{YC}, are also component load cases and thus require no superposition for their solution.

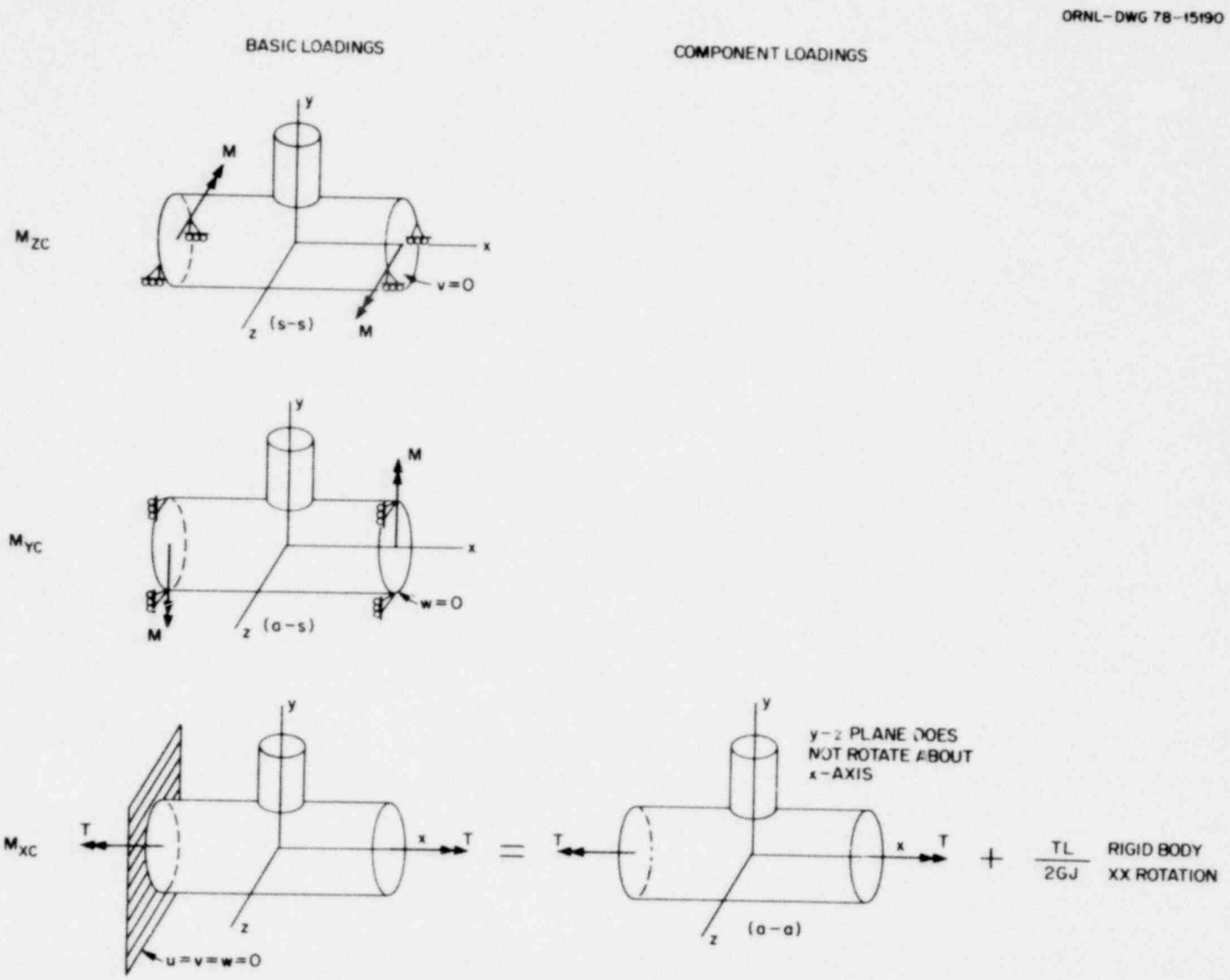

Fig. 5. External moment loadings on cylinder.

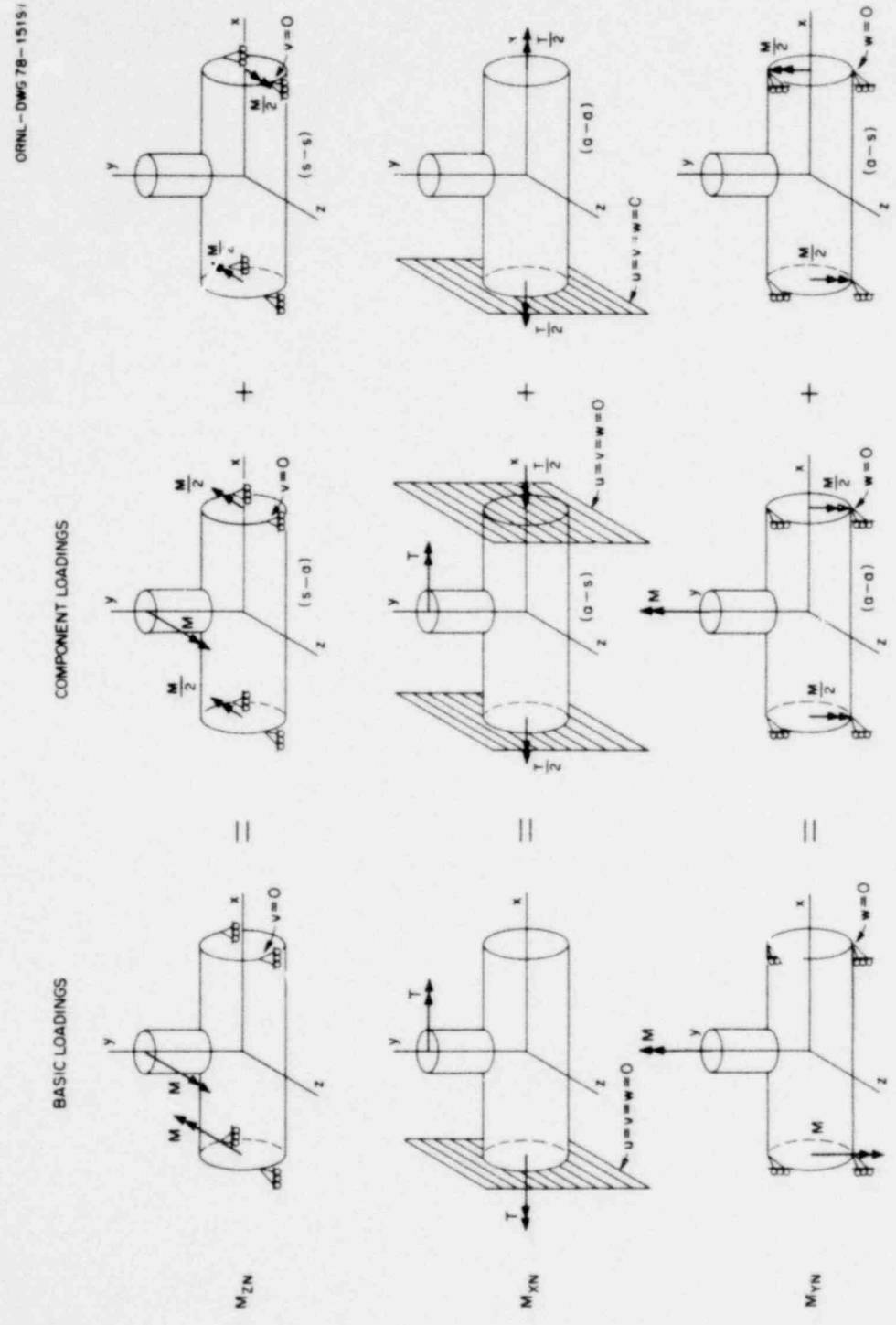

Fig. 6. External moment loadin[illegible] on nozzle.

Table 1. Basic load cases

LOADING	LOAD CASE	COMPONENT CASES
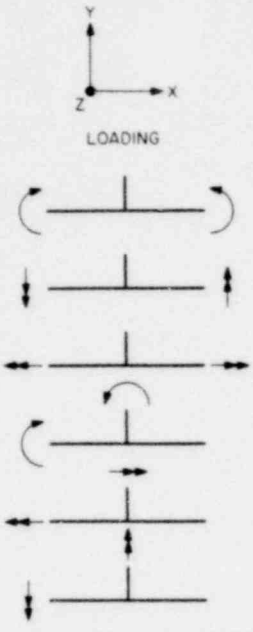	M_{ZC}	A
	M_{YC}	C
	M_{XC}	E
	M_{ZN}	$B + \frac{A}{2}$
	M_{XN}	$D + \frac{E}{2}$
	M_{YN}	$F + \frac{C}{2}$

Table 2. Component load cases

LOADING	LOAD CASE	BOUNDARY CONDITIONS AT CUT PLANE: X-Y PLANE	BOUNDARY CONDITIONS AT CUT PLANE: Y-Z PLANE
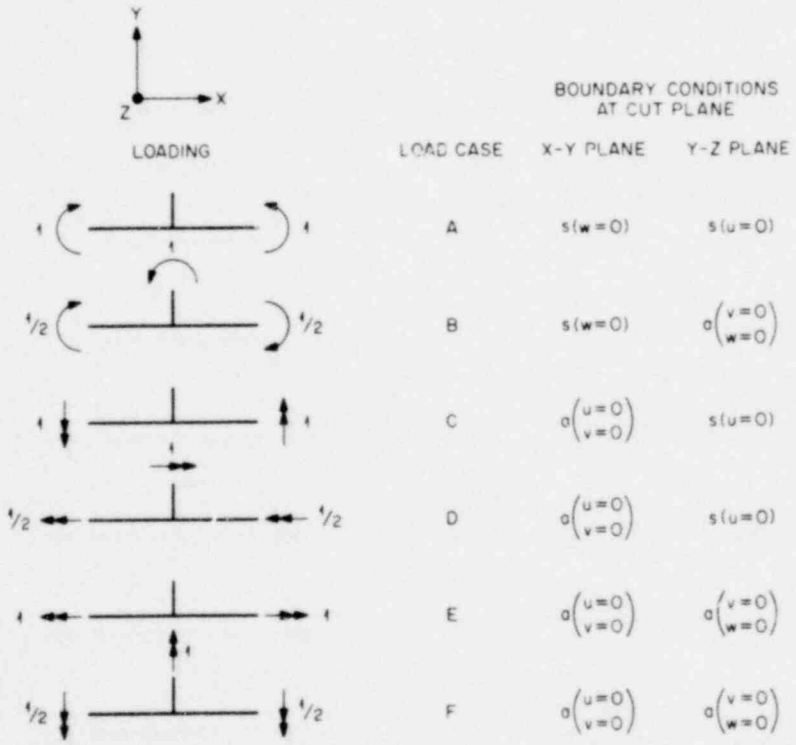	A	s(w=0)	s(u=0)
	B	s(w=0)	a(v=0, w=0)
	C	a(u=0, v=0)	s(u=0)
	D	a(u=0, v=0)	s(u=0)
	E	a(u=0, v=0)	a(v=0, w=0)
	F	a(u=0, v=0)	a(v=0, w=0)

s = SYMMETRY
a = ANTISYMMETRY

3. COMPUTER PROGRAM CHECKOUT

As was done for internal pressure loading in Ref. 1, a checkout of the computer program CORTES-SA was conducted to determine whether it would adequately predict the stress distributions for the relatively small d/D ratios ($0.08 \leq d/D \leq 0.50$) and wide range of D/T ratios ($10 \leq D/T \leq 100$) for individually applied moment loadings. At the outset of the study, it was realized that in-plane and out-of-plane moments applied to the nozzle (M_{ZN} and M_{XN}, respectively) were two of the more interesting loadings with regard to possible Code design rule modifications and/or revisions. Comparisons of results for these two loadings with experimental results for two of the checkout models of Ref. 1, ORNL-1 and ORNL-3, are given here. Similar comparisons are also shown for model ORNL-T8, a 12 × 12 × 6 in., sched-40, 304L stainless steel ANSI Standard B16.9 reducing piping tee.

Model ORNL-1[5] was an idealized thin-shell structure consisting of two stainless steel circular cylindrical shells intersecting at right angles. There were no transitions, reinforcements, or fillets in the junction region. The outside diameters of the cylinder and the nozzle were 254 mm (10 in.) and 127 mm (5 in.), respectively; the thicknesses of the cylinder and the nozzle were 2.54 mm (0.1 in.) and 1.27 mm (0.05 in.), respectively. A detailed discussion of model fabrication, strain-gage layout, and testing is given in Ref. 5.

For finite-element analysis, the appropriate model dimensions were input into CORTES-SA, but because the program requires an outside fillet radius r_2, an arbitrarily small value of 0.254 mm (0.01 in.) was also used. One element through the wall thickness was used, along with a total of 1226 nodes, 613 on each surface. The in-plane and out-of-plane moment loadings [271 N-M (2400 in.-lb) and 68 N-M (600 in.-lb), respectively] were the same as those used for the experimental study.

An isometric view of the mesh generated for the outside surface of the model is shown in Fig. 7, and cross-sectional views for 0 and 90° sections are shown in Fig. 8 for the junction region. Comparisons of

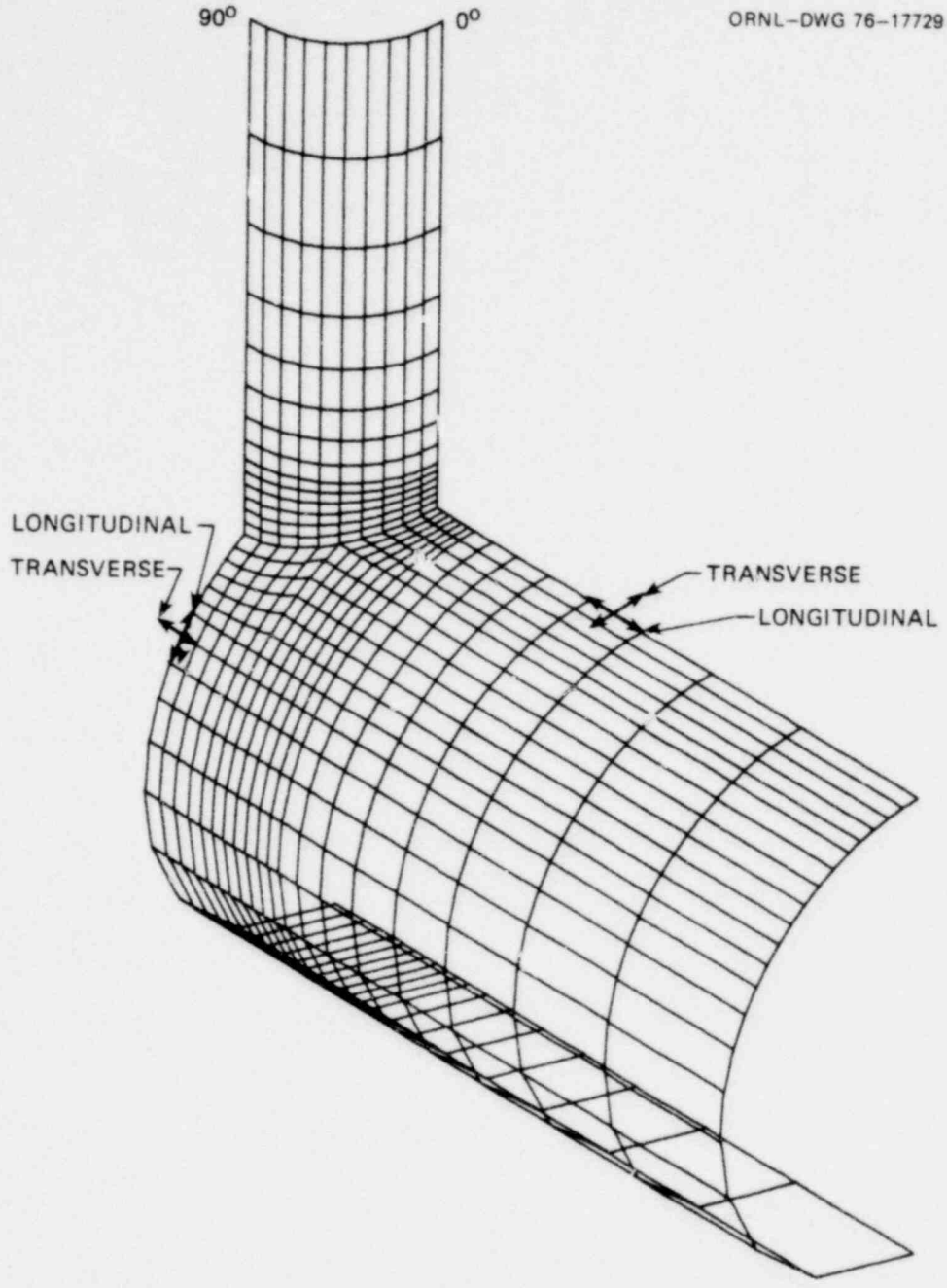

Fig. 7. Isometric view of outside surface for ORNL-1 generated mesh and definition of stresses for 0 and 90° sections.

experimental and calculated longitudinal and transverse stress distributions in plane sections normal to the moment-loading vector and containing the nozzle axis (0° section for M_{ZN} and 90° sections for M_{XN}) are shown in Figs. 9 and 10. Longitudinal stresses are those in the plane of

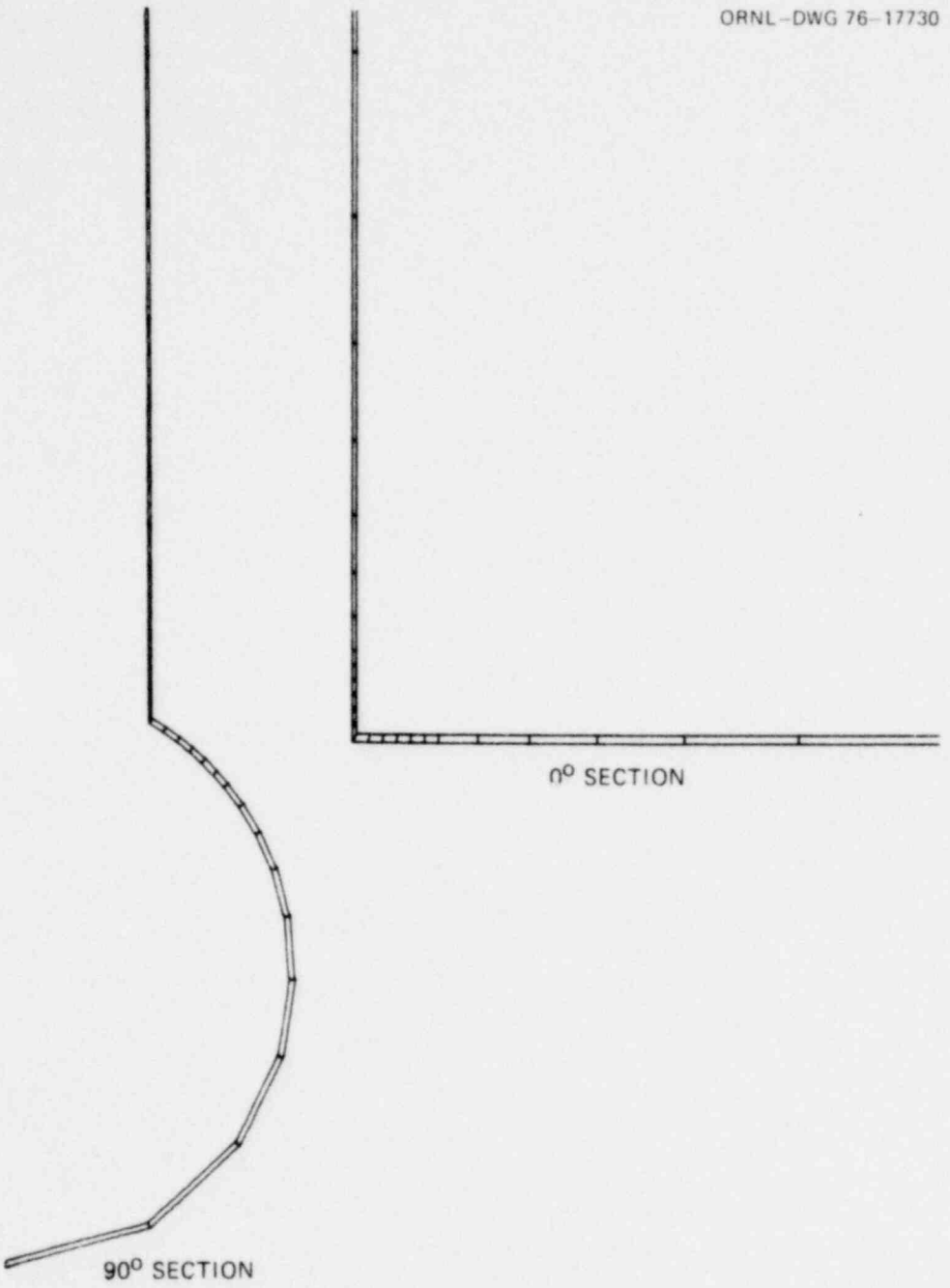

Fig. 8. Cross-sectional views for ORNL-1 generated mesh.

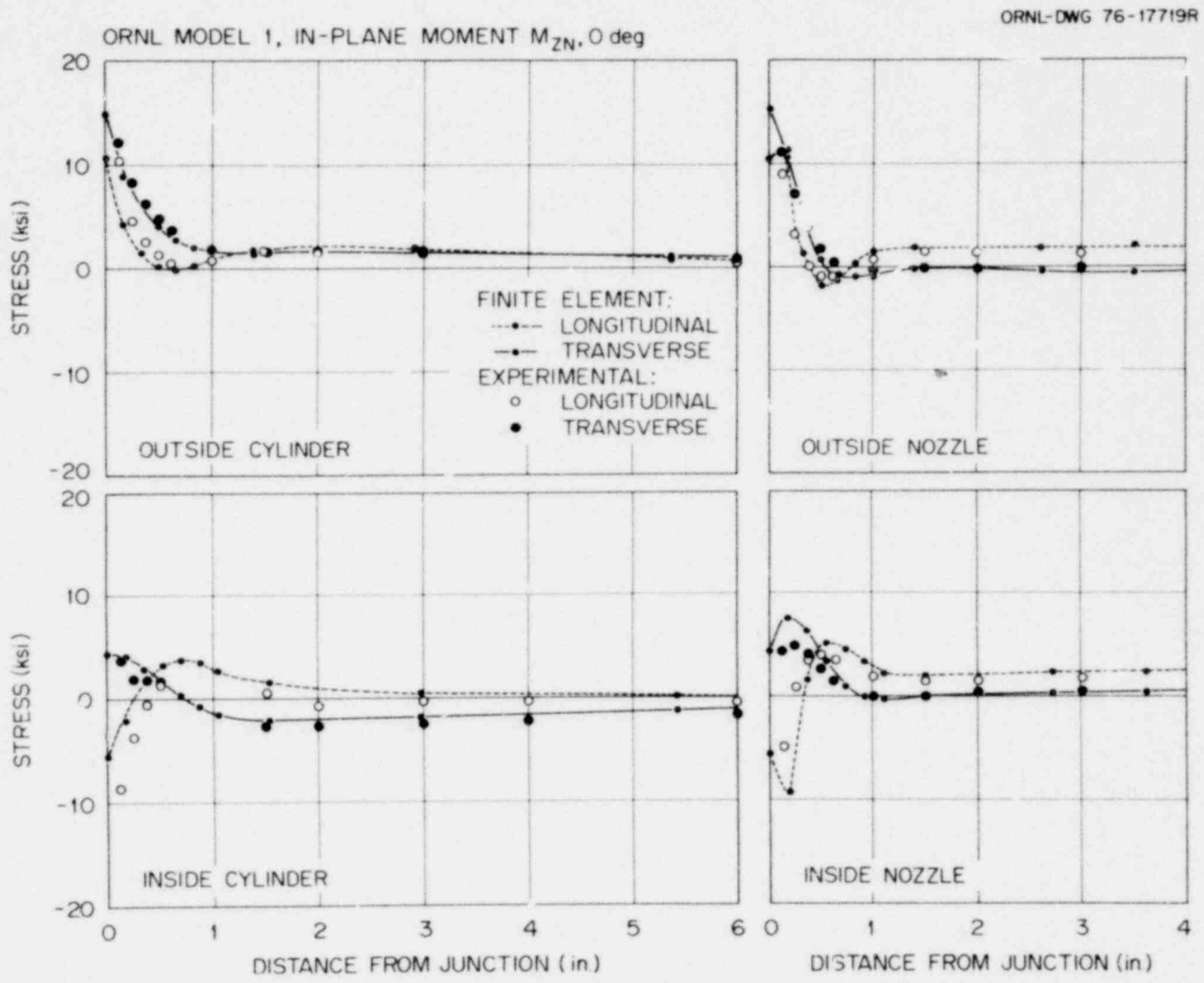

Fig. 9. Comparisons of experimental and theoretical stress distributions for 0° section of ORNL-1, in-plane moment loading M_{ZN} = 2400 in.-lb.

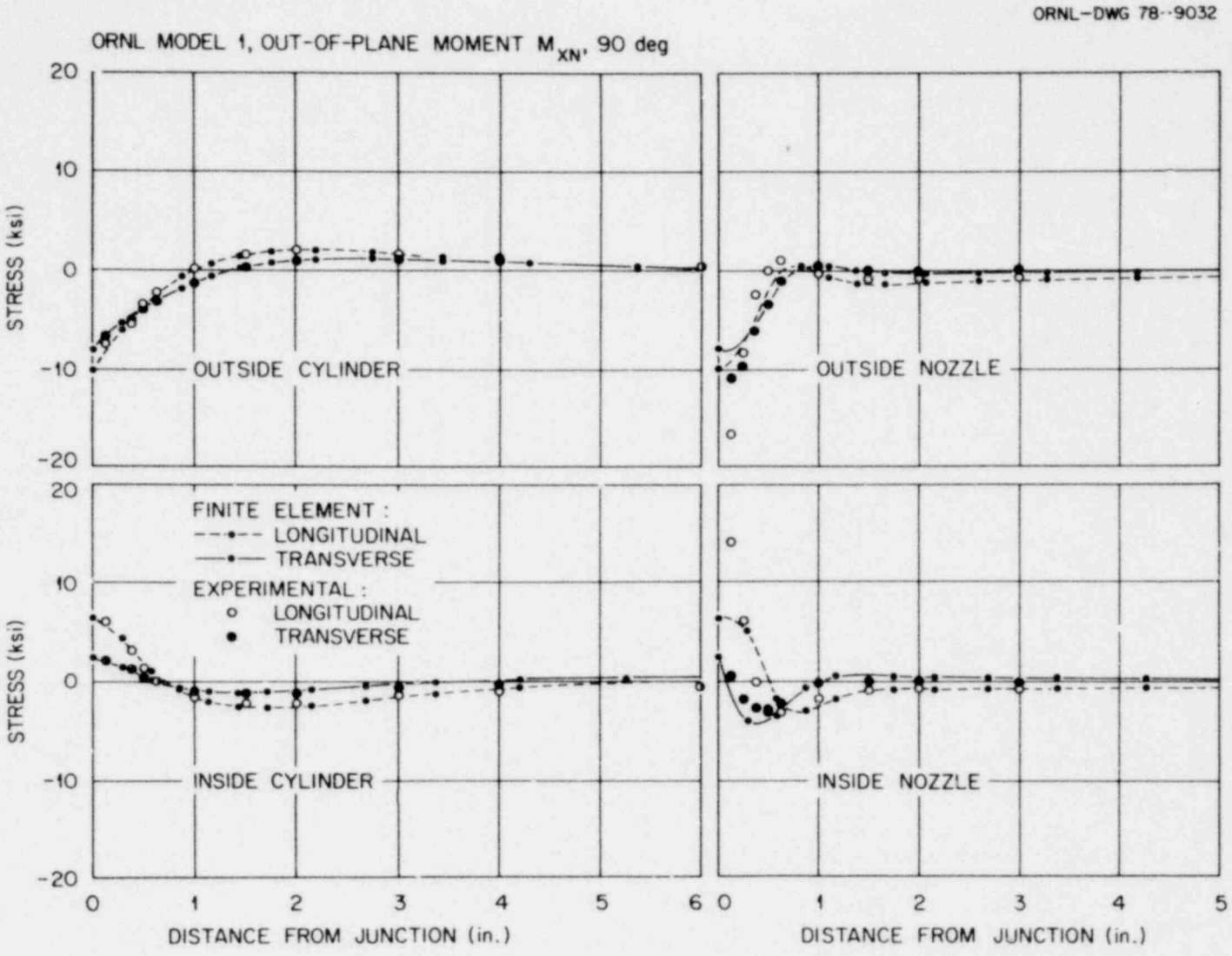

Fig. 10. Comparisons of experimental and theoretical stress distributions for 90° section of ORNL- · out-of-plane moment loading M_{XN} = 600 in.-lb.

the section *along* the node stringer, while transverse stresses are *normal* to the section (see Fig. 7). The comparisons shown in Fig. 9 for in-plane moment loading are generally good, except for the immediate junction region on the inside surface. Here the longitudinal stresses agree in magnitude; however, the experimental values are shifted somewhat more into the cylinder region than the calculated values. This discrepancy may result from the definition of the "junction." A slight misalignment in the abscissa values leads to a large discrepancy in the stress values due to the high stress gradient at the junction. The comparison for out-of-plane moment loading given in Fig. 10 shows generally good agreement, except for the longitudinal stress on the nozzle close to the junction. Here, the experimental values are roughly twice the calculated values.

For all of the loadings, the maximum values for the maximum principal stresses (and stress intensities) occurred on the outside surface at the junction between the nozzle and the cylinder, with the possible exception of the out-of-plane moment loading on the cylinder. For this loading, the finite-element analysis gave a value at the junction that was slightly less than the nominal bending stress in the cylinder that occurred along the outer surface of the cylinder in the X-Z plane. Figures 11 and 12 show comparisons between extrapolated experimental and calculated maximum principal stresses at the junction for in-plane and out-of-plane bending moments on the nozzle, respectively. Although the finite-element results are similar to the experimental results, they are on the order of 35% smaller at the indicated maximums. Part of this discrepancy can be attributed to experimental model inperfections (see Ref. 5); however, the major portion is probably due to a combination of factors, including the relative stiffness of the eight-node finite-element in CORTES and the difference in the boundary conditions between the experiment and the analysis, as discussed earlier in Chapter 2.

The second model for which comparisons of experimental and calculated results were made was ORNL-3.[6] Like ORNL-1, this model was an idealized structure with no transitions, reinforcements, or fillets in the junction region, but it had a smaller d/D ratio (0.129 vs 0.5) and a relatively thicker wall (D/T = 50 vs D/T = 100). The outside diameter of the cylinder was 254 mm (10 in.) and the thickness was 5.08 mm (0.2 in.); the

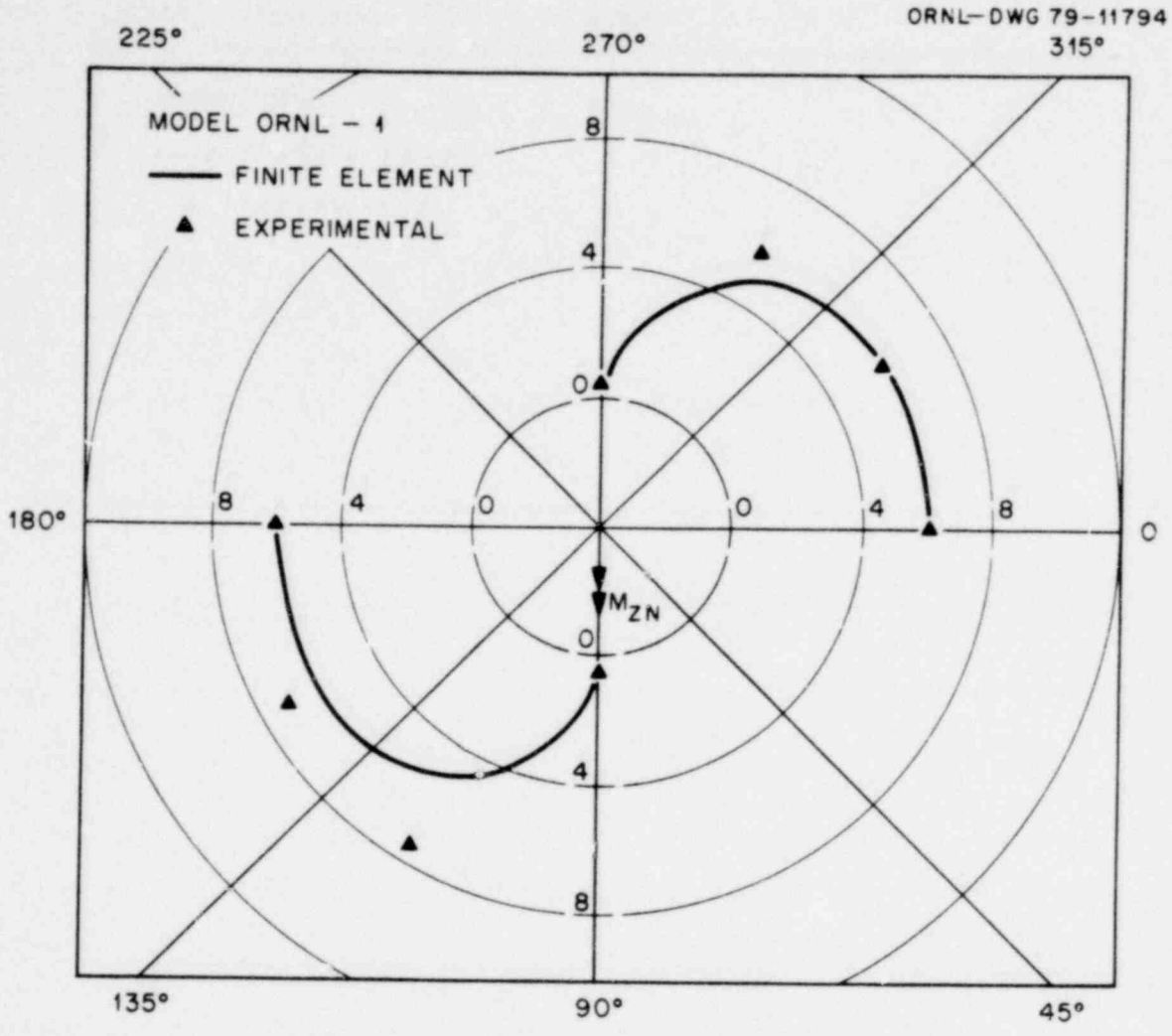

Fig. 11. Variation of maximum principal stress ratios around nozzle-cylinder junction for in-plane moment loading on nozzle M_{ZN} = 2400 in.-lb for ORNL-1.

outside diameter of the nozzle was 32.9 mm (1.29 in.) and the wall thickness was 4.27 mm (0.168 in.). Comparisons of experimental and calculated values for in-plane and out-of-plane moment loadings applied to the nozzle were made for this model primarily to investigate the ability of CORTES-SA to predict stress distributions for models with small d/D ratios.

An isometric view of the mesh generated for ORNL-3 is shown in Fig. 13 and cross-sectional views of the mesh generated for the 0 and 90° sections are shown in Fig. 14. Two elements were used through the wall

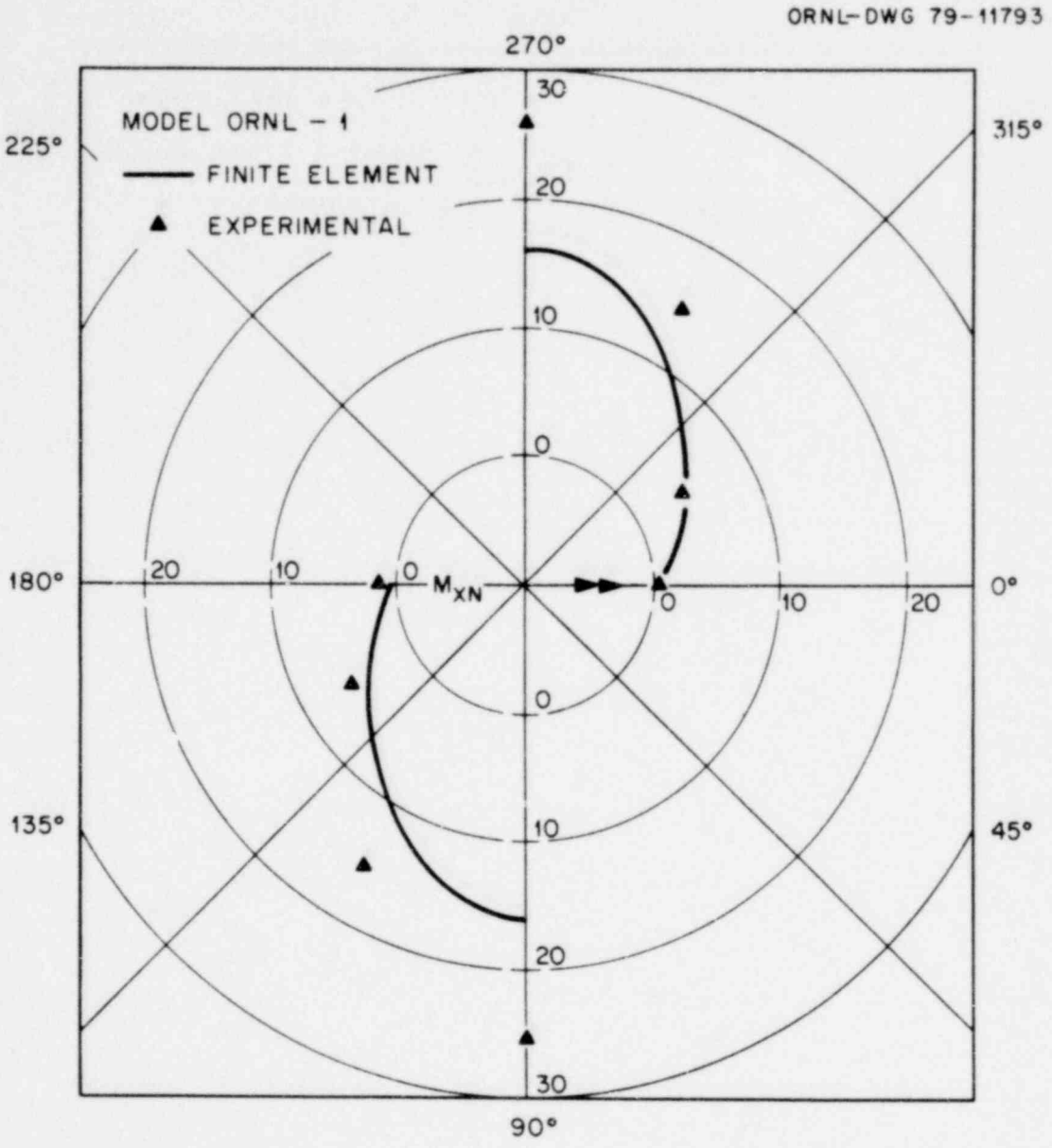

Fig. 12. Variation of maximum principal stress ratios around nozzle-cylinder junction for out-of-plane moment loading on nozzle M_{XN} = 600 in.-lb for ORNL-1.

thickness. The comparisons of experimental and calculated values for in-plane moment loading applied to the nozzle are given in Fig. 15, while those for out-of-plane moment loading are given in Fig. 16. As before, comparisons are shown for plane sections normal to the loading vector and containing the axis of the nozzle. The loadings were 136 N-M (1200 in.-lb)

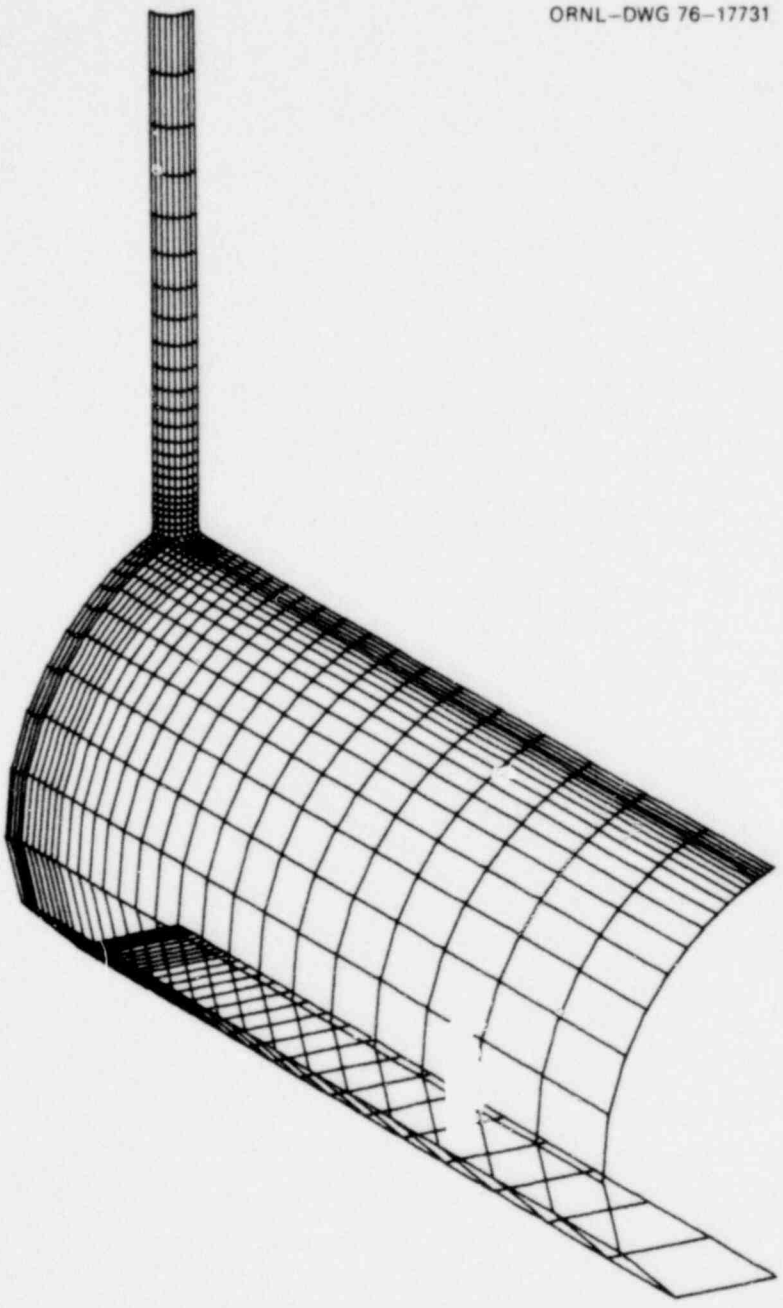

Fig. 13. Isometric view of outside surface for ORNL-3 generated mesh.

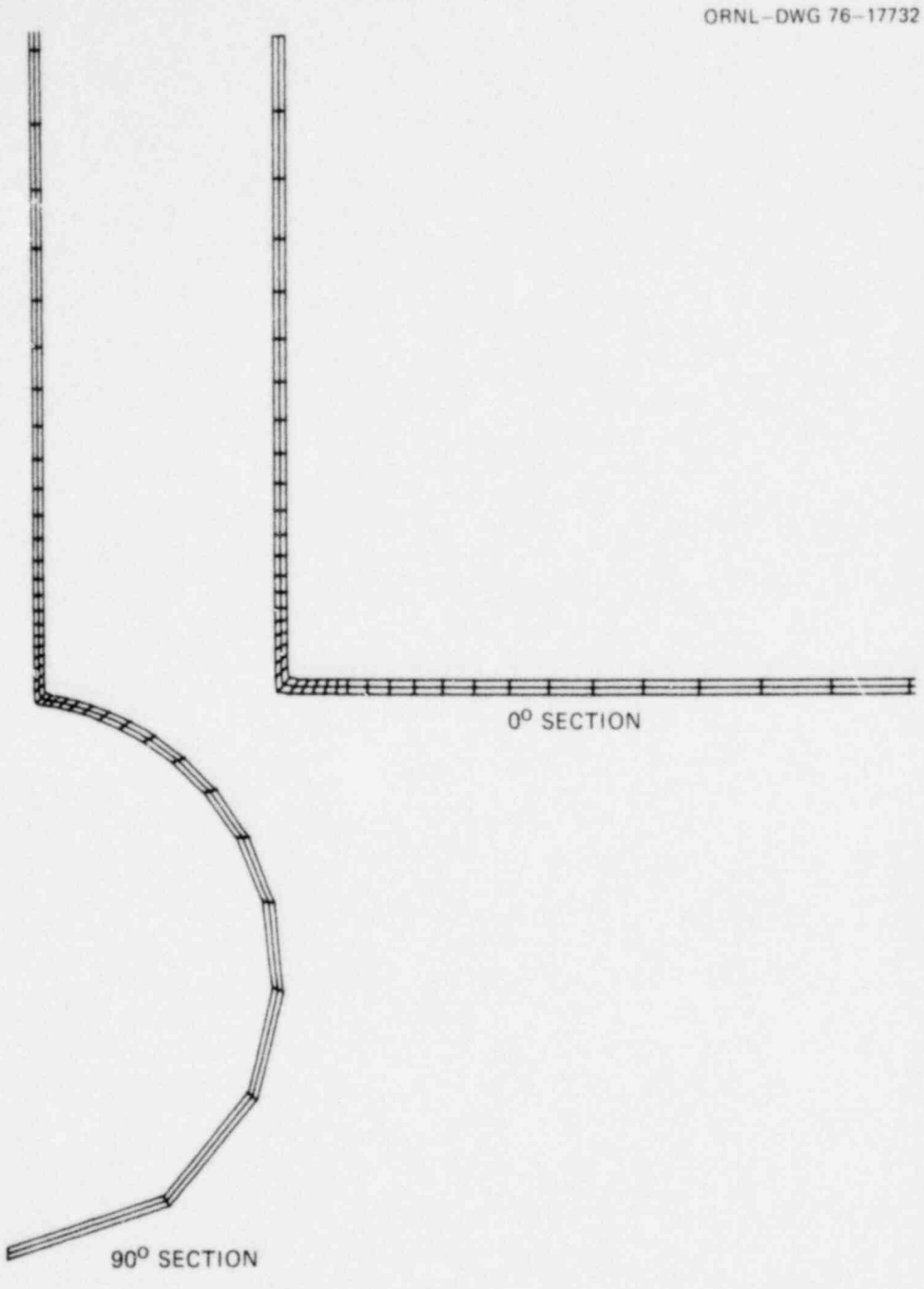

Fig. 14. Cross-sectional views of ORNL-3 mesh for 0 and 90° sections.

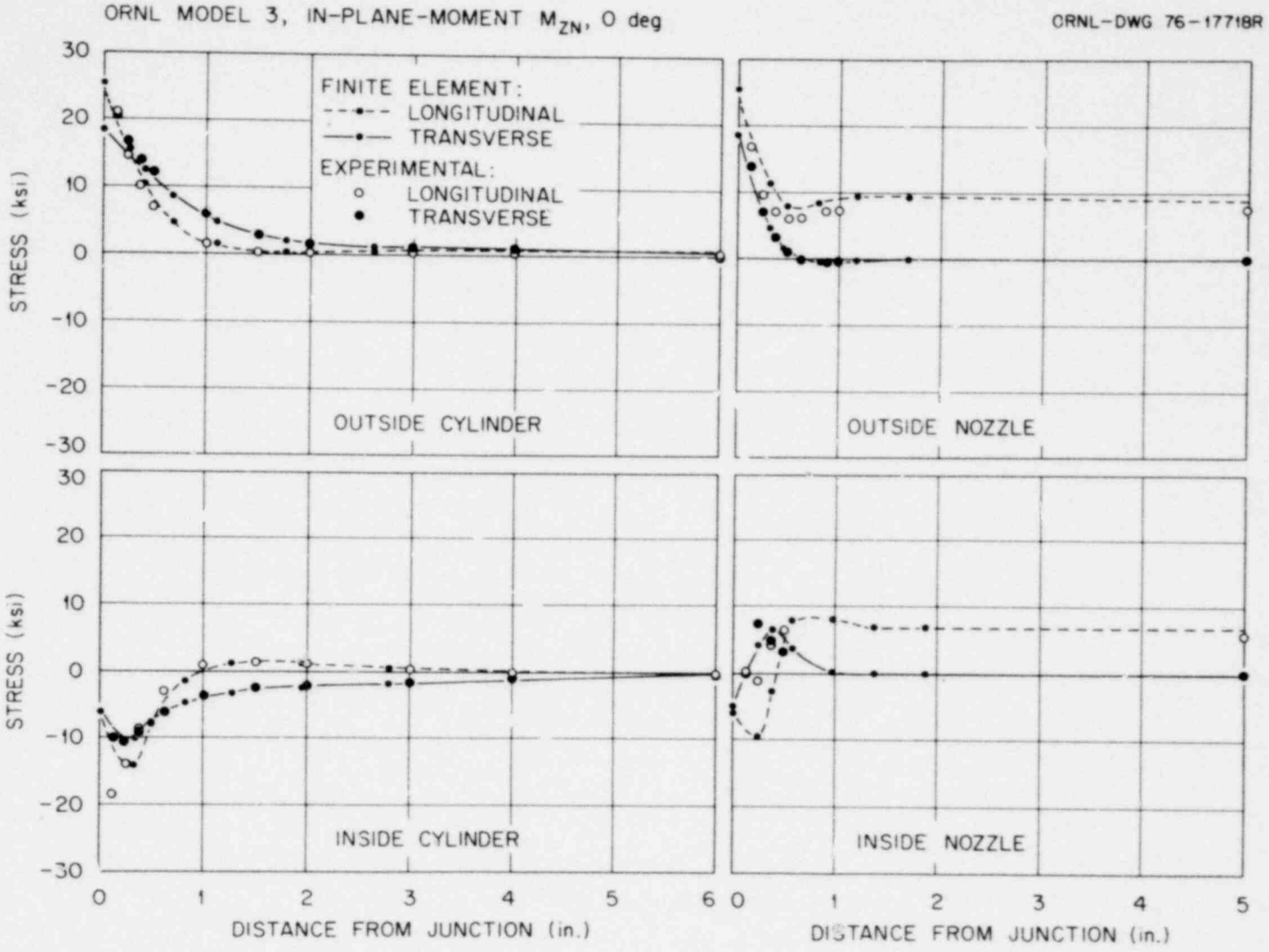

Fig. 15. Comparisons of experimental and theoretical stress distributions for 0° section of ORNL-3, in-plane moment loading M_{ZN} = 1200 in.-lb.

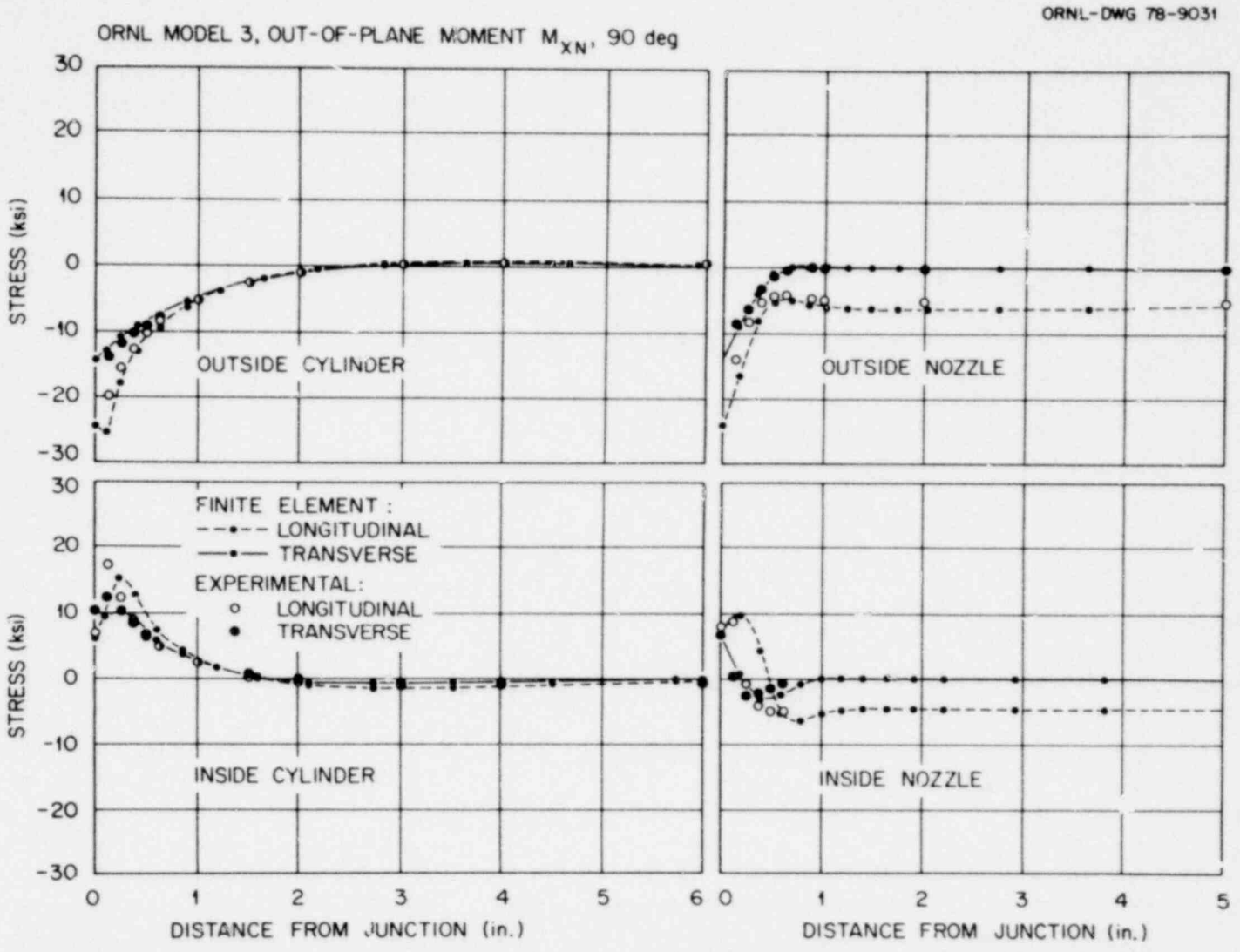

Fig. 16. Comparisons of experimental and theoretical stress distributions for 90° section of ORNL-3, out-of-plane momer . loading M_{XN} = 800 in.-lb.

and 90 N-M (800 in.-lb) for the in-plane and out-of-plane moments, respectively. The comparisons for in-plane moment loading at the 0° section are generally good, except for longitudinal stresses on the inside surface very near the junction. Unlike model ORNL-1, comparisons for out-of-plane moment loading at the 90° section show reasonably good agreement between calculated and experimental values.

For ORNL-3, the maximum principal stresses for all the loadings also occurred on the outside surface at the junction between the nozzle and the cylinder. Comparisons between experimental and finite-element results are shown in Figs. 17 and 18 for the in-plane and out-of-plane nozzle moment-loading cases. The agreement is excellent for both loadings, with maximum

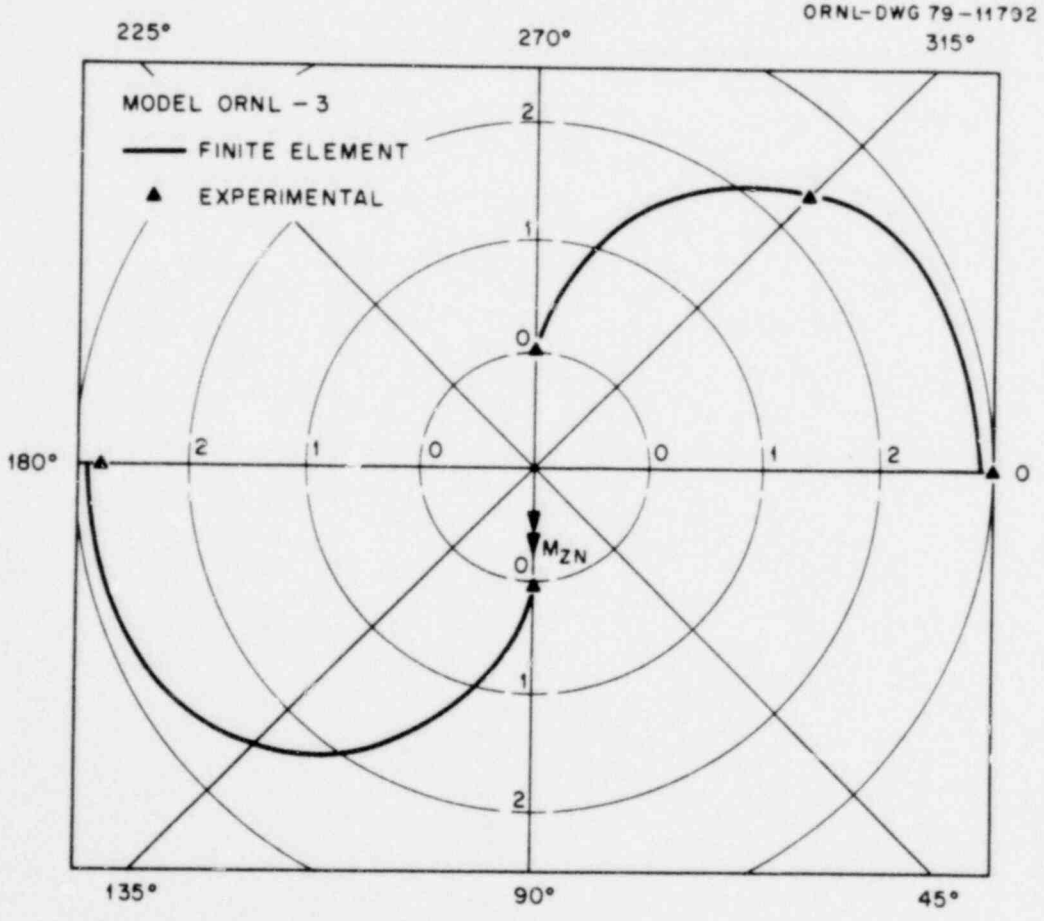

Fig. 17. Variation of maximum principal stress ratios around nozzle-cylinder junction for in-plane moment loading on nozzle M_{ZN} = 1200 in.-lb for ORNL-3.

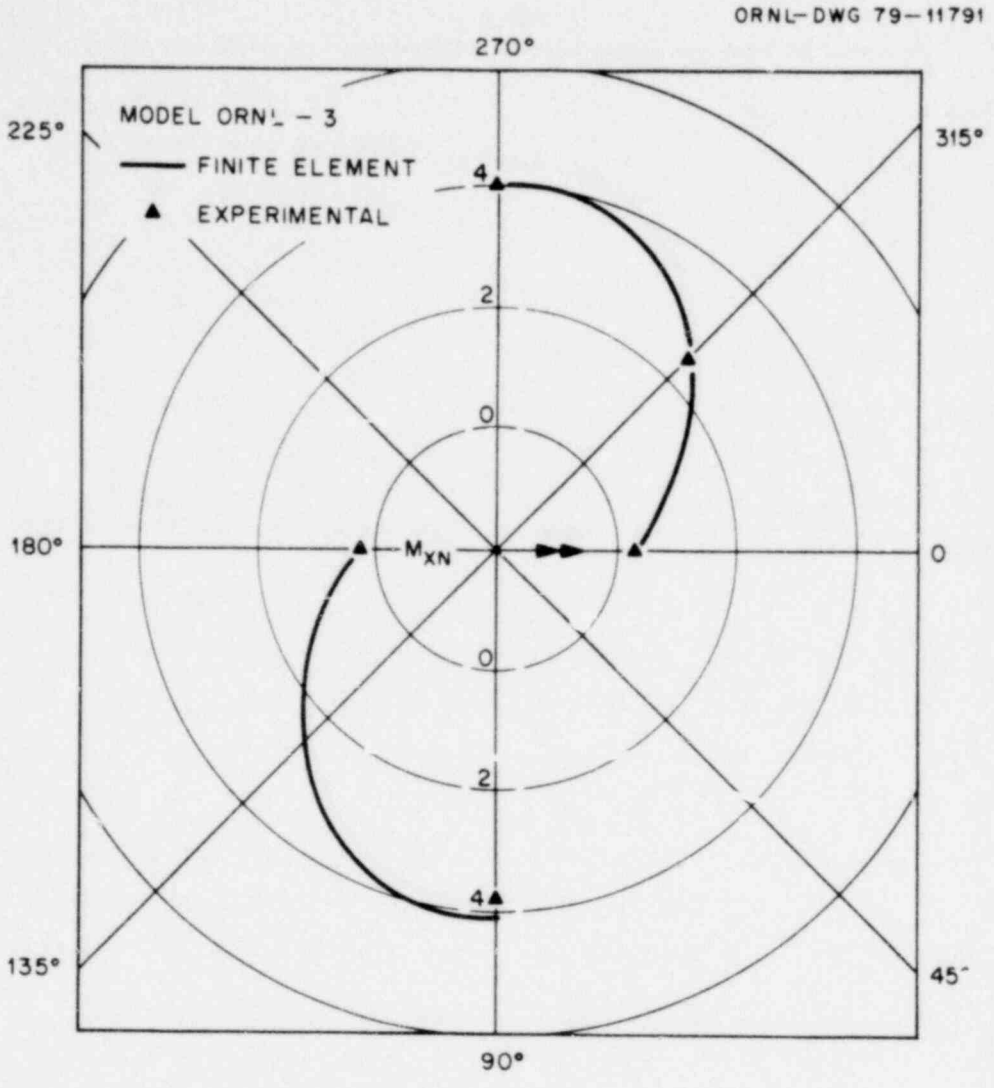

Fig. 18. Variation of maximum principal stress ratios around nozzle-cylinder junction for out-of-plane moment loading on nozzle M_{XN} = 80 n.-lb for ORNL-3.

differences of <5%. These results tend to support the conclusion, reached from the model ORNL-1 study, that differences between the experimental and finite-element results are caused primarily by the behavior of the particular finite element under bending and not by the mesh layout or the finite-element model boundary conditions. These factors, however, might also influence some of the parameter study results discussed in the next chapter.

Both ORNL-1 and ORNL-3 were flush cylinder-to-cylinder models with no reinforcing or fillet in the transition region. To examine whether the

computer program adequately predicts stress distributions for tees with a reinforced transition region, comparisons between experimental and calculated results were also made for model ORNL-T8. This model, a 12 × 12 × 6 in., sched-40, 304L stainless steel ANSI B16.9 Standard reducing piping tee that was tested[17] at Southwest Research Institute under subcontract to ORNL, had parameter ratios of d/D = 0.5 and D/T = 34. The outside diameter of the cylinder was 324 mm (12.750 in.) and the wall thickness was 9.5 mm (0.375 in.); the outside diameter of the nozzle was 168 mm (6.625 in.) and the wall thickness was 7.1 mm (0.280 in.).

Detailed wall thickness measurements were made at the transition region of the tee to accurately construct a finite-element mesh. Figure 19 gives an isometric view of the generated mesh for the outside surface using these thicknesses. Three layers of elements were used through the wall thickness.

Comparisons between experimental and calculated results for ORNL-T8 are shown in Figs. 20 and 21 for in-plane and out-of-plane moment loadings of 960 N-M (8500 in.-lb) applied to the nozzle. The abscissas in these figures represent arc distances measured from the point of attachment of the nozzle pipe extension to the tee. Figure 19 illustrates the various reference points. Good comparisons were obtained for both the in-plane and out-of-plane moment loadings. For in-plane moment loading, the maximum principal stress (absolute value) obtained experimentally was 8.4 MPa (1.22 ksi), while the maximum calculated value was 8.7 MPa (1.26 ksi), a difference of 3%. Both of these values were found on the outside surface in the middle of the transition region at 22-1/2°. For out-of-plane moment loading, the maximum experimental and calculated principal stresses (absolute value) obtained were 15.6 MPa (2.26 ksi) and 15.7 MPa (2.28 ksi), respectively, for a difference of 0.5%. Both of these occurred on the outside surface in the middle of the transition region at the 90° section.

In addition to the results for in-plane and out-of-plane moment loadings on the nozzle for the three models above, in-depth comparisons between experimental and calculated results were made for the other four moment loadings shown in Figs. 5 and 6. Generally good-to-excellent agreement was obtained for models ORNL-3 and ORNL-T8 for each of these

ORNL-DWG 78-19269

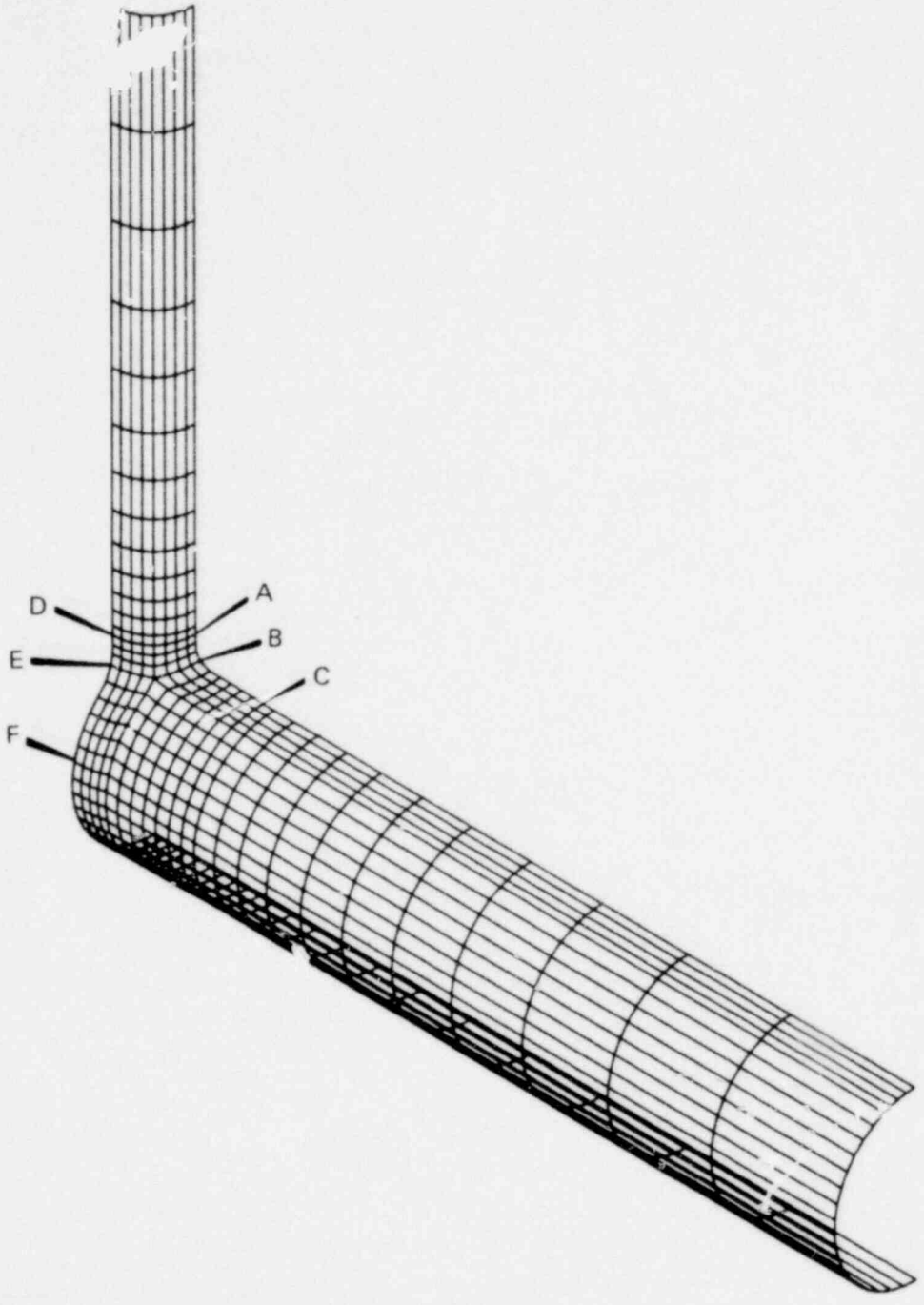

Fig. 19. Isometric view of outside surface for ORNL-T8 generated mesh.

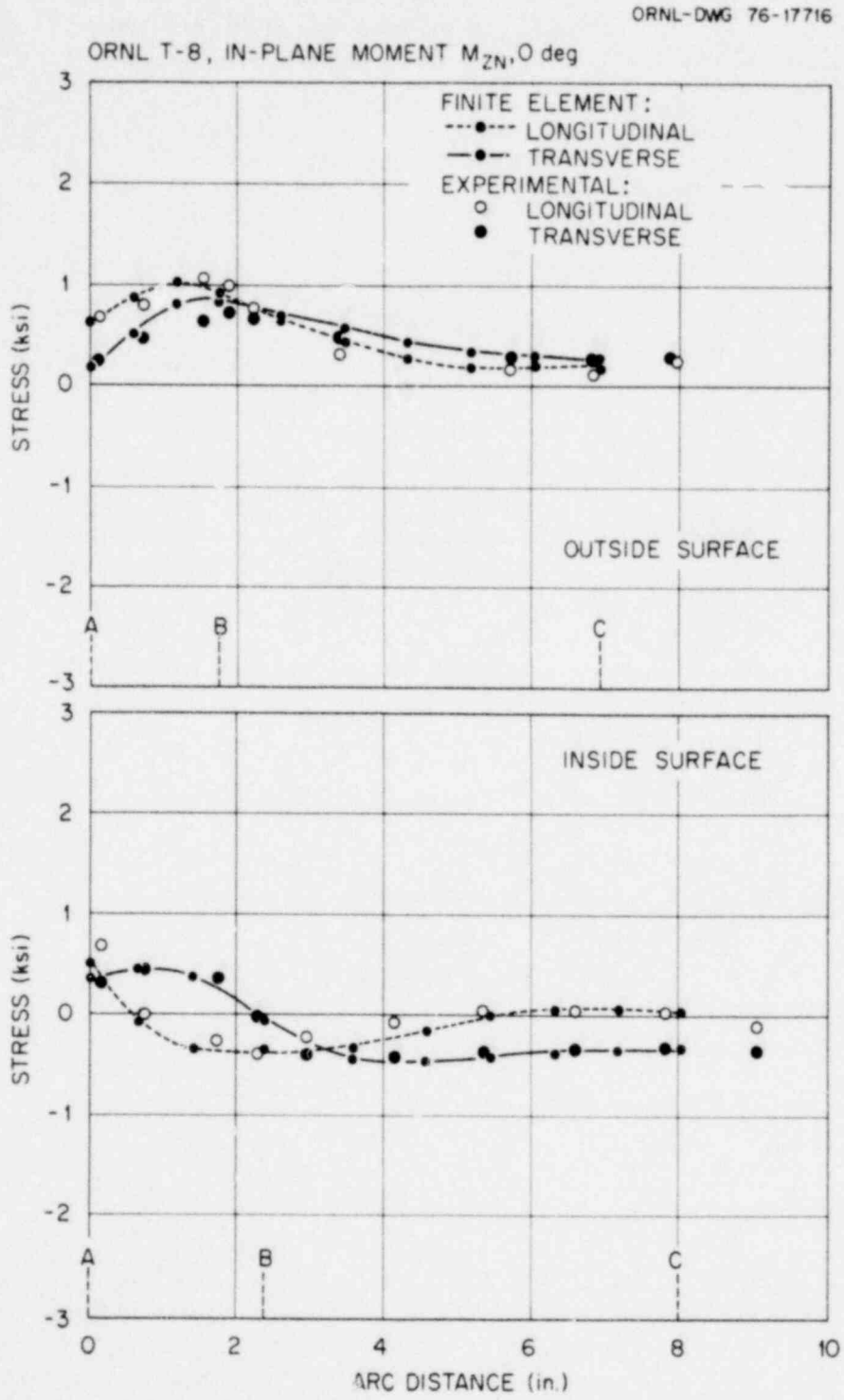

Fig. 20. Comparisons of experimental and theoretical stress distributions for 0° section of ORNL-T8, in-plane moment loading M_{ZN} = 850(in.-lb.

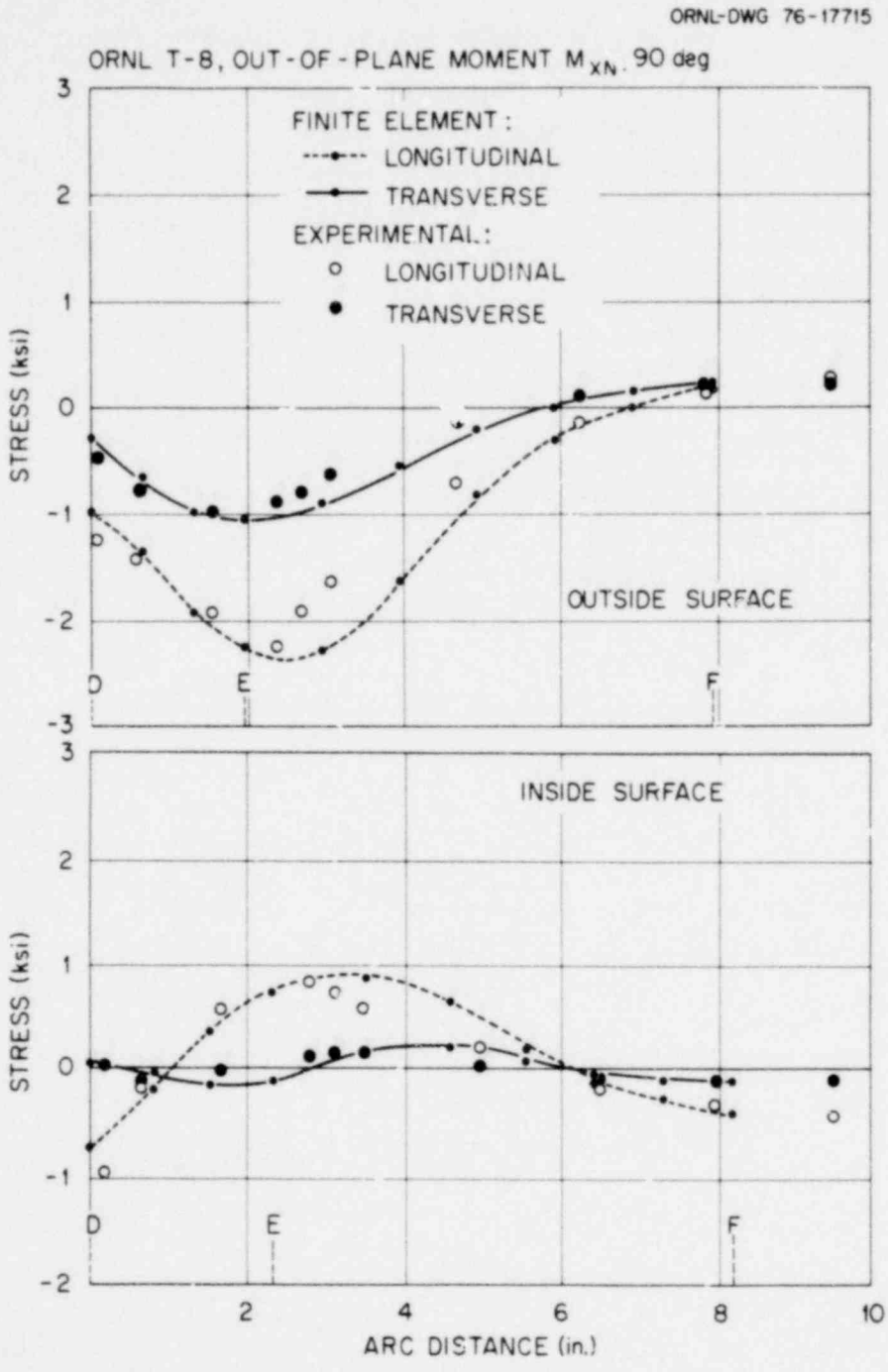

Fig. 21. Comparisons of experimental and theoretical stress distributions for 90° section of ORNL-T8, out-of-plane moment loading M_{XN} = 8500 in.-lb.

loadings. Somewhat less satisfactory comparisons were obtained for ORNL-1.

In light of the results above and other experience in using ORTES-SA, certain observations can be made about the program. As might be expected, the program gives the most "reliable" results for relatively thicker models having moderate to large d/D ratios and smooth transitions in the junction region, in the sense that good comparisons are obtained with experimental studies. Less reliable results are obtained for models with either very small d/D ratios or large D/T ratios. However, as Chapter 4 will show, only a few of the parameter study models have d/D or D/T ratios that might present difficulties for CORTES-SA. Also, the mesh-generation feature of the program and the minimal amount of input required make CORTES-SA economically attractive for conducting a parameter study of this magnitude.

4. THE PARAMETER STUDY

The 25 models listed in Table 3 were analyzed for the six individually applied external moment loadings shown earlier in Figs. 5 and 6. The models fall within the parameter ranges $10 \leq D/T \leq 100$ and $0.08 \leq d/D \leq 0.5$ and are the same models that were analyzed under internal pressure loading in Ref. 1. In fact, the finite-element meshes generated for the models in this study are identical to those generated in Ref. 1.

All of the nozzles were designed according to one of the sketches shown in Fig. 22 (NB-3338.2 of the Code). The six U models were essentially unreinforced, except for the minimum fillet (r_2) at the junction, as shown in Fig. 22(a). The fourteen S1 models (so-called "standard" reinforced) depicted in Fig. 22(b) and the five P30 models (30° pad reinforcement), Fig. 22(c), were fully reinforced in accordance with the rules of Code paragraphs NB-3332 through NB-3334. The primary emphasis of the study was placed on the S1 models because this reinforcement design is the most widely used at present for both nuclear pressure vessels and piping. Results from the U and P30 models provide a relative measure of the effect of reinforcement and the shape of the reinforcement on the calculated stress distributions when compared with results from the appropriate S1 models.

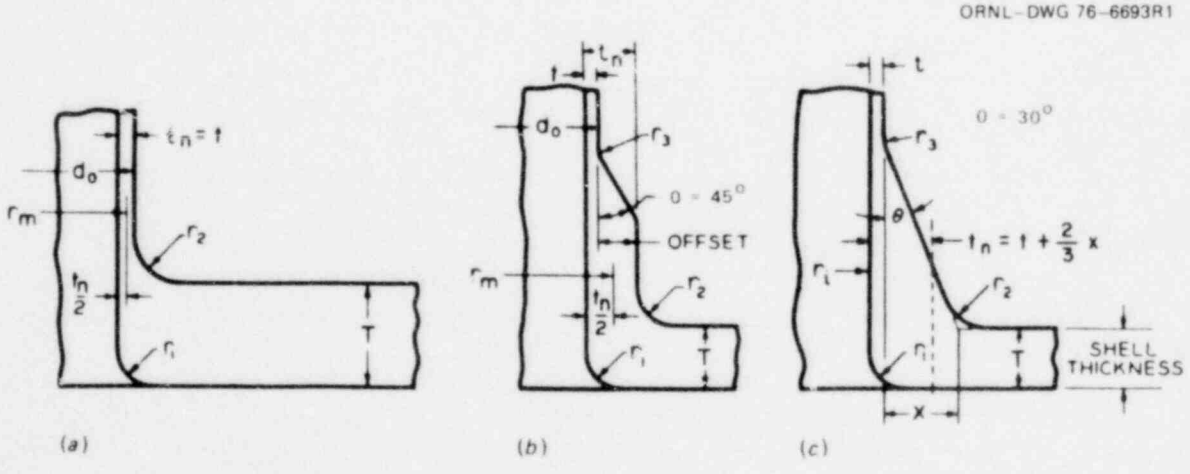

Fig. 22. Nozzle dimensions for various standard reinforcement designs: (*a*) unreinforced U models; (*b*) standard S1 models; and (*c*) reinforced P30 models.

Table 3. Dimensionless parameters for the study of isolated nozzles in cylindrical vessels

D/T[a]	d/D[b]			
	0.08	0.16	0.32	0.50
10	(0.2530)[c]	(0.5060)	(1.0119)	(1.5811)
	UF[d]			UE
	S1N[d]	S1K	S1H	S1E
	P30E[d]		P30D	[e]
20	(0.3578)	(0.7155)	(1.4311)	(2.2361)
				UD
	S1M	S1J	S1J	S1D
			P30C	[e]
40	(0.5060)	(1.0119)	(2.0239)	(3.1623)
				UC
	S1L	S1I	S1F	S1C
			P30B	[e]
80	(0.7155)	(1.4311)	(2.8622)	(4.4721)
				UB
				S1B
				[e]
100	(0.8000)	(1.600)	(3.2000)	(5.0000)
				UA
				S1A
			P30A	[e]

[a] D/T is the inside diameter-to-thickness ratio of the cylindrical vessel.

[b] d/D is the ratio of the inside diameters in the nozzle and cylindrical vessel.

[c] Numbers given in parentheses are values for the parameter $(d/D)\sqrt{D/T}$.

[d] U, S1, and P30 refer to nozzle designs shown in Figs. 22(*a*), 22(*b*), and 22(*c*), respectively.

[e] P30 models are geometrically impossible for these parameter values.

4.1 U Models

The U models (Table 4) were essentially unreinforced, except that a small outside fillet of radius $r_2 = T/2$, as required by Paragraph NB-3338.2, was used [see Fig. 22(a)]. This radius was taken as constant around the junction zone.

An inside shell diameter of 254 mm (10 in.) was chosen for these models as well as for all the others of the study. The other dimensional quantities were then determined from the parameter ratios (see Table 3). The relation $t = (d/D)T$ or $s/S = 1$ was used to determine the nozzle thickness for all the models; $s = pd/2t$ and $S = pD/2T$ are the nominal circumferential membrane stresses in the nozzle and cylinder, respectively.

Models UA through UE had nozzle-to-shell diameter ratios (d/D) of 0.50 and shell diameter-to-thickness ratios (D/T) from 10 to 100. Model UF had d/D and D/T values of 0.08 and 10, respectively.

Isometric views for the U models, as well as for the S1 and P30 models, can be found in Appendix B. Cross-sectional views for these same models may be found in the Appendices of Ref. 1. The largest and smallest principal stresses and maximum stress intensities obtained for each of the U models for each loading are tabulated and discussed in Chapter 5.

4.2 S1 Models

One of the most widely used reinforcement configurations for pressure vessel design is nozzle-thickening reinforcement [see Figs. 22(b) and 23]. Fourteen models of this type were investigated, and the dimensions are given in Table 5 and identified in Fig. 23.

The rules of Paragraphs NB-3332 through NB-3334 require that the total cross-sectional area of reinforcement A in any given plane for a vessel under internal pressure shall be not less than

$$A = dTF \ , \tag{4.1}$$

where F is a correction factor that compensates for the variation in pressure stresses on different planes with respect to the axis of a vessel. Paragraph NB-3332.2 provides a chart for determining the value of

Table 4. Dimensional parameters[a] for U models (1 in. = 25.4 mm)

Model (D/T, d/D)	D (in.)	d (in.)	T (in.)	t (in.)	L_c (in.)	L_b (in.)	r_1 (in.)	r_2 (in.)
UA (100, 0.50)	10	5	0.1	0.05	20	20	0.05	0.05
UB (80, 0.50)	10	5	0.125	0.0625	20	20	0.0625	0.0625
UC (40, 0.50)	10	5	0.25	0.125	20	20	0.125	0.125
UD (20, 0.50)	10	5	0.50	0.25	20	20	0.25	0.25
UE (10, 0.50)	10	5	1.0	0.5	20	20	0.5	0.5
UF (10, 0.08)	10	0.8	1.0	0.08	20	20	0.5	0.5

[a] D = inside diameter of run; same for all 25 models
d = inside diameter of branch
T = wall thickness of run
t = wall thickness of branch
L_c = length of run from intersection of run and branch axes
L_b = length of branch from intersection of run and branch axes
r_1 = inner transition radius [see Fig. 22(a)]
r_2 = outer fillet radius [see Fig. 22(a)]

Table 5. Dimensional parameters[a] for S1 models (1 in. = 25.4 mm)

Model (D/T, d/D)	D (in.)	d (in.)	T (in.)	t (in.)	L_c (in.)	L_b (in.)	L_n (in.)	t_n (in.)	r_1 (in.)	r_2 (in.)
S1A (100, 0.50)	10	5	0.1	0.05	20	20	0.651	0.434	0.05	0.217
S1B (80, 0.50)	10	5	0.125	0.0625	20	20	0.7123	0.5012	0.0625	0.251
S1C (40, 0.50)	10	5	0.25	0.125	20	20	0.9487	0.7838	0.125	0.392
S1D (20, 0.50)	10	5	0.5	0.25	20	20	1.2834	1.224	0.25	0.612
S1E (10, 0.50)	10	5	1	0.5	20	20	1.7658	1.9158	0.5	0.958
S1F (40, 0.32)	10	3.2	0.25	0.08	20	20	0.7143	0.64	0.125	0.32
S1G (20, 0.32)	10	3.2	0.5	0.16	20	20	0.9662	0.988	0.25	0.494
S1H (10, 0.32)	10	3.2	1	0.32	20	20	1.3293	1.5236	0.5	0.762
S1I (40, 0.16)	10	1.6	0.25	0.04	20	20	0.4658	0.4694	0.125	0.235
S1J (20, 0.16)	10	1.6	0.5	0.08	20	20	0.6321	0.7128	0.25	0.356
S1K (10, 0.16)	10	1.6	1	0.16	20	20	0.8707	1.0788	0.5	0.539
S1L (40, 0.08)	10	0.8	0.25	0.02	20	20	0.3081	0.3446	0.125	0.172
S1M (20, 0.08)	10	0.8	0.5	0.04	20	20	0.4203	0.5158	0.25	0.258
S1N (10, 0.08)	10	0.8	1	0.08	20	20	0.6213	0.7238	0.3619	0.5

[a] D = inside diameter of run
d = inside diameter of branch
T = wall thickness of run
t = wall thickness of branch
L_c = total length of run from intersection of run and branch axes
L_b = total length of branch from intersection of run and branch axes
L_n = reinforced length in junction zone (see Fig. 23)
t_n = reinforced thickness in junction zone (see Fig. 23)
r_1 = inner transition radius [see Fig. 22(*b*)]
r_2 = outer fillet radius [see Fig. 22(*b*)]

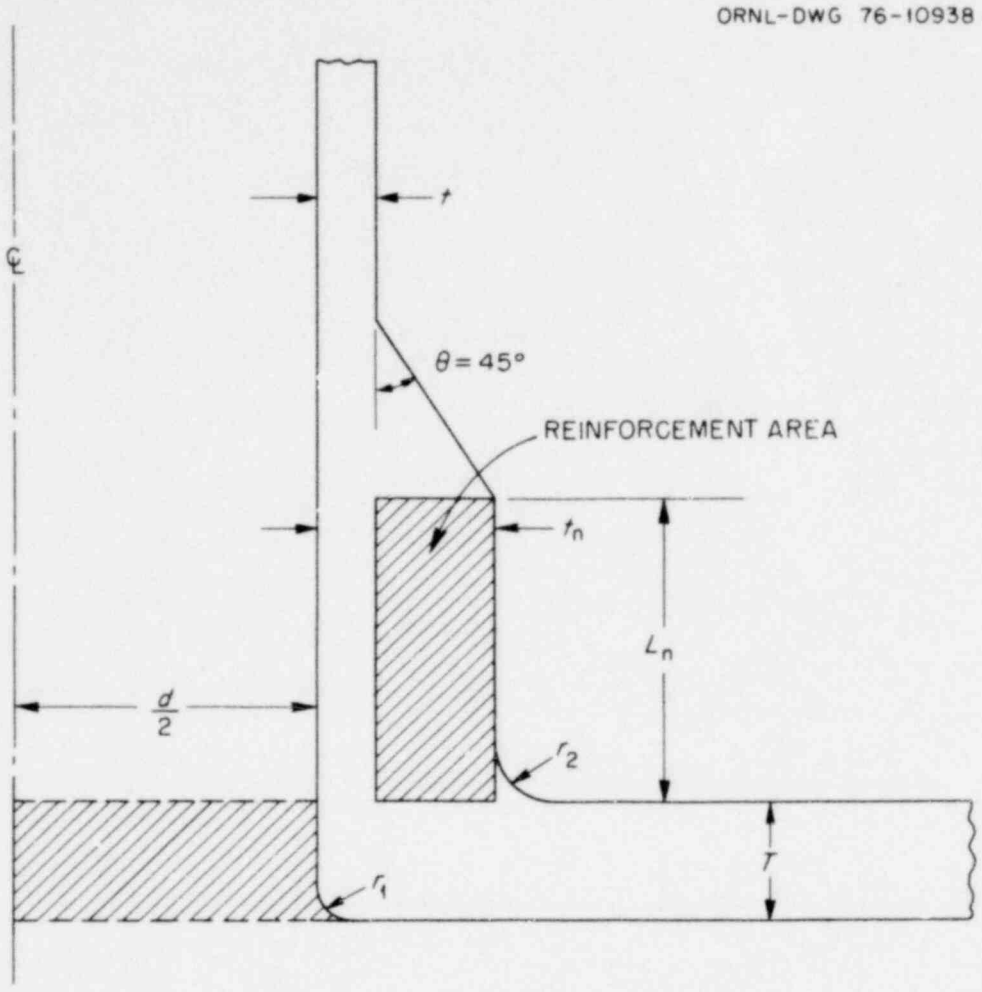

Fig. 23. Parameters for S1 standard reinforcement designs.

F for any given plane. A value of $F = 1.0$ was used in the parameter study. In terms of t_n, L_n, and t (see Fig. 23), Eq. (4.1) then becomes

$$A = dT = 2L_n(t_n - t) \quad . \tag{4.2}$$

The values for t_n and L_n were selected so that Eq. (4.2) was satisfied in the 0° (X-Y) plane. In other planes, L_n remained at the same distance above the vessel in the 0° plane; therefore, the reinforcement area was somewhat more than that required in these other planes.

An additional restriction on L_n, and hence on the shape of the reinforcement, is imposed by Paragraph NB-3334. This limitation is given

by

$$2L_n \leq \sqrt{0.5(d + t_n)\ t_n} + r_2 \ , \qquad (4.3)$$

where r_2 = max $(T/2,\ t_n/2)$ and is constant in all planes. Taking the upper limit on L_n, we then have two equations involving the two unknowns t_n and L_n, for any particular model. Equations (4.2) and (4.3) can be solved iteratively for the values of t_n and L_n; the results are given in Table 5 for each of the S1 models.

4.3 P30 Models

Five 30° pad reinforced models [see Figs. 22(c) and 24] were included in the study to investigate the influence of reinforcement shape. Four of

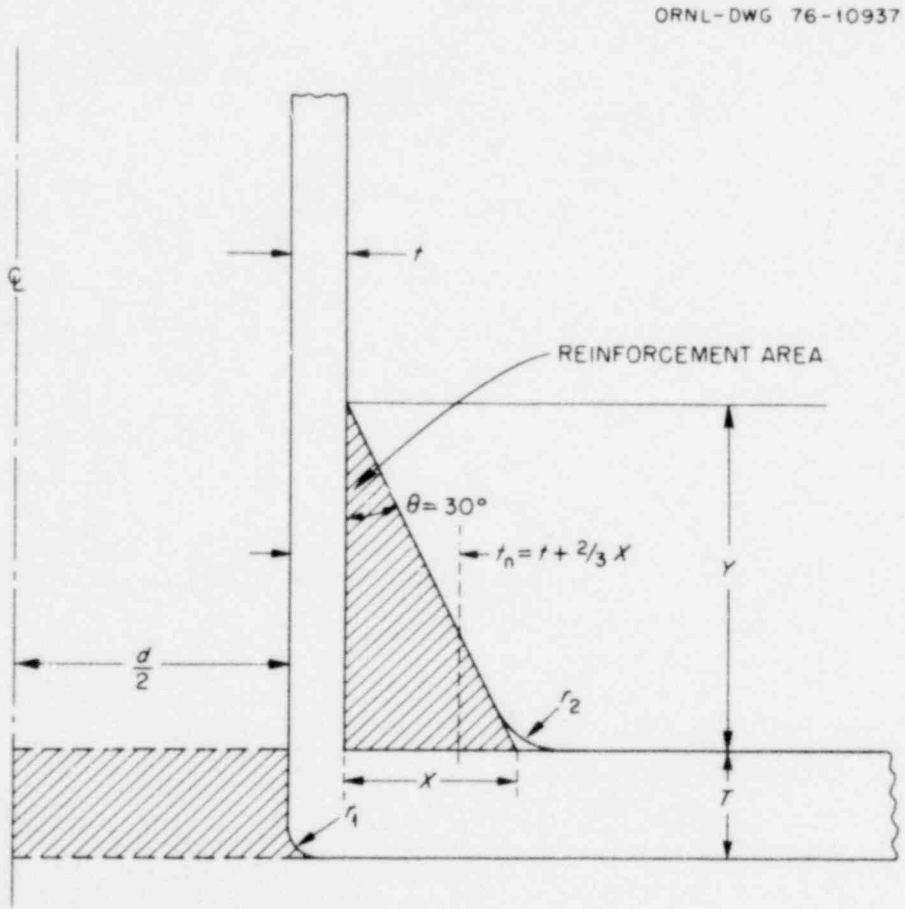

Fig. 24. Parameters for 30° pad reinforcement designs.

these models had d/D ratios of 0.32, and their results can be compared directly to the corresponding S1 models. For d/D = 0.5, however, 30° pad models are not geometrically possible.

The required reinforcement for the 30° pad models in the 0° plane [i.e., Eq. (4.1)] is given by

$$A = dT = XY = 1.732X^2$$

in terms of the dimensions X and Y shown in Fig. 24, since θ = 30°. The height of the reinformcement triangle remained at the same distance above the vessel in the 0° plane; hence, for these models, the reinforcement was also somewhat more than that required in the other planes. As for the S1 models, r_2 = max ($T/2$, $t_n/2$), where

$$t_n = t + \frac{2}{3} X \ . \qquad (4.5)$$

The radius r_2 was constant in all planes. Table 6 gives X and Y values as well as other dimensions for the triangular pad models.

4.4 Applied Loadings

Each of the 25 models in the parameter study was analyzed for in-plane, out-of-plane, and torsional moment loadings individually applied at the ends of the nozzle and cylinder. The values of the in-plane and out-of-plane moment loadings (M) on the nozzle or cylinder were chosen such that the bending stresses on the outside surfaces would equal 6.895 MPa (1 ksi) on the nozzle or cylinder (i.e., Mc/I = 1 ksi). Torsional moment loadings (T) were used such that the shear stress on the outside surfaces of the nozzle or cylinder computed by Tc/J would equal 3.448 MPa (0.5 ksi). The loading values are tabulated for each model, along with the largest and smallest principal stresses and maximum stress intensities obtained for these loadings in Chapter 5.

Table 6. Dimensional parameters[a] for P30 models (1 in. = 25.4 mm)

Model (D/T, d/D)	D (in.)	d (in.)	T (in.)	t (in.)	L_c (in.)	L_b (in.)	Y (in.)	X (in.)	r_1 (in.)	r_2 (in.)
P30A (100, 0.32)	10	3.2	0.1	0.032	20	20	0.7444	0.4298	0.05	0.1593
P30B (40, 0.32)	10	3.2	0.25	0.08	20	20	1.1771	0.6796	0.125	0.2665
P30C (20, 0.32)	10	3.2	0.5	0.16	20	20	1.6646	0.9611	0.25	0.4003
P30D (10, 0.32)	10	3.2	1.0	0.32	20	20	2.3543	1.3593	0.5	0.6131
P30E (10, 0.08)	10	0.8	1.0	0.08	20	20	1.1771	0.6796	0.5	0.5

[a] D = inside diameter of run
d = inside diameter of branch
T = wall thickness of run
t = wall thickness of branch
L_c = length of run from intersection of run and branch axes
L_b = length of branch from intersection of run and branch axes
Y = height of reinforcement triangle (see Fig. 24)
X = base of reinforcement triangle (see Fig. 24)
r_1 = inner transition radius [see Fig. 22(c)]
r_2 = outer fillet radius [see Fig. 22(c)]

5. RESULTS AND CONCLUSIONS

This 25-model parameter study of isolated nozzle-cylinder attachments under external moment loading is an extension of the work reported in Ref. 1 for the same models under internal pressure loading. These studies were undertaken as a first step in the assessment of existing design safety criteria and the development of improved Code rules for reinforced isolated and closely spaced nozzles in cylindrical pressure vessels. As stated earlier, the objective of this report is to summarize and present the more important and relevant results of the study. A follow-up document will relate these results to present design rules and include recommendations for improved design safety criteria for nozzles and branch connections.

The 25 models fall within the parameter ranges $0.08 \leq d/D \leq 0.50$ and $10 \leq D/T \leq 100$, ranges that include most reactor pressure vessel nozzles. The models were analyzed for the six external moment loadings and imposed boundary conditions shown in Figs. 5 and 6 (see Chapter 2). The emphasis of the study was on S1, or so-called standard reinforcement designs, since these are the most widely used; P30, or 30° triangular pad reinforcement, designs were investigated to examine the relative effects of reinforcement shape. The U or unreinforced models were included for comparison purposes with reinforced model results and with most of the available experimental data in the literature.

Tables 7 through 12 are summaries of the algebraically largest principal stresses and maximum stress intensities obtained on the outside and inside surfaces and their locations for each of the models. The stress intensity (not to be confused with the fracture mechanics parameter "stress-intensity factor") at any particular node on either surface represents twice the maximum shear stress ($2\tau_{max}$) and is given by

$$\bar{\sigma} = \max(|\sigma_1 - \sigma_2|,\ |\sigma_2 - 0|,\ |\sigma_1 - 0|)\ ,$$

where σ_1 and σ_2 represent principal stresses in a plane tangent to the surface at the particular node.

Table 7. Summary of maximum stress intensities and numerically largest principal stresses for in-plane moment loading, M_{ZN}, applied to the nozzle
(1 in.-lb = 0.113 N-m; 1 ksi = 6.895 MPa)

Model $\left(\frac{D}{T}, \frac{d}{D}\right)^{a,b}$	Number of elements through thickness	Load[c] (in.-lb)	$\bar{\sigma}_o d$ (ksi)	$\bar{\sigma}_i d$ (ksi)	Location[e] Quad: axis pos.	σ_{EQ}^f (ksi)	σ_{pt}^f (ksi)	Location[e] Quad: axis pos.	Direction cosines[g] ℓ	m	n
UA (100,0.5)	1	992	5.856		1:1-0-0-0-0	5.856		1:1-0-0-0-0	0.404	0.380	-0.832
				6.996	1:3-1-0-0-0		4.396	2:5-1-0-0-0	-0.046	-0.999	-0.029
UB (80,0.5)	1	1243	5.360		1:1-0-0-0-0	5.360		1:1-0-0-0-0	0.335	0.446	-0.830
				6.541	1:3-1-0-0-0		4.343	2:5-1-0-0-0	-0.057	-0.998	-0.028
UC (40,0.5)	2	2519	5.173		2:4-1-0-0-0	-5.173		2:4-1-0-0-0	0.145	0.989	-0.051
				4.642	1:5-2-0-0-0		3.300	2:5-2-0-0-0	-0.001	-1.000	-0.027
UD (20,0.5)	2	5178	3.277		2:4-1-0-0-0	-3.277		2:4-1-0-0-0	0.138	0.985	-0.099
				2.539	1:5-2-0-0-0		1.593	2:5-2-0-0-0	-0.001	-1.000	-0.028
UE (10,0.5)	4	10979	2.645		2:5-1-0-0-0	-2.645		2:5-1-0-0-0	0.241	0.971	0.017
				1.324	1:0-0-5-2-0		1.164	1:5-6-0-0-0	0.0	1.000	0.0
UF (10,0.08)	4	45	1.357		1:4-3-0-0-0	1.357		1:4-3-0-0-0	-0.030	1.000	0.003
				1.020	2:4-6-0-0-0		1.009	1:4-5-0-0-0	0.0	1.000	0.0
S1A (100,0.5)	1	992	2.190		2:5-0-0-0-1	-2.190		2:5-0-0-0-1	-0.982	-0.190	0.0
				2.138	1:0-0-5-3-0		-1.456	1:0-0-2-1-0	-0.730	0.359	-0.582
S1B (80,0.5)	1	1243	2.094		2:5-0-0-0-1	-2.094		2:5-0-0-0-1	-0.977	-0.216	0.0
				2.024	1:0-0-5-3-0		-1.431	1:0-0-1-1-0	-0.713	0.351	-0.607

Table 7 (continued)

Model $\left(\frac{D}{a},\frac{d}{D}\right)^{a,b}$	Number of elements through thickness	Load[c] (in.-lb)	$\bar{\sigma}_o$[d] (ksi)	$\bar{\sigma}_t$[d] (ksi)	Location[e] Quad: axis pos.	σ_{po}[f] (ksi)	σ_{pi}[f] (ksi)	Location[e] Quad: axis pos.	Direction cosines[g] ℓ	m	n
S1C (40,0.5)	2	2519	1.446		2:5-0-0-0-2	-1.446		2:5-0-0-0-2	-0.999	-0.045	0.0
				1.511	1:0-0-5-3-0		1.213	1:5-9-0-0-0	0.0	1.000	0.0
S1D (20,0.5)	3	5178	1.420		1:5-7-0-0-0	1.420		1:5-7-0-0-0	0.0	1.000	0.0
				1.181	1:5-9-0-0-0		1.181	1:5-9-0-0-0	0.0	1.000	0.0
S1E (10,0.5)	4	10979	1.492		1:5-7-0-0-0	1.492		1:5-7-0-0-0	0.0	1.000	0.0
				1.042	1:5-10-0-0-0		1.042	1:5-10-0-0-0	0.0	1.000	0.0
S1F (40,0.32)	2	660	1.182		1:5-7-0-0-0	1.182		1:5-7-0-0-0	0.0	1.000	0.0
				1.222	1:5-8-0-0-0		1.222	1:5-8-0-0-0	0.0	1.000	0.0
S1G (20,0.32)	3	1357	1.374		1:5-7-0-0-0	1.374		1:5-7-0-0-0	0.0	1.000	0.0
				1.138	1:5-9-0-0-0		1.138	1:5-9-0-0-0	0.0	1.000	0.0
S1H (10,0.32)	4	2878	1.366		1:5-7-0-0-0	1.366		1:5-7-0-0-0	0.0	1.000	0.0
				1.032	1:5-9-0-0-0		1.032	1:5-9-0-0-0	0.0	1.000	0.0
S1I (40,0.16)	2	83	1.208		2:4-24-0-0-0	1.200		1:4-7-0-0-0	0.0	1.000	0.0
				1.233	1:4-8-0-0-0		1.233	1:4-8-0-0-0	0.0	1.000	0.0
S1J (20,0.16)	3	170	1.252		1:4-7-0-0-0	1.252		1:4-7-0-0-0	0.0	1.000	0.0
				1.183	1:4-8-0-0-0		1.183	1:4-8-0-0-0	0.0	1.000	0.0
S1K (10,0.16)	4	360	1.318		1:4-7-0-0-0	1.318		1:4-7-0-0-0	0.0	1.000	0.0
				1.058	1:4-8-0-0-0		1.058	1:4-8-0-0-0	0.0	1.000	0.0

Table 7 (continued)

Model $\left(\frac{D}{T}, \frac{d}{D}\right)^{a,b}$	Number of elements through thickness	Load[c] (in.-lb)	$\bar{\sigma}_o^d$ (ksi)	$\bar{\sigma}_i^d$ (ksi)	Location[e] Quad: axis pos.	σ_{po}[f] (ksi)	σ_{pi}[f] (ksi)	Location[e] Quad: axis pos.	Direction cosines[g] ℓ	m	n
S1L (40,0.08)	2	10.32	1.211		2:4-24-0-0-0	1.181		1:4-9-0-0-0	0.0	1.000	0.0
				1.218	1:4-8-0-0-0		1.167	1:4-8-0-0-0	0.0	1.000	0.0
S1M (20,0.08)	3	21.20	1.206		1:4-24-0-0-0	1.178		1:4-9-0-0-0	0.0	1.000	0.0
				1.156	1:4-8-0-0-0		1.120	1:4-8-0-0-0	0.0	1.000	0.0
S1N (10,0.08)	4	45	1.203		1:4-7-0-0-0	1.203		1:4-7-0-0-0	0.0	1.000	0.0
				1.043	1:4-8-0-0-0		1.036	1:4-8-0-0-0	0.0	1.000	0.0
P30A (100,0.32)	1	260	1.178		2:5-18-0-0-0	1.126		1:5-17-0-0-0	0.0	1.000	0.0
				1.192	1:5-8-0-0-0		1.192	1:5-8-0-0-0	0.0	1.000	0.0
P30B (40,0.32)	2	660	1.208		1:5-6-0-0-0	1.208		1:5-6-0-0-0	-0.261	0.965	-0.021
				1.236	1:5-8-0-0-0		1.236	1:5-8-0-0-0	0.0	1.000	0.0
P30C (20,0.32)	3	1357	1.319		1:5-6-0-0-0	1.319		1:5-6-0-0-0	-0.261	0.965	-0.021
				1.146	1:5-8-0-0-0		1.146	1:5-8-0-0-0	0.0	1.000	0.0
P30D (10,0.32)	4	2878	1.352		1:5-6-0-0-0	1.352		1:5-6-0-0-0	-0.261	0.965	-0.021
				1.020	1:5-9-0-0-0		1.020	1:5-9-0-0-0	0.0	1.000	0.0
P30E (10,0.08)	4	45	1.202		1:4-24-0-0-0	1.188		1:4-7-0-0-0	0.0	1.000	0.0
				1.033	1:4-8-0-0-0		1.025	1:4-8-0-0-0	0.0	1.000	0.0

[a] D and d are inside diameters of cylinder and nozzle, respectively.

[b] Young's modulus E = 206.8 GPa (30 × 10^6 psi); Poisson's ratio ν = 0.3 for all models.

[c] Moment loading used such that the axial bending stress on the outside surface of the nozzle = $\frac{Mc}{I}$ = 1 ksi.

[d] $\bar{\sigma}$ = max ($|\sigma_{max} - \sigma_{min}|$, $|\sigma_{max} - 0|$, $|\sigma_{min} - 0|$); o = outside surface, i = inside surface.

[e] Location is given by Quadrant Number: A1-A2-A3-A4-A5, where A1 through A5 represent the number of divisions along each of the respective axes (see Figs. 3, 4, and 25).

[f] σ_p = numerically largest principal stress (positive value denotes tensile stress, negative value denotes compressive stress); o = outside surface; i = inside surface.

[g] Direction cosines for σ_p relative to X-Y-Z global coordinate system (see Fig. 1).

Table 8. Summary of maximum stress intensities and numerically largest principal stresses for out-of-plane moment loading, M_{XN}, applied to the nozzle (1 in.-lb = 0.113 N-m; 1 ksi = 6.895 MPa)

Model $\left(\frac{D}{T},\frac{d}{D}\right)^{a,b}$	Number of elements through thickness	Load[c] (in.-lb)	$\bar{\sigma}_o^d$ (ksi)	$\bar{\sigma}_i^d$ (ksi)	Location[e] Quad: axis pos.	σ_{po}^f (ksi)	σ_{pi}^f (ksi)	Location[e] Quad: axis pos.	Direction cosines[g] ℓ	m	n
UA (100,0.5)	1	992	16.599		1:0-0-5-0-0	-16.599		1:0-0-3-0-0	0.017	0.868	-0.496
				15.361	1:0-1-5-0-0		10.565	1:0-0-5-0-0	-0.010	0.869	-0.495
UB (80,0.5)	1	1243	15.047		1:0-0-5-0-0	-15.047		1:0-0-5-0-0	0.018	0.868	-0.496
				13.876	1:0-1-5-0-0		9.444	1:0-1-5-0-0	-0.002	1.000	-0.016
UC (40,0.5)	2	2519	10.846		1:0-1-5-0-0	-10.846		1:0-1-5-0-0	0.014	0.999	-0.036
				7.911	1:0-1-4-0-0		7.728	1:0-1-5-0-0	-0.004	1.000	-0.031
UD (20,0.5)	2	5178	5.772		1:0-0-5-0-0	-5.772		1:0-0-5-0-0	0.036	0.875	-0.482
				3.319	1:0-1-3-0-0		3.181	2:0-1-4-0-0	0.014	0.999	-0.037
UE (10,0.5)	4	10979	3.500		1:0-0-5-0-0	-3.500		1:0-0-5-0-0	0.044	0.886	-0.463
				1.575	2:0-0-0-1-1		1.575	2:0-0-0-1-1	0.238	-0.444	0.864
UF (10,0.08)	4	45	1.266		1:0-3-4-0-0	-1.266		1:0-3-4-0-0	0.0	-1.000	0.0
				1.016	1:0-5-4-0-0		-1.016	1:0-5-4-0-0	0.0	1.000	0.0
S1A (100,0.5)	1	992	11.070		1:0-0-5-2-0	-11.070		1:0-0-5-2-0	0.019	0.642	-0.766
				5.208	1:0-0-5-1-0		5.208	1:0-0-5-1-0	-0.017	0.561	-0.828
S1B (80,0.5)	1	1243	9.839		1:0-0-5-2-0	-9.839		1:0-0-5-2-0	0.020	0.653	-0.757
				5.074	1:0-0-5-1-0		5.074	1:0-0-5-1-0	-0.017	0.565	-0.825
S1C (40,0.5)	2	2519	5.638		1:0-0-5-1-0	-5.638		1:0-0-5-1-0	0.025	0.718	-0.696
				3.498	1:0-0-5-2-0		3.498	1:0-0-5-2-0	-0.023	0.624	-0.782

Table 8 (continued)

Model $\left(\frac{D}{T}, \frac{d}{D}\right)^{a,b}$	Number of elements through thickness	Load[c] (in.-lb)	$\bar{\sigma}_o d$ (ksi)	$\bar{\sigma}_i d$ (ksi)	Location[e] Quad: axis pos.	$\sigma_{po}{}^f$ (ksi)	$\sigma_{pi}{}^f$ (ksi)	Location[e] Quad: axis pos.	Direction cosines[g] ℓ	m	n
S1D (20,0.5)	3	5178	2.814	1.689	1:0-0-5-1-0 2:0-0-4-3-0	-2.814	1.689	1:0-0-5-1-0 2:0-0-4-3-0	0.039 0.015	0.778 -0.704	-0.627 0.710
S1E (10,0.5)	4	10979	1.564	1.031	1:0-7-5-0-0 1:0-10-5-0-0	-1.564	-1.031	1:0-7-5-0-0 1:0-10-5-0-0	0.0 0.0	-1.000 1.000	0.0 0.0
S1F (40,0.32)	2	660	2.564	1.750	1:0-0-5-1-0 1:0-0-5-2-0	-2.564	1.750	1:0-0-5-1-1 1:0-0-5-2-0	0.013 -0.012	0.553 0.466	-0.833 -0.885
S1G (20,0.32)	3	1357	1.434	1.133	1:0-7-5-0-0 1:0-9-5-0-0	-1.434	-1.133	1:0-7-5-0-0 1:0-9-5-0-0	0.0 0.0	-1.000 1.000	0.0 0.0
S1H (10,0.32)	4	2878	1.391	1.031	1:0-7-5-0-0 1:0-9-5-0-0	-1.391	-1.031	1:0-7-5-0-0 1:0-9-5-0-0	0.0 0.0	-1.000 1.000	0.0 0.0
S1I (40,0.16)	2	83	1.223	1.244	1:0-7-4-0-0 1:0-8-4-0-0	-1.223	-1.234	1:0-7-4-0-0 1:0-8-4-0-0	0.0 0.0	-1.000 -1.000	0.0 0.0
S1J (20,0.16)	3	170	1.264	1.182	1:0-7-4-0-0 1:0-8-4-0-0	-1.264	-1.182	1:0-7-4-0-0 1:0-8-4-0-0	0.0 0.0	-1.000 -1.000	0.0 0.0
S1K (10,0.16)	4	360	1.326	1.057	1:0-7-4-0-0 1:0-8-4-0-0	-1.326	-1.057	1:0-7-4-0-0 1:0-8-4-0-0	0.0 0.0	-1.000 1.000	0.0 0.0
S1L (40,0.08)	2	10.32	1.211	1.220	1:0-24-4-0-0 1:0-8-4-0-0	-1.182	-1.168	1:0-9-4-0-0 1:0-8-4-0-0	0.0 0.0	-1.000 -1.000	0.0 0.0

Table 8 (continued)

Model $\left(\frac{D}{T}, \frac{d}{D}\right)^{a,b}$	Number of elements through thickness	Load[c] (in.-lb)	$\bar{\sigma}_o^d$ (ksi)	$\bar{\sigma}_i^d$ (ksi)	Location[e] Quad: axis pos.	σ_{po}[f] (ksi)	σ_{pi}[f] (ksi)	Location[e] Quad: axis pos.	Direction cosines[g] ℓ	m	n
S1M (20,0.08)	3	21.20	1.206		1:0-24-4-0-0	-1.182		1:0-7-4-0-0	0.0	-1.000	0.0
				1.157	1:0-8-4-0-0		-1.120	1:0-8-4-0-0	0.0	-1.000	0.0
S1N (10,0.08)	4	45	1.208		1:0-7-4-0-0	-1.208		1:0-7-4-0-0	0.0	-1.000	0.0
				1.045	1:0-8-4-0-0		-1.037	1:0-8-4-0-0	0.0	-1.000	0.0
P30A (100,0.32)	1	260	3.725		1:0-0-5-3-0	-3.725		1:0-0-5-3-0	0.013	0.580	-0.815
				1.470	1:0-8-5-0-0		-1.334	1:0-8-5-0-0	0.0	-1.000	0.0
P30B (40,0.32)	2	660	1.843		1:0-0-5-1-0	-1.843		1:0-0-5-1-0	0.017	0.585	-0.811
				1.265	1:0-8-5-0-0		-1.227	1:0-8-5-0-0	0.0	1.000	0.0
P30C (20,0.32)	3	1357	1.387		1:0-7-5-0-0	-1.387		1:0-7-5-0-0	0.0	-1.000	0.0
				1.138	1:0-9-5-0-0		-1.117	1:0-8-5-0-0	0.0	1.000	0.0
P30D (10,0.32)	4	2878	1.332		1:0-7-5-0-0	-1.332		1:0-7-5-0-0	0.0	-1.000	0.0
				1.018	1:0-9-5-0-0		-1.018	1:0-9-5-0-0	0.0	1.000	0.0
P30E (10,0.08)	4	45	1.202		1:0-24-4-0-0	-1.190		1:0-7-4-0-0	0.0	-1.000	0.0
				1.034	1:0-8-4-0-0		-1.025	1:0-8-4-0-0	0.0	1.000	0.0

[a] D and d are inside diameters of cylinder and nozzle, respectively.

[b] Young's modulus E = 206.8 GPa (30 × 10^6 psi); Poisson's ratio ν = 0.3 for all models.

[c] Moment loading used such that the axial bending stress on the outside surface of the nozzle = $\frac{Mc}{I}$ = 1 ksi.

[d] $\bar{\sigma}$ = max ($|\sigma_{max} - \sigma_{min}|$, $|\sigma_{max} - 0|$, $|\sigma_{min} - 0|$); o = outside surface, i = inside surface.

[e] Location is given by Quadrant Number: A1-A2-A3-A4-A5, where A1 through A5 represent the number of divisions along each of the respective axes (see Figs. 3, 4, and 25).

[f] σ_p = numerically largest principal stress (positive value denotes tensile stress, negative value denotes compressive stress); o = outside surface; i = inside surface.

[g] Direction cosines for σ_p relative to X-Y-Z global coordinate system (see Fig. 1).

Table 9. Summary of maximum stress intensities and numerically largest principal stresses for torsional moment loading, M_{YN}, applied to the nozzle
(1 in.-lb = 0.113 N-m; 1 ksi = 6.895 MPa)

Model $\left(\frac{D}{T},\frac{d}{D}\right)^{a,b}$	Number of elements through thickness	Load[c] (in.-lb)	$\bar{\sigma}_o^d$ (ksi)	$\bar{\sigma}_i^d$ (ksi)	Location[e] Quad: axis pos.	σ_{po}^f (ksi)	σ_{pi}^f (ksi)	Location[e] Quad: axis pos.	Direction cosines[g] ℓ	m	n
UA (100,0.5)	1	992	1.312	1.390	2:0-1-0-0-0 1:0-1-1-0-0	-1.312	1.034	2:0-1-0-0-0 1:0-2-1-0-0	0.427 0.535	-0.784 0.750	0.450 -0.390
UB (80,0.5)	1	1243	1.261	1.316	2:0-1-0-0-0 1:0-1-1-0-0	-1.261	1.010	2:0-1-0-0-0 1:0-2-1-0-0	0.410 0.539	-0.799 0.745	0.440 -0.393
UC (40,0.5)	2	2519	1.252	1.076	1:5-1-0-0-0 2:5-16-0-0-0	-0.977	-0.913	2:0-1-0-0-0 2:0-2-1-0-0	0.377 0.545	-0.812 -0.738	0.446 0.397
UD (20,0.5)	2	5178	1.392	1.005	1:5-1-0-0-0 2:5-15-0-0-0	-0.726	0.828	2:2-6-0-0-0 1:0-0-1-0-0	-0.280 -0.702	0.786 -0.389	-0.551 0.597
UE (10,0.5)	4	10979	1.431	0.888	1:5-1-0-0-0 1:0-4-5-0-0	0.765	0.656	2:3-1-0-0-0 1:0-0-1-0-0	-0.395 -0.755	-0.620 -0.333	-0.678 0.565
UF (10,0.08)	4	45	1.020	0.853	1:0-5-4-0-0 1:0-5-4-0-0	0.523	0.433	1:1-3-0-0-0 2:0-5-1-0-0	-0.411 0.588	-0.701 0.707	-0.582 0.392
S1A (100,0.5)	1	992	1.156	1.102	2:5-9-0-0-0 2:5-18-0-0-0	-0.820	-0.707	2:1-7-0-0-0 2:1-8-0-0-0	-0.339 -0.340	0.818 0.816	-0.466 -0.468
S1B (80,0.5)	1	1243	1.160	1.092	2:5-7-0-0-0 2:5-16-0-0-0	-0.806	-0.675	2:1-7-0-0-0 2:1-8-0-0-0	-0.341 -0.347	0.814 0.807	-0.470 -0.477

Table 9 (continued)

Model $\left(\frac{D}{T}, \frac{d}{D}\right)^{a,b}$	Number of elements through thickness	Load[c] (in.-lb)	$\bar{\sigma}_o$[d] (ksi)	$\bar{\sigma}_i$[d] (ksi)	Location[e] Quad: axis pos.	σ_{po}[f] (ksi)	σ_{pi}[f] (ksi)	Location[e] Quad: axis pos.	Direction cosines[g] ℓ	m	n
S1C (40,0.5)	2	2519	1.172		2:5-7-0-0-0	-0.740		2:1-7-0-0-0	-0.360	0.790	-0.496
				1.042	2:5-16-0-0-0		-0.561	2:1-9-0-0-0	-0.366	0.783	-0.503
S1D (20,0.5)	3	5178	1.157		2:5-7-0-0-0	-0.661		2:1-7-0-0-0	-0.384	0.757	-0.529
				0.965	2:5-15-0-0-0		0.492	2:3-15-0-0-0	-0.223	-0.693	-0.685
S1E (10,0.5)	4	10979	1.128		2:5-7-0-0-0	-0.597		2:2-7-0-0-0	-0.312	0.727	-0.612
				0.862	2:5-12-0-0-0		0.435	2:3-13-0-0-0	-0.221	-0.699	-0.680
S1F (40,0.32)	2	660	1.064		2:5-7-0-0-0	-0.588		2:1-7-0-0-0	-0.399	0.735	-0.549
				0.978	2:5-13-0-0-0		0.503	2:1-14-0-0-0	-0.426	-0.689	-0.587
S1G (20,0.32)	3	1357	1.072		2:5-7-0-0-0	-0.566		2:1-7-0-0-0	-0.406	0.723	-0.559
				0.929	2:5-11-0-0-0		0.473	2:1-13-0-0-0	-0.422	-0.697	-0.581
S1H (10,0.32)	4	2878	1.054		1:5-7-0-0-0	-0.543		2:1-7-0-0-0	-0.413	0.712	-0.568
				0.847	2:5-9-0-0-0		0.426	2:2-10-0-0-0	-0.323	-0.702	-0.635
S1I (40,0.16)	2	83	1.023		2:4-7-0-0-0	0.523		1:1-7-0-0-0	0.391	0.710	-0.586
				0.970	2:4-11-0-0-0		0.488	2:1-13-0-0-0	-0.395	-0.704	-0.590
S1J (20,0.16)	3	170	1.021		2:4-7-0-0-0	0.517		1:0-7-0-0-0	0.499	0.708	-0.499
				0.92?	2:4-8-0-0-0		0.462	2:1-10-0-0-0	-0.394	-0.705	-0.589
S1K (10,0.16)	4	360	1.032		1:0-7-4-0-0	0.517		1:0-7-1-0-0	0.588	0.707	-0.393
				0.843	2:4-8-0-0-0		0.421	2:4-8-0-0-0	0.0	-0.851	-0.525

Table 9 (continued)

Model $\left(\frac{D}{T}, \frac{d}{D}\right)^{a,b}$	Number of elements through thickness	Load[c] (in.-lb)	$\bar{\sigma}_o^d$ (ksi)	$\bar{\sigma}_i^d$ (ksi)	Location[e] Quad: axis pos.	σ_{po}[f] (ksi)	σ_{pi}[f] (ksi)	Location[e] Quad: axis pos.	Direction cosines[g] ℓ	m	n
S1L (40,0.08)	2	10.32	1.011		2:4-7-0-0-0	0.507		1:0-7-0-0-0	0.500	0.707	-0.500
				0.962	2:4-7-0-0-0		0.481	2:2-7-0-0-0	-0.271	-0.707	-0.654
S1M (20,0.08)	3	21.20	1.012		1:0-7-4-0-0	0.506		1:0-7-2-0-0	0.653	0.707	-0.271
				0.918	2:4-7-0-0-0		0.459	1:3-7-0-0-0	0.138	0.707	-0.694
S1N (10,0.08)	4	45	1.015		1:0-7-4-0-0	0.507		2:0-7-3-0-0	0.694	0.707	0.138
				0.845	2:4-7-0-0-0		0.423	1:0-7-0-0-0	0.500	0.707	-0.500
P30A (100,0.32)	1	260	1.080		2:5-7-0-0-0	-0.628		2:1-7-0-0-0	-0.381	0.762	-0.524
				1.021	2:5-16-0-0-0		0.558	1:0-8-0-0-0	0.456	0.764	-0.456
P30B (40,0.32)	2	660	1.080		2:5-7-0-0-0	-0.610		2:1-7-0-0-0	-0.395	0.741	-0.543
				0.983	2:5-13-0-0-0		0.509	2:1-14-0-0-0	-0.429	-0.684	-0.590
P30C (20,0.32)	3	1357	1.069		2:5-7-0-0-0	0.579		1:1-7-0-0-0	0.405	0.725	-0.557
				0.935	2:5-10-0-0-0		0.479	2:1-13-0-0-0	-0.424	-0.693	-0.583
P30D (10,0.32)	4	2878	1.049		2:5-7-0-0-0	0.544		1:1-7-0-0-0	0.412	0.713	-0.567
				0.851	2:5-9-0-0-0		0.430	2:2-10-0-0-0	-0.324	-0.700	-0.636
P30E (10,0.08)	4	45	1.012		1:0-7-4-0-0	0.506		1:0-7-3-0-0	0.694	0.707	0.138
				0.846	2:4-7-0-0-0		0.423	1:1-7-0-0-0	0.393	0.707	-0.588

[a] D and d are inside diameters of cylinder and nozzle, respectively.

[b] Young's modulus E = 206.8 GPa (30 × 10^6 psi); Poisson's ratio ν = 0.3 for all models.

[c] Moment loading used such that the shear stress on the outside surface of the cylinder = $\frac{Tc}{J}$ = 0.5 ksi.

[d] $\bar{\sigma}$ = max ($|\sigma_{max} - \sigma_{min}|$, $|\sigma_{max} - 0|$, $|\sigma_{min} - 0|$); o = outside surface, i = inside surface.

[e] Location is given by Quadrant Number: A1-A2-A3-A4-A5, where A1 through A5 represent the number of divisions along each of the respective axes (see Figs. 3, 4, and 25).

[f] σ_p = numerically largest principal stress (positive value denotes tensile stress, negative value denotes compressive stress); o = outside surface; i = inside surface.

[g] Direction cosines for σ_p relative to X-Y-Z global coordinate system (see Fig. 1).

Table 10. Summary of maximum stress intensities and numerically largest principal stresses for in-plane moment loading, M_{ZC}, applied to the cylinder (1 in.-lb = 0.113 N-m; 1 ksi = 6.895 MPa)

Model $\left(\frac{D}{T}, \frac{d}{D}\right)^{a,b}$	Number of elements through thickness	Load[c] (in.-lb)	$\bar{\sigma}_o^d$ (ksi)	$\bar{\sigma}_t^d$ (ksi)	Location[e] Quad: axis pos.	σ_{pc}^e (ksi)	σ_{pt}^e (ksi)	Location[e] Quad: axis pos.	Direction cosines[f] ℓ	m	n
UA (100,0.5)	1	7934	4.167		1:0-0-5-0-0	-4.167		1:0-0-5-0-0	-1.000	0.0	0.0
				4.616	1:0-0-5-0-0		-3.825	1:0-0-5-0-0	-1.000	0.0	0.0
UB (80,0.5)	1	9943	3.976		1:0-0-5-0-0	-3.976		1:0-0-5-0-0	-1.000	0.0	0.0
				4.541	1:0-0-5-0-0		-3.772	1:0-0-5-0-0	-1.000	0.0	0.0
UC (40,0.5)	2	20150	2.964		1:0-0-5-0-0	-2.964		1:0-0-5-0-0	-1.000	0.0	0.0
				4.090	1:0-0-5-0-0		-3.780	1:0-0-5-0-0	-1.000	0.0	0.0
UD (20,0.5)	2	41421	1.949		1:0-0-2-1-0	-1.949		1:0-0-2-1-0	-0.985	0.116	-0.129
				3.595	1:0-0-5-0-0		-3.595	1:0-0-5-0-0	-1.000	0.0	0.0
UE (10,0.5)	4	87834	2.009		1:0-0-0-1-0	-1.883		1:0-0-0-0-1	-0.993	0.060	0.106
				3.173	1:0-1-5-0-0		-3.173	1:0-1-5-0-0	1.000	0.0	0.0
UF (10,0.08)	4	87834	1.582		1:0-0-0-1-1	-1.353		1:0-0-0-1-2	-0.997	0.054	0.051
				3.112	1:0-1-4-0-0		-3.112	1:0-1-4-0-0	1.000	0.0	0.0
SIA (100,0.5)	1	7934	2.071		1:0-0-1-1-0	-1.786		1:0-0-0-1-1	-0.999	-0.005	0.044
				2.185	1:0-0-5-0-0		-2.185	1:0-0-5-0-0	-1.000	0.0	0.0
SIB (80,0.5)	1	9943	1.989		1:0-0-1-1-0	-1.837		1:0-0-0-1-1	-0.999	-0.002	0.040
				2.234	1:0-0-5-0-0		-2.234	1:0-0-5-0-0	-1.000	0.0	0.0
SIC (40,0.5)	2	20150	1.860		1:1-0-0-0-1	-1.860		1:1-0-0-0-1	-0.981	0.056	0.188
				2.251	1:0-0-5-0-0		-2.251	1:0-0-5-0-0	-1.000	0.0	0.0

Table 10 (continued)

Model $\left(\frac{a}{2c}, \frac{a}{t}\right)^{a,b}$	Number of elements through thickness	Load[c] (in.-lb)	$\bar{\sigma}_o$[d] (ksi)	$\bar{\sigma}_i$[d] (ksi)	Location[e] Quad: axis pos.	σ_{fo}[f] (ksi)	σ_{fi}[f] (ksi)	Location[e] Quad: axis pos.	Direction cosines[g] ℓ	m	n
S1D (20,0.5)	3	41421	1.977		1:3-0-0-0-2	-1.977		1:3-0-0-0-2	-0.984	0.071	0.162
				2.069	1:0-0-5-0-0		-2.069	1:0-0-5-0-0	-1.000	0.0	0.0
S1E (10,0.5)	4	87834	2.067		1:5-0-0-0-2	-2.067		1:5-0-0-0-2	0.958	-0.286	0.0
				1.821	1:0-1-5-0-0		-1.821	1:0-1-5-0-0	1.000	0.0	0.0
S1F (40,0.32)	2	20150	1.729		1:1-0-0-0-1	-1.729		1:1-0-0-0-1	-0.982	0.084	0.167
				2.355	1:0-0-5-0-0		-2.355	1:0-0-5-0-0	-1.000	0.0	0.0
S1G (20,0.32)	3	41421	1.765		1:2-0-0-0-1	-1.765		1:2-0-0-0-1	-0.966	0.182	0.184
				2.226	1:0-0-5-0-0		-2.226	1:0-0-5-0-0	-1.000	0.0	0.0
S1H (10,0.32)	4	87834	1.981		1:5-0-0-0-2	-1.981		1:5-0-0-0-2	0.986	-0.166	0.0
				2.080	1:0-1-5-0-0		-2.080	1:0-1-5-0-0	1.000	0.0	0.0
S1I (40,0.16)	2	20150	1.633		1:1-0-0-0-2	-1.633		1:1-0-0-0-2	-0.993	-0.005	0.121
				2.486	1:0-0-4-0-0		-2.486	1:0-0-4-0-0	-1.000	0.0	0.0
S1J (20,0.16)	3	41421	1.745		1:4-0-0-0-2	-1.745		1:4-0-0-0-2	0.994	-0.107	0.0
				2.375	1:0-1-4-0-0		-2.375	1:0-1-4-0-0	1.000	0.0	0.0
S1K (10,0.16)	4	87834	1.840		1:4-0-0-0-2	-1.840		1:4-0-0-0-2	0.984	-0.176	0.0
				2.334	1:0-1-4-0-0		-2.334	1:0-1-4-0-0	1.000	0.0	0.0
S1L (40,0.08)	2	20150	1.477		1:2-0-0-0-2	-1.477		1:2-0-0-0-2	-0.996	0.0	0.090
				2.523	1:0-0-4-0-0		-2.523	1:0-0-4-0-0	-1.000	0.0	0.0

Table 10 (continued)

Model $\left(\frac{D}{T}, \frac{d}{D}\right)^{a,b}$	Number of elements through thickness	Load[c] (in.-lb)	$\bar{\sigma}_o$[d] (ksi)	$\bar{\sigma}_i$[d] (ksi)	Location[e] Quad: axis pos.	σ_{po}[f] (ksi)	σ_{pi}[f] (ksi)	Location[e] Quad: axis pos.	Direction cosines[g] ℓ	m	n
S1M (20,0.08)	3	41421	1.559		1:4-0-0-0-1	-1.559		1:4-0-0-0-1	0.960	-0.280	0.0
				2.609	1:0-1-4-0-0		-2.609	1:0-1-4-0-0	1.000	0.0	0.0
S1N (10,0.08)	4	87834	1.696		1:4-0-0-0-2	-1.696		1:4-0-0-0-2	0.993	-0.120	0.0
				2.627	1:0-1-4-0-0		-2.627	1:0-1-4-0-0	1.000	0.0	0.0
P30A (100,0.32)	1	7934	1.893		1:0-0-0-0-1	-1.852		1:0-0-0-1-0	-0.999	0.032	-0.038
				2.241	1:0-0-5-0-0		-2.241	1:0-0-5-0-0	-1.000	0.0	0.0
P30B (40,0.32)	2	20150	2.037		1:1-0-0-0-1	-2.037		1:1-0-0-0-1	-0.988	0.004	0.155
				2.390	1:0-0-5-0-0		-2.390	1:0-0-5-0-0	-1.000	0.0	0.0
P30C (20,0.32)	3	41421	2.009		1:1-0-0-0-1	-2.009		1:1-0-0-0-1	-0.994	0.030	0.103
				2.269	1:0-0-5-0-0		-2.269	1:0-0-5-0-0	-1.000	0.0	0.0
P30D (10,0.32)	4	87834	1.948		1:2-0-0-0-1	-1.948		1:2-0-0-0-1	-0.990	0.083	0.110
				2.054	1:0-1-5-0-0		-2.054	1:0-1-5-0-0	1.000	0.0	0.0
P30E (10,0.08)	4	87834	1.531		1:4-0-0-0-1	-1.531		1:4-0-0-0-1	0.969	-0.247	0.0
				2.676	1:0-1-4-0-0		-2.676	1:0-1-4-0-0	1.000	0.0	0.0

[a] D and d are inside diameters of cylinder and nozzle, respectively.

[b] Young's modulus E = 206.8 GPa (30×10^6 psi); Poisson's ratio ν = 0.3 for all models.

[c] Moment loading used such that the axial bending stress on the outside surface of the cylinder = $\frac{Mc}{I}$ = 1 ksi.

[d] $\bar{\sigma}$ = max ($|\sigma_{max} - \sigma_{min}|$, $|\sigma_{max} - 0|$, $|\sigma_{min} - 0|$); o = outside surface, i = inside surface.

[e] Location is given by Quadrant Number: A1-A2-A3-A4-A5, where A1 through A5 represent the number of divisions along each of the respective axes (see Figs. 3, 4, and 25).

[f] σ_p = numerically largest principal stress (positive value denotes tensile stress, negative value denotes compressive stress); o = outside surface; i = inside surface.

[g] Direction cosines for σ_p relative to X-Y-Z global coordinate system (see Fig. 1).

Table 11. Summary of maximum stress intensities and numerically largest principal stresses for out-of-plane moment loading, M_{y_C}, applied to the cylinder (1 in.-lb = 0.113 N-m; 1 ksi = 6.895 MPa)

Model $\left(\frac{D}{t}, \frac{d}{D}\right)^{a,b}$	Number of elements through thickness	Load[c] (in.-lb)	$\bar{\sigma}_o d$ (ksi)	$\bar{\sigma}_i d$ (ksi)	Location[e] Quad: axis pos.	σ_{po} (ksi)	σ_{pi} (ksi)	Location[e] Quad: axis pos.	Direction cosines[d] ℓ	m	n
UA (100,0.5)	1	7934	1.044		1:0-0-0-11-17	1.031		1:0-0-0-11-16	-1.000	0.0	0.0
				1.098	1:0-0-5-0-0		1.020	1:0-0-5-0-0	-1.000	0.0	0.0
UB (80,0.5)	1	9943	1.044		1:0-0-0-11-17	1.034		1:0-0-0-11-16	-1.000	0.0	0.0
				1.093	1:0-0-5-0-0		1.014	1:0-0-5-0-0	-1.000	0.0	0.0
UC (40,0.5)	2	20150	1.044		1:0-0-0-11-16	1.044		1:0-0-0-11-16	-1.000	0.0	0.0
				1.049	1:0-0-5-0-0		1.021	1:0-0-5-0-0	-1.000	0.0	0.0
UD (20,0.5)	2	41421	1.041		1:0-0-0-11-16	1.041		1:0-0-0-11-16	-1.000	0.0	0.0
				0.991	1:0-0-0-11-17		0.977	1:0-0-5-0-0	-1.000	0.0	0.0
UE (10,0.5)	4	87834	1.032		1:0-0-0-11-16	1.028		1:0-0-0-11-14	-1.000	0.0	0.0
				0.919	1:0-0-0-11-17		0.919	1:0-0-0-11-17	-1.000	0.0	0.0
UF (10,0.08)	4	87834	1.043		1:0-0-0-13-20	1.037		1:0-0-0-13-20	-1.000	0.0	0.0
				0.934	1:0-0-0-13-23		0.934	1:0-0-0-13-23	-1.000	0.0	0.0
S1A (100,0.5)	1	7934	1.035		1:0-0-0-11-17	1.023		1:0-0-0-11-14	1.000	0.0	0.0
				1.024	1:0-0-0-11-18		1.010	1:0-0-0-11-18	-1.000	0.0	0.0
S1B (80,0.5)	1	9943	1.037		1:0-0-0-11-17	1.026		1:0-0-0-11-16	-1.000	0.0	0.0
				1.014	1:0-0-0-11-18		1.007	1:0-0-0-11-18	-1.000	0.0	0.0
S1C (40,0.5)	2	20150	1.035		1:0-0-0-11-16	1.035		1:0-0-0-11-16	1.000	0.0	0.0
				1.013	1:0-0-0-11-17		0.989	1:0-0-0-10-18	-1.000	0.0	0.0

Table II (continued)

Model $\left(\frac{D}{T}, \frac{a}{D}\right)^{a,b}$	Number of elements through thickness	Load[c] (in.-lb)	$\bar{\sigma}_o^d$ (ksi)	$\bar{\sigma}_i^d$ (ksi)	Location[e] Quad: axis pos.	σ_{po}^f (ksi)	σ_{pi}^f (ksi)	Location[e] Quad: axis pos.	Direction cosines[g] ℓ	m	n
S1D (20,0.5)	3	41421	1.037		1:0-0-0-10-16	1.024		1:0-0-0-10-16	1.000	0.0	0.0
				0.993	1:0-0-0-10-17		0.987	1:0-0-0-10-17	1.000	0.0	0.0
S1E (10,0.5)	4	87834	1.034		1:0-0-0-10-18	1.034		1:0-0-0-10-18	1.000	0.0	0.0
				0.926	1:0-0-0-10-17		0.926	1:0-0-0-10-17	1.000	0.0	0.0
S1F (40,0.32)	2	20150	1.042		1:0-0-0-11-17	1.040		1:0-0-0-11-16	-1.000	0.0	0.0
				1.009	1:0-0-0-11-17		0.990	1:0-0-0-11-18	-1.000	0.0	0.0
S1G (20,0.32)	3	41421	1.040		1:0-0-0-11-16	1.040		1:0-0-0-11-16	-1.000	0.0	0.0
				0.988	1:0-0-0-11-17		0.972	1:0-0-0-11-17	-1.000	0.0	0.0
S1H (10,0.32)	4	87834	1.029		1:0-0-0-11-16	1.020		1:0-0-0-11-14	1.000	0.0	0.0
				0.919	1:0-0-0-11-17		0.919	1:0-0-0-11-17	-1.000	0.0	0.0
S1I (40,0.16)	2	20150	1.048		1:0-0-0-12-22	1.048		1:0-0-0-12-22	-1.000	0.0	0.0
				1.039	1:0-0-0-12-23		1.021	1:0-0-0-12-23	1.000	0.0	0.0
S1J (20,0.16)	3	41421	1.040		1:0-0-0-12-22	1.033		1:0-0-0-12-22	-1.000	0.0	0.0
				0.991	1:0-0-0-12-23		0.982	1:0-0-0-12-23	-1.000	0.0	0.0
S1K (10,0.16)	4	87834	1.022		1:0-0-0-11-20	1.020		1:0-0-0-11-20	-1.000	0.0	0.0
				0.928	1:0-0-0-11-23		0.928	1:0-0-0-11-23	-1.000	0.0	0.0
S1L (40,0.08)	2	20150	1.061		1:0-0-0-13-1	1.053		1:0-0-0-13-1	-1.000	0.0	0.0
				1.034	1:0-0-4-13-0		1.034	1:0-0-4-13-0	-1.000	0.0	0.0

Table 11 (continued)

Model $\left(\frac{D}{R_i}, \frac{d}{D}\right)^{a,b}$	Number of elements through thickness	Load[c] (in.-lb)	$\bar{\sigma}_o d$ (ksi)	$\bar{\sigma}_i d$ (ksi)	Location[e] Quad: axis pos.	σ_{po}[f] (ksi)	σ_{pi}[f] (ksi)	Location[e] Quad: axis pos.	Direction cosines[g] ℓ	m	n
S1M (20,0.08)	3	41421	1.044		1:0-0-0-12-22	1.030		1:0-0-0-12-21	-1.000	0.0	0.0
				1.000	1:0-0-0-12-23		1.000	1:0-0-0-12-23	-1.000	0.0	0.0
S1N (10,0.08)	4	87834	1.033		1:0-0-0-12-22	1.030		1:0-0-0-12-20	-1.000	0.0	0.0
				0.929	1:0-0-0-12-23		0.929	1:0-0-0-12-23	-1.000	0.0	0.0
P30A (100,0.	1	7934	1.033		1:0-0-0-11-17	1.026		1:0-0-0-11-0	-1.000	0.0	0.0
				1.027	1:0-0-0-11-18		1.010	1:0-0-0-11-18	-1.000	0.0	0.0
P30B (40,0.32)	2	20150	1.036		1:0-0-0-11-17	1.036		1:0-0-0-11-16	-1.000	0.0	0.0
				1.010	1:0-0-0-11-17		0.988	1:0-0-0-11-18	-1.000	0.0	0.0
P30C (20,0.32)	3	41421	1.031		1:0-0-0-10-16	1.031		1:0-0-0-10-16	1.000	0.0	0.0
				0.982	1:0-0-0-10-17		0.965	1:0-0-0-11-17	-1.000	0.0	0.0
P30D (10,0.32)	4	87834	1.027		1:0-0-0-10-16	1.018		1:0-0-0-10-14	1.000	0.0	0.0
				0.917	1:0-0-0-10-17		0.917	1:0-0-0-10-17	1.000	0.0	0.0
P30E (10,0.08)	4	87834	1.031		1:0-0-0-12-22	1.028		1:0-0-0-12-20	-1.000	0.0	0.0
				0.974	1:0-0-0-12-23		0.924	1:0-0-0-12-23	-1.000	0.0	0.0

[a] D and d are inside diameters of cylinder and nozzle, respectively.

[b] Young's modulus E = 206.8 GPa (30×10^6 psi); Poisson's ratio ν = 0.3 for all models.

[c] Moment loading used such that the axial bending stress on the outside surface of the cylinder = $\frac{Mc}{I}$ = 1 ksi.

[d] $\bar{\sigma}$ = max ($|\sigma_{max} - \sigma_{min}|$, $|\sigma_{max} - 0|$, $|\sigma_{min} - 0|$); o = outside surface, i = inside surface.

[e] Location is given by Quadrant Number: A1-A2-A3-A4-A5, where A1 through A5 represent the number of divisions along each of the respective axes (see Figs. 3, 4, and 25).

[f] σ_p = numerically largest principal stress (positive value denotes tensile stress, negative value denotes compressive stress); o = outside surface; i = inside surface.

[g] Direction cosines for σ_p relative to X-Y-Z global coordinate system (see Fig. 1).

Table 12. Summary of maximum stress intensities and numerically largest principal stresses for torsional moment loading, M_{xC}, applied to the cylinder
(1 in.-lb = 0.113 N-m; 1 ksi = 6.895 MPa)

Model $\left(\frac{D}{T}, \frac{d}{D}\right)^{a,b}$	Number of elements through thickness	Load[c] (in.-lb)	$\bar{\sigma}_o d$ (ksi)	$\bar{\sigma}_i d$ (ksi)	Location[e] Quad: axis pos.	σ_{po}[f] (ksi)	σ_{pi}[f] (ksi)	Location[e] Quad: axis pos.	Direction cosines[g] ℓ	m	n
UA (100,0.5)	1	7934	4.242		1:0-0-1-0-0	4.242		2:0-0-1-0-0	0.750	-0.311	0.584
				4.352	1:0-0-1-0-0		3.542	2:0-0-1-0-0	0.803	-0.225	0.553
UB (80,0.5)	1	9943	3.920		1:0-0-1-0-0	3.920		2:0-0-1-0-0	0.739	-0.327	0.589
				4.177	1:0-0-1-0-0		3.469	2:0-0-1-0-0	0.802	-0.227	0.552
UC (40,0.5)	2	20150	2.900		1:0-0-5-4-0	2.594		2:0-0-1-0-0	0.672	-0.414	0.615
				3.533	1:0-0-1-0-0		3.513	2:0-0-1-0-0	0.801	-0.234	0.552
UD (20,0.5)	2	41421	2.832		1:0-0-5-1-0	1.528		1:0-0-3-4-0	-0.813	0.396	-0.426
				3.411	1:0-0-1-0-0		3.411	2:0-0-1-0-0	0.806	-0.232	0.545
UE (10,0.5)	4	87834	2.760		1:0-0-5-1-0	1.442		1:0-0-4-1-0	-0.776	0.403	-0.485
				2.789	1:0-0-1-0-0		2.789	2:0-0-1-0-0	0.821	-0.216	0.528
UF (10,0.08)	4	87834	1.568		1:0-0-4-2-0	0.784		1:0-0-4-2-0	-0.525	0.255	-0.812
				2.123	1:0-1-0-0-0		2.123	2:0-1-0-0-0	-0.724	0.038	-0.688
SIA (100,0.5)	1	7934	2.985		1:0-0-5-1-0	1.492		1:0-0-5-1-0	-0.525	0.555	-0.645
				2.846	1:0-0-5-2-0		2.002	2:0-0-1-0-0	0.853	-0.122	0.508
SIB (80,0.5)	1	9943	2.868		1:0-0-5-1-0	1.487		1:0-0-4-2-0	-0.776	0.410	-0.479
				2.666	1:0-0-5-2-0		2.065	2:0-0-1-0-0	0.851	-0.129	0.510
SIC (40,0.5)	2	20150	2.433		1:0-0-5-1-0	1.645		1:0-0-3-2-0	-0.799	0.406	-0.445
				2.092	1:0-0-1-0-0		2.092	2:0-1-0-0-0	0.812	-0.214	0.543

Table 12 (continued)

Model $\left(\frac{D}{P},\frac{d}{D}\right)^{a,b}$	Number of elements through thickness	Load[c] (in.-lb)	$\bar{\sigma}_o d$ (ksi)	$\bar{\sigma}_i d$ (ksi)	Location[e] Quad: axis pos.	σ_{po}[f] (ksi)	σ_{pi}[f] (ksi)	Location[e] Quad: axis pos.	Direction cosines[g] ℓ	m	n
S1D (20,0.5)	3	41421	2.114		1:0-0-5-1-0	1.789		1:0-0-2-1-0	-0.783	0.478	-0.398
				1.980	1:0-1-0-0-0		1.980	2:0-1-0-0-0	-0.708	0.131	-0.694
S1E (10,0.5)	4	87834	1.705		1:0-0-5-1-0	1.608		1:0-0-2-1-0	-0.740	0.549	-0.388
				1.637	1:0-1-0-0-0		1.637	2:0-1-0-0-0	-0.712	0.140	-0.689
S1F (40,0.32)	2	20150	2.005		1:0-0-5-1-0	1.229		1:0-0-5-2-0	-0.792	0.313	-0.525
				1.972	1:1-0-0-0-0		1.972	2:1-0-0-0-0	-0.613	0.073	-0.787
S1G (20,0.32)	3	41421	1.831		1:0-0-5-1-0	1.285		1:0-0-2-1-0	-0.796	0.381	-0.471
				1.915	1:0-1-0-0-0		1.915	2:0-1-0-0-0	-0.710	0.097	-0.698
S1H (10,0.32)	4	87834	1.596		1:0-0-5-1-0	1.250		1:0-0-2-1-0	-0.754	0.453	-0.475
				1.678	1:0-1-0-0-0		1.678	2:0-1-0-0-0	-0.715	0.101	-0.692
S1I (40,0.16)	2	20150	1.663		1:4-0-0-0-2	0.974		1:0-0-2-2-0	-0.795	0.182	-0.579
				1.813	1:0-1-0-0-0		1.813	2:0-1-0-0-0	-0.709	0.053	-0.703
S1J (20,0.16)	3	41421	1.583		1:4-0-0-0-2	0.999		1:0-0-2-1-0	-0.780	0.333	-0.531
				1.781	1:0-1-0-0-0		1.781	2:0-1-0-0-0	-0.712	0.057	-0.700
S1K (10,0.16)	4	87834	1.471		1:4-0-0-0-2	1.045		1:0-0-0-1-0	0.700	-0.381	0.604
				1.637	1:0-1-0-0-0		1.637	2:0-1-0-0-0	-0.718	0.061	-0.694
S1L (40,0.08)	2	20150	1.458		1:4-0-0-0-1	0.844		1:2-0-0-0-1	0.586	-0.220	0.780
				1.761	1:0-1-0-0-0		1.761	2:0-1-0-0-0	-0.710	0.031	-0.704

Table 12 (continued)

Model $\left(\frac{D}{T}, \frac{d}{D}\right)^{a,b}$	Number of elements through thickness	Load[c] (in.-lb)	$\bar{\sigma}_o^d$ (ksi)	$\bar{\sigma}_i^d$ (ksi)	Location[e] Quad: axis pos.	σ_{po}[f] (ksi)	σ_{pi}[f] (ksi)	Location[e] Quad: axis pos.	Direction cosines[g] ℓ	m	n
S1M (20,0.08)	3	41421	1.392	1.753	1:4-0-0-0-1 1:0-1-0-0-0	0.929	1.753	1:0-0-0-1-0 2:0-1-0-0-0	0.714 -0.713	-0.294 0.034	0.635 -0.701
S1N (10,0.08)	4	87834	1.367	1.678	1:4-0-0-0-2 1:0-1-0-0-0	0.975	1.678	1:1-0-0-0-1 2:0-1-0-0-0	0.609 -0.721	-0.407 0.038	0.681 -0.692
P30A (100,0.32)	1	7934	2.299	1.964	1:5-0-0-0-1 1:1-0-0-0-0	1.255	1.964	1:0-0-2-3-0 2:1-0-0-0-0	-0.789 -0.543	0.339 0.158	-0.512 -0.825
P30B (40,0.32)	2	20150	2.075	2.126	1:5-0-0-0-1 1:1-0-0-0-0	1.511	2.126	1:0-0-3-1-0 2:1-0-0-0-0	-0.798 -0.607	0.342 0.083	-0.496 -0.790
P30C (20,0.32)	3	41421	1.901	1.969	1:5-0-0-0-1 1:0-1-0-0-0	1.542	1.969	1:0-0-2-1-0 2:0-1-0-0-0	-0.784 -0.711	0.372 0.092	-0.497 -0.698
P30D (10,0.32)	4	87834	1.732	1.668	1:5-0-0-0-1 1:0-1-0-0-0	1.269	1.668	1:0-0-2-1-0 2:0-1-0-0-0	-0.751 -0.716	0.441 0.094	-0.491 -0.691
P30E (10,0.08)	4	87834	1.368	1.725	1:4-0-0-0-1 2:0-1-0-0-0	0.868	1.725	1:1-0-0-0-1 2:0-1-0-0-0	0.638 -0.722	-0.273 0.038	0.720 -0.691

[a] D and d are inside diameters of cylinder and nozzle, respectively.

[b] Young's modulus E = 206.8 GPa (30 × 10^6 psi); Poisson's ratio ν = 0.3 for all models.

[c] Moment loading used such that the shear stress on the outside surface of the cylinder = $\frac{\tau_o}{f}$ = 0.5 ksi.

[d] $\bar{\sigma}$ = max ($|\sigma_{max} - \sigma_{min}|$, $|\sigma_{max} - 0|$, $|\sigma_{min} - 0|$); o = outside surface, i = inside surface.

[e] Location is given by Quadrant Number: A1-A2-A3-A4-A5, where A1 through A5 represent the number of divisions along each of the respective axes (see Figs. 3, 4, and 25).

[f] σ_p = numerically largest principal stress (positive value denotes tensile stress, negative value denotes compressive stress); o = outside surface; i = inside surface.

[g] Direction cosines for σ_p relative to X-Y-Z global coordinate system (see Fig. 1).

The external moment loadings were chosen such that the stress intensity on the outside surface of the nozzle or cylinder would equal 1 ksi in regions removed from the junction [i.e., Mc/I = 1 ksi for bending moment loadings (M_{XN}, M_{ZN}, M_{YC}, and M_{ZC}) and Tc/J = 0.5 ksi for torsional moment loadings (M_{YN} and M_{XC})]. Hence, the values in Tables 7 through 12 represent "normalized" values. A Young's modulus of E = 206.8 GPa (30×10^6 psi) and a Poisson's ratio of ν = 0.3 were used for all models. The locations of the maximum stress values are given in terms of the model quadrant and the number of divisions along axes A1 through A5 [e.g., 1:1-0-0-0-0 (see Figs. 1, 3, and 4)]. The first number in the identification is the model quadrant (see Fig. 25), and the next five numbers (e.g., 1-0-0-0-0) locate the node with respect to the isometric views of the mesh layouts given in Appendix B.

For all but 4 of the 25 models, the calculated stresses are essentially symmetrical about the transverse plane through the nozzle. The results for models S1C, S1D, S1E, and S1H, which are relatively thick-walled models with large d/D ratios, however, are obviously influenced by

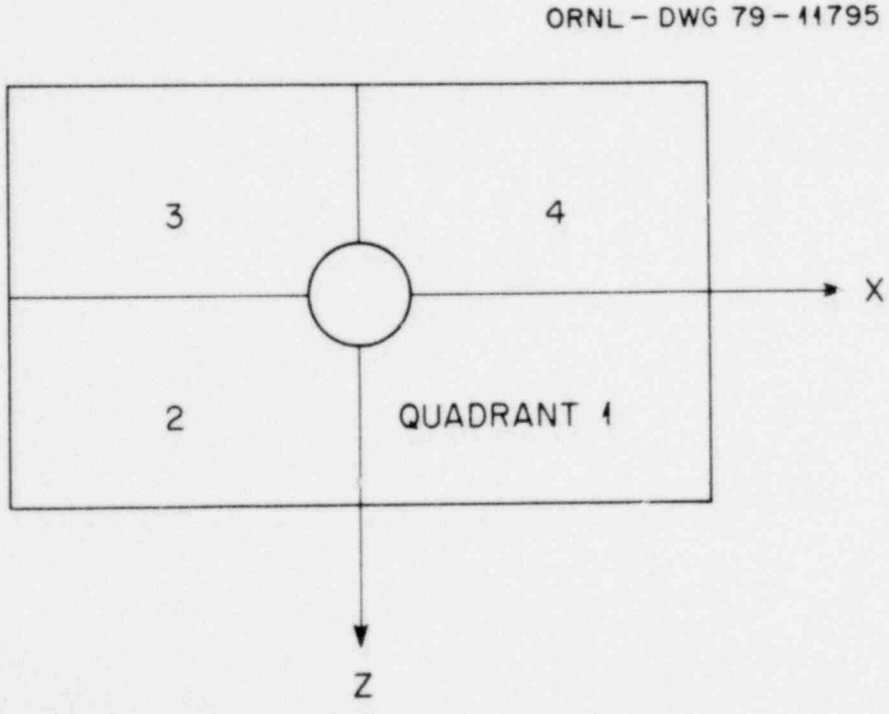

Fig. 25. Model quadrant identification.

the model boundary conditions discussed earlier in Chapter 2. Although there is no reason to suspect that the results presented here are inaccurate, they should not be applied indiscriminately in situations where the support boundary conditions are different (e.g., for a cantilivered structure or the simply supported structure analyzed by Bijlaard[8]).

At the outset of the parameter study, the authors anticipated that either of two loadings, out-of-plane bending on the nozzle M_{XN}, or in-plane bending on the nozzle M_{ZN}, would consistently give the highest stress intensities for both the unreinforced and reinforced models. This expectation was realized for out-of-plane bending on the nozzle M_{XN}. Table 8 shows that loading M_{XN} gives stress intensities that are markedly higher for all the unreinforced models and also for the reinforced models with $D/T \geq 20$ and $d/D = 0.50$ than those given by any other loading. This trend is not observed, however, for relatively small, thick-walled nozzle attachments ($D/T < 20$, $d/D < 0.50$). Thus, one conclusion of the study is that out-of-plane bending on the nozzle is the most "critical" loading condition for relatively large, thin nozzle attachments. This is true in the sense that very high stress concentrations are obtained that might lead to fatigue failure under cyclic loading conditions. As expected, in-plane bending on the nozzle M_{ZN} produced relatively high stress intensities for the unreinforced models (see Table 7) but not nearly as high as those obtained for out-of-plane bending (M_{XN}). Further examination of Table 7 reveals that Code reinforcement significantly reduces stress intensities to the point that in-plane bending M_{ZN} is no more "critical" than, for example, torsional moment loading on the cylinder M_{XC} (see Table 12), or in-plane bending on the cylinder M_{ZC} (see Table 10). Somewhat surprisingly, the two loadings, torsional moment loading on the nozzle M_{YN} and out-of-plane bending on the cylinder M_{YC}, showed practically no concentration of stress [i.e., all stress intensities were very nearly 1.0 ksi (see Tables 9 and 11)].

The largest stress intensity obtained in the study for an unreinforced model was a value of 16.599 ksi for out-of-plane bending on the nozzle M_{XN}. This value was found on the outside surface of model UA at 90° in the junction region. Out-of-plane bending M_{XN} also gave the largest stress intensity for a reinforced model, 11.070 ksi on the outside

surface of model S1A at 90° in the junction region. The largest stress intensity obtained for a reinforced model under loadings other than M_{XN} was 2.985 ksi on the outside surface of model S1A at the 90° junction region for torsional moment loading on the cylinder M_{XC}.

Like the results from the internal pressure loading parameter study,[1] there appears to be little difference (<5%) in the maximum stress intensities obtained for corresponding S1 and P30 models for the external moment loadings considered here. However, in contrast to the internal pressure loading study, it is more difficult to recognize trends for the variation of stress intensity with respect to D/T or d/D.

In summary, the results of this parameter study indicate that the reinforcement designs of Subsections NB-3330 through NB-3338, Section III, of the Code significantly reduce the maximum stresses in nozzle-to-cylinder attachments for all of the external moment loadings. However, for out-of-plane bending on the nozzle M_{XN} the maximum stresses, though substantially reduced in magnitude by the Code reinforcement designs, may still be sufficiently high for relatively large, thin (d/D = 0.5, $D/T \geq 20$) nozzle attachments to be of concern from a design viewpoint, particularly for cyclic loading conditions.

ACKNOWLEDGMENTS

The authors wish to express their indebtedness to E. C. Rodabaugh, Battelle-Columbus Laboratories, and to members of the PVRC Subcommittee on Reinforced Openings and External Loadings for their assistance in planning the parameter study reported here. Special thanks are extended to J. L. Mershon for his review of the preliminary results.

The finite-element computer program CORTES-SA was developed at the University of California, Berkeley, by A. M. Gantayat and G. H. Powell.

P. G. Fowler, Computer Sciences Division, UCC-ND, wrote all the plotting routines for the CORTES package of programs. The help of B. D. Nelson, also of the Computer Sciences Division, in generating input and executing the computer program is very much appreciated.

Finally, the authors gratefully acknowledge Linda Dockery for final typing of the report and the Engineering Technology Division Publications Office for editing, makeup, and final processing.

REFERENCES

1. J. W. Bryson, W. G. Johnson, and B. R. Bass, *Stresses in Reinforced Nozzle-Cylinder Attachments Under Internal Pressure Loading Analyzed by the Finite-Element Method — A Parameter Study*, ORNL/NUREG-4, (October 1977).

2. A. M. Gantayat and G. H. Powell, *Stress Analysis of Tee Joints by the Finite-Element Method*, Report UC-SESM 73-6, Structural Engineering Laboratory, University of California, Berkeley (February 1973).

3. B. M. Irons and O. C. Zienkiewicz, "The ISO Parametric Element System — A New Concept in Finite Element Analysis," Proceedings of Conference on Recent Advances in Stress Analysis, Royal Aeronautical Society, London, England, 1968.

4. E. L. Wilson, *SAP — A General Purpose Structural Analysis Program*, Report 70-20, SESM Laboratory, University of California, Berkeley (September 1970).

5. J. M. Corum et al., *Theoretical and Experimental Stress Analysis of ORNL Thin-Shell Cylinder-to-Cylinder Model No. 1*, ORNL-4553 (October 1972).

6. R. C. Gwaltney et al., *Theoretical and Experimental Stress Analysis of ORNL Thin-Shell Cylinder-to-Cylinder Model 3*, ORNL-5020 (June 1975).

7. S. C. Grigory, *Experimental Stress Analysis and Fatigue Test of ASA Standard B16.9 Tees, 304L Stainless Steel Tee No. T-8*, Southwest Research Institute (Dec. 8, 1971).

8. P. P. Bijlaard, "Stresses from Radial Loads and External Moments in Cylindrical Pressure Vessels," *Welding J., Res. Suppl.* 34(12), 608-17 (1955).

9. Ojars Greste, *Finite Element Analysis of Tubular K Joints*, Report UCSESM 70-11, University of California, Berkeley (June 1970).

APPENDIXES

INTRODUCTION

A complete tabulation of the results from the moment loading parameter study is provided on microfiche in the envelope attached to the back cover. Results are given by loading for each of the 25 models. Coordinates (in.), principal stresses (psi) and their direction cosines, and the stress intensity (psi) are printed for each nodal point on the outer and inner surfaces. The tabulated quantities are those obtained for the loading values shown in Tables 7 through 12 and, hence, represent normalized values (see Chapter 5). The stress intensity reported here represents twice the maximum shear stress ($2\tau_{max}$) and is defined by

$$\bar{\sigma} = \max\left(|\sigma_1 - \sigma_2|,\ |\sigma_2 - 0|,\ |\sigma_1 - 0|\right) ,$$

where $\sigma_1 = \sigma_{max}$ and $\sigma_2 = \sigma_{min}$.

Results are given for one-half ($Z \geq 0$) of each model [i.e., for quadrant 1 ($X \geq 0$, $Z \geq 0$) and quadrant 2 ($X \leq 0$, $Z \geq 0$)]. The appropriate symmetry, skew-symmetry arguments discussed in Chapter 2 can be used to determine the desired quantities for the other half ($Z \leq 0$) of each model. A five-column identification (A1-A2-A3-A4-A5), each of which gives the number of divisions along the respective axis, is used for each node (see Figs. 3 and 4). Nodes in quadrant 2 are located by taking mirror image projections of corresponding nodes in quadrant 1. Results for nodes located on the end caps are not given, because an artificially large modulus of elasticity was assigned to the end cap elements to represent stiff diaphragms.

In addition to the microfiche, displacement values at selected points on the end caps are given in Appendix A for loadings M_{ZN} and M_{XN} (see Fig. 6). Finally, Appendix B provides isometric views of the finite-element meshes for each of the 25 models in the parameter study. These figures are helpful in identifying the locations of the stress values listed in Tables 7 through 12.

Appendix A

END CAP DISPLACEMENTS FOR LOADINGS M_{ZN} AND M_{XN}

Subsection NB-3687.5 of the ASME Boiler and Pressure Vessel Code gives flexibility factors of small branch connections for use in a piping system flexibility analysis. The two flexibility factors k_{z3} and k_{x3} receive special treatment in NB-3687.5. These two factors are associated with in-plane and out-of-plane bending moment loadings applied to the nozzle. Because an examination and evaluation of the current flexibility factors in the Code will be the subject of a follow-up document, displacement values at selected reference points on the end caps of the models are given in Tables A.1 through A.25 for loadings M_{ZN} and M_{XN} (see Fig. 6). The reference points in these tables are shown in Fig. A.1. Displacements are printed with a format such that 1.052-02 means 1.052×10^{-2}.

ORNL-DWG 78-19268

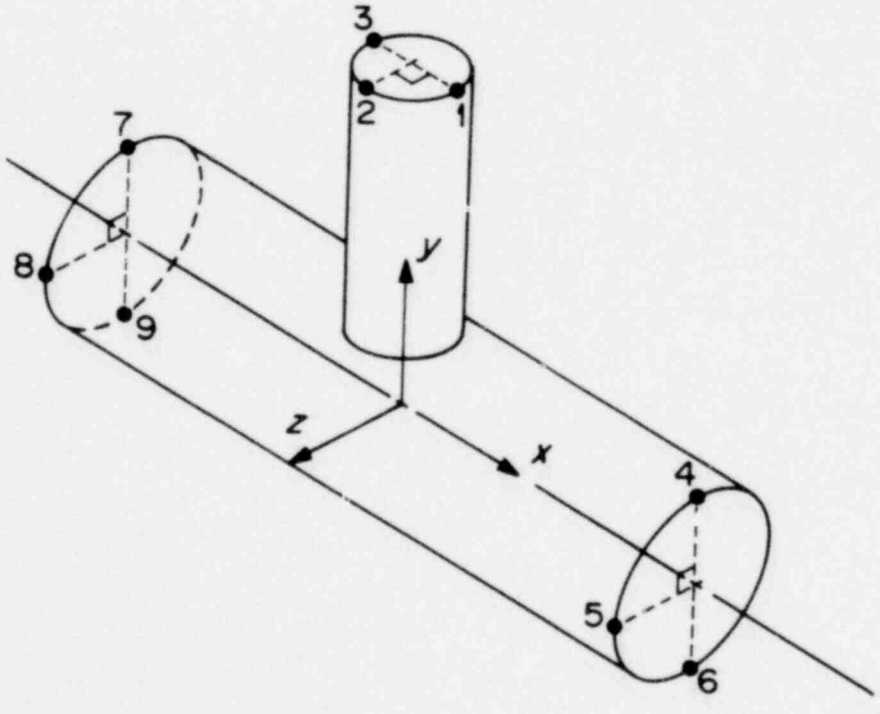

Fig. A.1. Reference points for displacements.

Table A.1. End cap displacements (in.)
for parameter study model *UA*

Loading (in.-lb)	Reference point	Outside			Inside		
		Δ_x	Δ_y	Δ_z	Δ_x	Δ_y	Δ_z
M_{ZN} (992)	1	-1.052-02	1.867-03	0.0	-1.052-02	1.828-03	0.0
	2	-1.052-02	-1.248-04	-1.002-07	-1.052-02	-1.248-04	-1.001-07
	3	-1.052-02	-2.116-03	0.0	-1.052-02	-2.077-03	0.0
	4	-2.064-05	-3.041-07	0.0	-2.050-05	-3.015-07	0.0
	5	-1.127-05	0.0	4.838-07	-1.123-05	0.0	4.797-07
	6	1.356-05	4.723-07	0.0	1.306-05	4.711-07	0.0
	7	8.167-05	2.945-07	0.0	7.989-05	2.919-07	0.0
	8	-6.618-06	0.0	-5.203-07	-6.591-06	0.0	-5.156-07
	9	-7.751-05	-5.580-07	0.0	-7.614-05	-5.567-07	0.0
M_{XN} (992)	1	0.0	0.0	4.639-02	0.0	0.0	4.639-02
	2	-2.048-05	-8.531-03	4.637-02	-2.009-05	-8.363-03	4.637-02
	3	0.0	0.0	4.635-02	0.0	0.0	4.635-02
	4	0.0	0.0	1.255-04	0.0	0.0	1.230-04
	5	3.621-06	-1.254-04	0.0	3.553-06	-1.230-04	0.0
	6	0.0	0.0	-1.254-04	0.0	0.0	-1.230-04
	7	0.0	0.0	0.0	0.0	0.0	0.0
	8	0.0	0.0	0.0	0.0	0.0	0.0
	9	0.0	0.0	0.0	0.0	0.0	0.0

Table A.2. End cap displacements (in.)
for parameter study model *UB*

Loading (in.-lb)	Reference point	Outside			Inside		
		Δ_x	Δ_y	Δ_z	Δ_x	Δ_y	Δ_z
M_{ZN} (1243)	1	-9.254-03	1.672-03	0.0	-9.254-03	1.629-03	0.0
	2	-9.254-03	-1.200-04	-7.054-08	-9.254-03	-1.200-04	-7.054-08
	3	-9.254-03	-1.912-03	0.0	-9.254-03	-1.869-03	0.0
	4	-2.018-05	-3.024-08	0.0	-1.992-05	-2.751-08	0.0
	5	-9.089-06	0.0	2.661-07	-9.057-06	0.0	2.627-07
	6	1.487-05	3.354-07	0.0	1.427-05	3.342-07	0.0
	7	8.127-05	3.720-10	0.0	7.917-05	3.047-09	0.0
	8	-4.606-06	0.0	-2.781-07	-4.588-06	0.0	-2.741-07
	9	-7.603-05	-3.949-07	0.0	-7.431-05	-3.936-07	0.0
M_{XN} (1243)	1	0.0	0.0	3.686-02	0.0	0.0	3.686-02
	2	-1.930-05	-6.870-03	3.686-02	-1.878-05	-6.720-03	3.686-02
	3	0.0	0.0	3.686-02	0.0	0.0	3.686-02
	4	0.0	0.0	1.246-04	0.0	0.0	1.216-04
	5	3.423-06	-1.246-04	0.0	3.343-06	-1.215-04	0.0
	6	0.0	0.0	-1.246-04	0.0	0.0	-1.215-04
	7	0.0	0.0	0.0	0.0	0.0	0.0
	8	0.0	0.0	0.0	0.0	0.0	0.0
	9	0.0	0.0	0.0	0.0	0.0	0.0

Table A.3. End cap displacements (in.)
for parameter study model *UC*

Loading (in.-lb)	Reference point	Outside			Inside		
		Δ_x	Δ_y	Δ_z	Δ_x	Δ_y	Δ_z
M_{ZN} (2519)	1	-5.961-03	1.174-03	0.0	-5.961-03	1.113-03	0.0
	2	-5.961-03	-1.057-04	-2.180-08	-5.961-03	-1.057-04	-2.179-08
	3	-5.961-03	-1.385-03	0.0	-5.961-03	-1.324-03	0.0
	4	-1.561-05	3.487-08	0.0	-1.494-05	3.885-08	0.0
	5	-2.356-06	0.0	1.147-07	-2.313-06	0.0	1.116-07
	6	2.090-05	2.461-07	0.0	1.974-05	2.441-07	0.0
	7	8.343-05	-5.383-08	0.0	7.958-05	-5.769-08	0.0
	8	1.466-06	0.0	-1.182-07	1.480-06	0.0	-1.143-07
	9	-6.938-05	-2.880-07	0.0	-6.606-05	-2.858-07	0.0
M_{XN} (2519)	1	0.0	0.0	1.678-02	0.0	0.0	1.678-02
	2	-1.681-05	-3.368-03	1.676-02	-1.601-05	-3.208-03	1.676-02
	3	0.0	0.0	1.675-02	0.0	0.0	1.675-02
	4	0.0	0.0	1.223-04	0.0	0.0	1.165-04
	5	2.900-06	-1.223-04	0.0	2.765-06	-1.165-04	0.0
	6	0.0	0.0	-1.223-04	0.0	0.0	-1.165-04
	7	0.0	0.0	0.0	0.0	0.0	0.0
	8	0.0	0.0	0.0	0.0	0.0	0.0
	9	0.0	0.0	0.0	0.0	0.0	0.0

Table A.4. End cap displacements (in.)
for parameter study model *UD*

Loading (in.-lb)	Reference point	Outside			Inside		
		Δ_x	Δ_y	Δ_z	Δ_x	Δ_y	Δ_z
M_{ZN} (5178)	1	-3.838-03	8.629-04	0.0	-3.838-03	7.760-04	0.0
	2	-3.838-03	-9.313-05	-5.576-09	-3.838-03	-9.313-05	-5.586-09
	3	-3.838-03	-1.049-03	0.0	-3.838-03	-9.622-04	0.0
	4	-1.358-05	1.276-07	0.0	-1.199-05	1.334-07	0.0
	5	2.090-06	0.0	-1.905-08	2.131-06	0.0	-1.911-08
	6	2.287-05	6.457-08	0.0	2.095-05	6.260-08	0.0
	7	8.319-05	-1.425-07	0.0	7.629-05	-1.482-07	0.0
	8	5.302-06	0.0	2.523-08	5.300-06	0.0	2.585-08
	9	-6.681-05	-8.432-08	0.0	-6.029-05	-8.236-08	0.0
M_{XN} (5178)	1	0.0	0.0	7.876-03	0.0	0.0	7.875-03
	2	-1.434-05	-1.789-03	7.861-03	-1.304-05	-1.626-03	7.861-03
	3	0.0	0.0	7.847-03	0.0	0.0	7.848-03
	4	0.0	0.0	1.201-04	0.0	0.0	1.092-04
	5	2.444-06	-1.201-04	0.0	2.223-06	-1.092-04	0.0
	6	0.0	0.0	-1.201-04	0.0	0.0	-1.092-04
	7	0.0	0.0	0.0	0.0	0.0	0.0
	8	0.0	0.0	0.0	0.0	0.0	0.0
	9	0.0	0.0	0.0	0.0	0.0	0.0

Table A.5. End cap displacements (in.)
for parameter study model *UE*

Loading (in.-lb)	Reference point	Outside			Inside		
		Δ_x	Δ_y	Δ_z	Δ_x	Δ_y	Δ_z
M_{ZN} (10979)	1	-2.453-03	6.73[illegible]4	0.0	-2.453-03	5.481-04	0.0
	2	-2.453-03	-7.938-05	-1.590-09	-2.453-03	-7.938-05	-1.578-09
	3	-2.453-03	-8.323-04	0.0	-2.453-03	-7.069-04	0.0
	4	-1.49[illegible]-05	4.862-08	0.0	-1.212-05	5.587-08	0.0
	5	9.795-07	0.0	1.982-09	1.045-06	0.0	2.815-09
	6	1.977-05	3.325-08	0.0	1.663-05	3.103-08	0.0
	7	7.888-05	-5.823-08	0.0	6.655-05	-6.563-08	0.0
	8	3.300-06	0.0	-1.016-09	3.301-06	0.0	-1.432-09
	9	-6.887-05	-5.275-08	0.0	-5.686-05	-5.084-08	0.0
M_{XN} (10979)	1	0.0	0.0	3.875-03	0.0	0.0	3.873-03
	2	-1.134-05	-1.071-03	3.863-03	-9.454-06	-8.926-04	3.863-03
	3	0.0	0.0	3.852-03	0.0	0.0	3.854-03
	4	0.0	0.0	1.171-04	0.0	0.0	9.762-03
	5	1.846-06	-1.171-04	0.0	1.539-06	-9.761-05	0.0
	6	0.0	0.0	-1.171-04	0.0	0.0	-9.761-04
	7	0.0	0.0	0.0	0.0	0.0	0.0
	8	0.0	0.0	0.0	0.0	0.0	0.0
	9	0.0	0.0	0.0	0.0	0.0	0.0

Table A.6. End cap displacements (in.)
for parameter study model *UF*

Loading (in.-lb)	Reference point	Outside			Inside		
		Δ_x	Δ_y	Δ_z	Δ_x	Δ_y	Δ_z
M_{ZN} (45)	1	-7.696-03	5.109-04	0.0	-7.696-03	4.257-04	0.0
	2	-7.696-03	-2.892-07	2.986-17	-7.696-03	-2.892-07	3.099-17
	3	-7.696-03	-5.114-04	0.0	-7.696-03	-4.263-04	0.0
	4	-3.664-08	3.596-10	0.0	-2.676-08	3.820-10	0.0
	5	1.594-08	0.0	-8.081-11	1.573-08	0.0	-7.466-11
	6	7.911-08	7.108-11	0.0	6.866-08	7.269-11	0.0
	7	3.112-07	-5.502-10	0.0	2.621-07	-5.710-10	0.0
	8	4.413-09	0.0	1.799-10	2.917-09	0.0	1.962-10
	9	-2.779-07	-1.397-10	0.0	-2.299-07	-1.593-10	0.0
M_{XN} (45)	1	0.0	0.0	7.744-03	0.0	0.0	7.744-03
	2	-3.374-09	-5.128-04	7.744-03	-2.812-09	-4.274-04	7.744-03
	3	0.0	0.0	7.744-03	0.0	0.0	7.744-03
	4	0.0	0.0	4.579-07	0.0	0.0	3.816-07
	5	-1.903-09	-4.579-07	0.0	-1.590-09	-3.816-07	0.0
	6	0.0	0.0	-4.579-07	0.0	0.0	-3.816-07
	7	0.0	0.0	0.0	0.0	0.0	0.0
	8	0.0	0.0	0.0	0.0	0.0	0.0
	9	0.0	0.0	0.0	0.0	0.0	0.0

Table A.7. End cap displacements (in.)
for parameter study model *S1A*

Loading (in.-lb)	Reference point	Outside			Inside		
		Δ_x	Δ_y	Δ_z	Δ_x	Δ_y	Δ_z
M_{ZN} (992)	1	-4.152-03	8.470-04	0.0	-4.152-03	8.285-04	0.0
	2	-4.152-03	-9.751-05	-1.357-07	-4.152-03	-9.750-05	-1.357-07
	3	-4.152-03	-1.042-03	0.0	-4.152-03	-1.023-03	0.0
	4	-2.009-05	-6.631-07	0.0	-1.993-05	-6.603-07	0.0
	5	-9.156-06	0.0	4.411-07	-9.016-06	0.0	4.433-07
	6	1.407-05	5.343-07	0.0	1.359-05	5.333-07	0.0
	7	7.183-05	7.038-07	0.0	7.025-05	7.010-07	0.0
	8	-6.428-06	0.0	-4.666-07	-6.293-06	0.0	-4.684-07
	9	-7.092-05	-6.265-07	0.0	-6.969-05	-6.254-07	0.0
M_{XN} (992)	1	0.0	0.0	1.821-02	0.0	0.0	1.821-02
	2	-1.338-05	-3.556-03	1.820-02	-1.313-05	-3.487-03	1.820-02
	3	0.0	0.0	1.819-02	0.0	0.0	1.819-02
	4	0.0	0.0	1.165-04	0.0	0.0	1.142-04
	5	2.125-06	-1.164-04	0.0	2.083-06	-1.142-04	0.0
	6	0.0	0.0	-1.164-04	0.0	0.0	-1.142-04
	7	0.0	0.0	0.0	0.0	0.0	0.0
	8	0.0	0.0	0.0	0.0	0.0	0.0
	9	0.0	0.0	0.0	0.0	0.0	0.0

Table A.8. End cap displacements (in.)
for parameter study model *S1B*

Loading (in.-lb)	Reference point	Outside			Inside		
		Δ_x	Δ_y	Δ_z	Δ_x	Δ_y	Δ_z
M_{ZN} (1243)	1	-3.845-03	8.009-04	0.0	-3.845-03	7.791-04	0.0
	2	-3.845-03	-9.[illegible]9-05	-9.082-08	-3.845-03	-9.638-05	-9.079-08
	3	-3.845-03	-9.9[illegible]4-04	0.0	-3.845-03	-9.716-04	0.0
	4	-1.945-05	-4.344-07	0.0	-1.920-05	-4.817-07	0.0
	5	-7.505-06	0.0	3.654-07	-7.373-06	0.0	3.665-07
	6	1.495-05	4.558-07	0.0	1.438-05	4.546-07	0.0
	7	7.220-05	5.174-07	0.0	7.028-05	5.146-07	0.0
	8	-5.079-06	0.0	-3.894-07	-4.953-06	0.0	-3.901-07
	9	-7.054-05	-5.319-07	0.0	-6.898-05	-5.306-07	0.0
M_{XN} (1243)	1	0.0	0.0	1.509-02	0.0	0.0	1.509-02
	2	-1.319-05	-3.007-03	1.508-02	-1.287-05	-2.934-03	1.508-02
	3	0.0	0.0	1.507-02	0.0	0.0	1.507-02
	4	0.0	0.0	1.164-04	0.0	0.0	1.136-04
	5	2.011-06	-1.164-04	0.0	1.962-06	-1.136-04	0.0
	6	0.0	0.0	-1.164-04	0.0	0.0	-1.135-04
	7	0.0	0.0	0.0	0.0	0.0	0.0
	8	0.0	0.0	0.0	0.0	0.0	0.0
	9	0.0	0.0	0.0	0.0	0.0	0.0

Table A.9. End cap displacements (in.)
for parameter study model *S1C*

Loading (in.-lb)	Reference point	Outside			Inside		
		Δ_x	Δ_y	Δ_z	Δ_x	Δ_y	Δ_z
M_{ZN} (2519)	1	-2.778-03	6.428-04	0.0	-2.778-03	6.079-04	0.0
	2	-2.778-03	-9.028-05	-2.205-08	-2.778-03	-9.028-05	-2.206-08
	3	-2.778-03	-8.232-04	0.0	-2.778-03	-7.884-04	0.0
	4	-1.446-05	-1.295-07	0.0	-1.384-05	-1.262-07	0.0
	5	-1.349-06	0.0	1.716-07	-1.246-06	0.0	1.695-07
	6	1.971-05	2.900-07	0.0	1.865-05	2.881-07	0.0
	7	7.565-05	1.377-07	0.0	7.206-05	1.344-07	0.0
	8	1.990-07	0.0	-1.840-07	2.852-07	0.0	-1.812-07
	9	-6.634-05	-3.383-07	0.0	-6.324-05	-3.363-07	0.0
M_{XN} (2519)	1	0.0	0.0	7.358-03	0.0	0.0	7.358-03
	2	-1.197-05	-1.634-03	7.346-03	-1.140-05	-1.556-03	7.346-03
	3	0.0	0.0	7.334-03	0.0	0.0	7.335-03
	4	0.0	0.0	1.153-04	0.0	0.0	1.098-04
	5	1.598-06	-1.153-04	0.0	1.523-06	-1.098-04	0.0
	6	0.0	0.0	-1.153-04	0.0	0.0	1.098-04
	7	0.0	0.0	0.0	0.0	0.0	0.0
	8	0.0	0.0	0.0	0.0	0.0	0.0
	9	0.0	0.0	0.0	0.0	0.0	0.0

Table A.10. End cap displacements (in.)
for parameter study model S1D

Loading (in.-lb)	Reference point	Outside			Inside		
		Δ_x	Δ_y	Δ_z	Δ_x	Δ_y	Δ_z
M_{ZN} (5178)	1	-1.926-03	5.230-04	0.0	-1.926-03	4.681-04	0.0
	2	-1.926-03	-8.114-05	-4.233-09	-1.926-03	-8.113-05	-4.247-09
	3	-1.926-03	-6.852-04	0.0	-1.926-03	-6.303-04	0.0
	4	-1.201-05	3.152-08	0.0	-1.069-05	3.618-08	0.0
	5	1.957-06	0.0	2.950-09	2.044-06	0.0	1.836-09
	6	2.062-05	9.771-08	0.0	1.885-05	9.556-08	0.0
	7	7.549-05	-3.881-08	0.0	6.894-05	-4.364-08	0.0
	8	2.696-06	0.0	-1.317-09	2.760-06	0.0	-3.762-10
	9	-6.479-05	-1.244-07	0.0	-5.873-05	-1.221-07	0.0
M_{XN} (5178)	1	0.0	0.0	3.590-03	0.0	0.0	3.589-03
	2	-9.883-06	-9.472-04	3.580-03	-8.985-06	-8.611-04	3.580-03
	3	0.0	0.0	3.570-03	0.0	0.0	3.571-03
	4	0.0	0.0	1.129-04	0.0	0.0	1.026-04
	5	1.066-06	-1.129-04	0.0	9.696-07	-1.026-04	0.0
	6	0.0	0.0	-1.129-04	0.0	0.0	-1.026-04
	7	0.0	0.0	0.0	0.0	0.0	0.0
	8	0.0	0.0	0.0	0.0	0.0	0.0
	9	0.0	0.0	0.0	0.0	0.0	0.0

Table A.11. End cap displacements (in.) for parameter study model *S1E*

Loading (in.-lb)	Reference point	Outside			Inside		
		Δ_x	Δ_y	Δ_z	Δ_x	Δ_y	Δ_z
M_{ZN} (10979)	1	-1.276-03	4.362-04	0.0	-1.276-03	3.522-04	0.0
	2	-1.276-03	-6.830-05	-1.197-09	-1.276-03	-6.830-05	-1.172-09
	3	-1.276-03	-5.729-04	0.0	-1.276-03	-4.888-04	0.0
	4	-1.314-05	7.022-09	0.0	-1.080-05	1.315-08	0.0
	5	4.706-07	0.0	-5.669-09	5.680-07	0.0	-6.753-09
	6	1.653-05	2.266-08	0.0	1.383-05	2.071-08	0.0
	7	7.071-05	-1.423-08	0.0	5.911-05	-2.140-08	0.0
	8	3.624-07	0.0	3.298-09	4.480-07	0.0	4.680-09
	9	-6.714-05	-3.915-08	0.0	-5.594-05	-3.708-08	0.0
M_{XN} (10979)	1	0.0	0.0	1.925-03	0.0	0.0	1.924-03
	2	-7.652-06	-6.401-04	1.917-03	-6.377-06	-5.334-04	1.917-03
	3	0.0	0.0	1.910-03	0.0	0.0	1.911-03
	4	0.0	0.0	1.093-04	0.0	0.0	9.108-05
	5	4.663-07	-1.093-04	0.0	3.892-07	-9.108-05	0.0
	6	0.0	0.0	-1.093-04	0.0	0.0	-9.107-05
	7	0.0	0.0	0.0	0.0	0.0	0.0
	8	0.0	0.0	0.0	0.0	0.0	0.0
	9	0.0	0.0	0.0	0.0	0.0	0.0

Table A.12. End cap displacements (in.)
for parameter study model *S1F*

Loading (in.-lb)	Reference point	Outside			Inside		
		Δ_x	Δ_y	Δ_z	Δ_x	Δ_y	Δ_z
M_{ZN} (660)	1	-3.083-03	5.760-04	0.0	-3.083-03	5.475-04	0.0
	2	-3.083-03	-2.218-05	1.068-10	-3.083-03	-2.218-05	1.046-10
	3	-3.083-03	-6.203-04	0.0	-3.083-03	-5.918-04	0.0
	4	-3.161-06	-6.553-08	0.0	-3.025-06	-6.459-08	0.0
	5	-3.662-07	0.0	6.277-08	-3.350-07	0.0	6.215-08
	6	5.067-06	9.898-08	0.0	4.792-06	9.839-08	0.0
	7	1.918-05	6.127-08	0.0	1.825-05	6.037-08	0.0
	8	-4.899-07	0.0	-5.981-08	-4.664-07	0.0	-5.890-08
	9	-1.708-05	-1.098-07	0.0	-1.631-05	-1.092-07	0.0
M_{XN} (660)	1	0.0	0.0	5.857-03	0.0	0.0	5.85 03
	2	-1.430-06	-9.393-04	5.855-03	-1.362-06	-8.946-04	5.855-03
	3	0.0	0.0	5.854-03	0.0	0.0	5.854-03
	4	0.0	0.0	2.912-05	0.0	0.0	2.773-05
	5	1.022-07	-2.911-05	0.0	9.728-08	-2.773-05	0.0
	6	0.0	0.0	-2.911-05	0.0	0.0	-2.772-05
	7	0.0	0.0	0.0	0.0	0.0	0.0
	8	0.0	0.0	0.0	0.0	0.0	0.0
	9	0.0	0.0	0.0	0.0	0.0	0.0

Table A.13. End cap displacements (in.) for parameter study model *SIG*

Loading (in.-lb)	Reference point	Outside			Inside		
		Δ_x	Δ_y	Δ_z	Δ_x	Δ_y	Δ_z
M_{ZN} (1357)	1	-2.316-03	5.042-04	0.0	-2.316-03	4.565-04	0.0
	2	-2.316-03	-2.038-05	3.410-11	-2.316-03	-2.038-05	3.239-11
	3	-2.316-03	-5.450-04	0.0	-2.316-03	-4.973-04	0.0
	4	-2.520-06	7.748-09	0.0	-2.195-06	9.015-09	0.0
	5	8.125-07	0.0	5.286-09	8.248-07	0.0	4.813-09
	6	5.586-06	3.582-08	0.0	5.134-06	3.518-08	0.0
	7	1.958-05	-1.334-08	0.0	1.788-05	-1.457-08	0.0
	8	6.280-07	0.0	-1.567-09	6.277-07	0.0	-7.905-10
	9	-1.661-05	-4.294-08	0.0	-1.506-05	-4.230-08	0.0
M_{XN} (1357)	1	0.0	0.0	3.195-03	0.0	0.0	3.195-03
	2	-1.239-06	-6.407-04	3.194-03	-1.126-06	-5.824-04	3.194-03
	3	0.0	0.0	3.193-03	0.0	0.0	3.193-03
	4	0.0	0.0	2.894-05	0.0	0.0	2.631-05
	5	4.671-08	-2.894-05	0.0	4.246-08	-2.631-05	0.0
	6	0.0	0.0	-2.894-05	0.0	0.0	-2.631-05
	7	0.0	0.0	0.0	0.0	0.0	0.0
	8	0.0	0.0	0.0	0.0	0.0	0.0
	9	0.0	0.0	0.0	0.0	0.0	0.0

Table A.14. End cap displacements (in.)
for parameter study model *S1H*

Loading (in.-lb)	Reference point	Outside			Inside		
		Δ_x	Δ_y	Δ_z	Δ_x	Δ_y	Δ_z
M_{ZN} (2878)	1	-1.648-03	4.424-04	0.0	-1.648-03	3.657-04	0.0
	2	-1.648-03	-1.782-05	1.622-12	-1.648-03	-1.782-05	4.804-13
	3	-1.648-03	-4.780-04	0.0	-1.648-03	-4.013-04	0.0
	4	-3.056-06	8.880-09	0.0	-2.431-06	1.061-08	0.0
	5	4.802-07	0.0	-1.168-09	4.913-07	0.0	-1.191-09
	6	4.604-06	8.236-09	0.0	3.911-06	7.744-09	0.0
	7	1.869-05	-1.226-08	0.0	1.566-05	-1.412-08	0.0
	8	2.527-07	0.0	2.570-09	2.477-07	0.0	2.738-09
	9	-1.745-05	-1.293-08	0.0	-1.451-05	-1.250-08	0.0
M_{XN} (2878)	1	0.0	0.0	1.933-03	0.0	0.0	1.933-03
	2	-1.074-06	-5.005-04	1.932-03	-8.951-07	-4.171-04	1.932-03
	3	0.0	0.0	1.931-03	0.0	0.0	1.931-03
	4	0.0	0.0	2.864-05	0.0	0.0	2.387-05
	5	-7.313-09	-2.864-05	0.0	-6.267-09	-2.387-05	0.0
	6	0.0	0.0	-2.864-05	0.0	0.0	-2.387-05
	7	0.0	0.0	0.0	0.0	0.0	0.0
	8	0.0	0.0	0.0	0.0	0.0	0.0
	9	0.0	0.0	0.0	0.0	0.0	0.0

Table A.15. End cap displacements (in.)
for parameter study model *S1I*

Loading (in.-lb)	Reference point	Outside			Inside		
		Δ_x	Δ_y	Δ_z	Δ_x	Δ_y	Δ_z
M_{ZN} (83)	1	-4.964-03	5.417-04	0.0	-4.964-03	5.058-04	0.0
	2	-4.964-03	-2.715-06	2.646-13	-4.964-03	-2.715-06	2.650-13
	3	-4.964-03	-5.472-04	0.0	-4.964-03	-5.212-04	0.0
	4	-3.827-07	-3.967-09	0.0	-3.625-07	-3.857-09	0.0
	5	1.194-08	0.0	4.327-09	1.435-08	0.0	4.256-09
	6	6.102-07	6.883-09	0.0	5.814-07	6.793-09	0.0
	7	2.383-06	3.240-09	0.0	2.268-06	3.137-09	0.0
	8	-6.937-08	0.0	-3.839-09	-6.856-08	0.0	-3.722-09
	9	-2.284-06	-8.166-09	0.0	-2.178-06	-8.060-09	0.0
M_{XN} (83)	1	0.0	0.0	5.788-03	0.0	0.0	5.788-03
	2	-6.162-08	-5.939-04	5.788-03	-5.869-08	-5.656-04	5.788-03
	3	0.0	0.0	5.787-03	0.0	0.0	5.787-03
	4	0.0	0.0	3.668-06	0.0	0.0	3.494-06
	5	-1.724-08	-3.668-06	0.0	-1.645-08	-3.494-06	0.0
	6	0.0	0.0	-3.668-06	0.0	0.0	-3.493-06
	7	0.0	0.0	0.0	0.0	0.0	0.0
	8	0.0	0.0	0.0	0.0	0.0	0.0
	9	0.0	0.0	0.0	0.0	0.0	0.0

Table A.16. End cap displacements (in.)
for parameter study model *S1J*

Loading (in.-lb)	Reference point	Outside			Inside		
		Δ_x	Δ_y	Δ_z	Δ_x	Δ_y	Δ_z
M_{ZN} (170)	1	-4.160-03	5.061-04	0.0	-4.160-03	4.598-04	0.0
	2	-4.160-03	-2.489-04	-9.471-14	-4.160-03	-2.489-06	-9.388-14
	3	-4.160-03	-5.111-04	0.0	-4.160-03	-4.648-04	0.0
	4	-2.741-07	2.362-09	0.0	-2.340-07	2.531-09	0.0
	5	1.240-07	0.0	-1.095-09	1.255-07	0.0	-1.110-09
	6	6.788-07	1.972-09	0.0	6.295-07	1.893-09	0.0
	7	2.449-06	-3.629-09	0.0	2.238-06	-3.793-09	0.0
	8	7.098-08	0.0	2.380-09	7.023-08	0.0	2.430-09
	9	-2.116-06	-2.249-09	0.0	-1.915-06	-2.166-09	0.0
M_{XN} (170)	1	0.0	0.0	4.385-03	0.0	0.0	4.385-03
	2	-5.601-08	-5.232-04	4.385-03	-5.091-08	-4.756-04	4.385-03
	3	0.0	0.0	4.385-03	0.0	0.0	4.385-03
	4	0.0	0.0	3.598-06	0.0	0.0	3.271-06
	5	-1.007-08	-3.598-06	0.0	-9.164-09	-3.271-06	0.0
	6	0.0	0.0	-3.598-06	0.0	0.0	-3.270-06
	7	0.0	0.0	0.0	0.0	0.0	0.0
	8	0.0	0.0	0.0	0.0	0.0	0.0
	9	0.0	0.0	0.0	0.0	0.0	0.0

Table A.17. End cap displacements (in.)
for parameter study model *S1K*

Loading (in.-lb)	Reference point	Outside			Inside		
		Δ_x	Δ_y	Δ_z	Δ_x	Δ_y	Δ_z
M_{ZN} (360)	1	-3.249-03	4.661-04	0.0	-3.249-03	3.880-04	0.0
	2	-3.249-03	-2.202-06	-6.375-15	-3.249-03	-2.202-06	-6.165-15
	3	-3.249-03	-4.705-04	0.0	-3.249-03	-3.924-04	0.0
	4	-3.270-07	1.582-09	0.0	-2.531-07	1.808-09	0.0
	5	8.146-08	0.0	-6.082-10	8.337-08	0.0	-6.139-10
	6	5.756-07	2.344-10	0.0	4.960-07	1.519-10	0.0
	7	2.363-06	-2.136-09	0.0	1.985-06	-2.383-09	0.0
	8	4.877-08	0.0	1.084-09	4.849-08	0.0	1.114-09
	9	-2.160-06	-3.659-10	0.0	-1.788-06	-2.906-10	0.0
M_{XN} (360)	1	0.0	0.0	3.310-03	0.0	0.0	3.310-03
	2	-5.369-08	-4.726-04	3.310-03	-4.474-08	-3.939-04	3.310-03
	3	0.0	0.0	3.310-03	0.0	0.0	3.310-03
	4	0.0	0.0	3.552-06	0.0	0.0	2.960-06
	5	-6.677-09	-3.552-06	0.0	-5.556-09	-2.960-06	0.0
	6	0.0	0.0	-3.552-06	0.0	0.0	-2.960-06
	7	0.0	0.0	0.0	0.0	0.0	0.0
	8	0.0	0.0	0.0	0.0	0.0	0.0
	9	0.0	0.0	0.0	0.0	0.0	0.0

Table A.18. End cap displacements (in.)
for parameter study model *S1L*

Loading (in.-lb)	Reference point	Outside			Inside		
		Δ_x	Δ_y	Δ_z	Δ_x	Δ_y	Δ_z
M_{ZN} (10.32)	1	-9.374-03	5.269-04	0.0	-9.374-03	5.018-04	0.0
	2	-9.374-03	-3.390-07	1.587-17	-9.374-03	-3.390-07	1.576-17
	3	-9.374-03	-5.276-04	0.0	-9.374-03	-5.024-04	0.0
	4	-4.209-08	-2.532-10	0.0	-3.944-08	-2.405-10	0.0
	5	1.076-08	0.0	3.570-10	1.120-08	0.0	3.577-10
	6	8.326-08	6.616-10	0.0	7.969-08	6.478-10	0.0
	7	3.046-07	2.904-10	0.0	2.901-07	2.790-10	0.0
	8	-4.869-09	0.0	-4.526-10	-4.698-09	0.0	-4.432-10
	9	-2.877-07	-9.362-10	0.0	-2.741-07	-9.188-10	0.0
M_{XN} (10.32)	1	0.0	0.0	9.528-03	0.0	0.0	9.528-03
	2	-3.118-09	-5.318-04	9.528-03	-2.970-09	-5.065-04	9.528-03
	3	0.0	0.0	9.528-03	0.0	0.0	9.528-03
	4	0.0	0.0	4.640-07	0.0	0.0	4.419-07
	5	-3.482-09	-4.640-07	0.0	3.327-09	-4.419-07	0.0
	6	0.0	0.0	-4.640-07	0.0	0.0	-4.419-07
	7	0.0	0.0	0.0	0.0	0.0	0.0
	8	0.0	0.0	0.0	0.0	0.0	0.0
	9	0.0	0.0	0.0	0.0	0.0	0.0

Table A.19. End cap displacements (in.)
for parameter study model *S1M*

Loading (in.-lb)	Reference point	Outside			Inside		
		Δ_x	Δ_y	Δ_z	Δ_x	Δ_y	Δ_z
M_{ZN} (21.20)	1	-8.293-03	5.071-04	0.0	-8.293-03	4.610-04	0.0
	2	-8.293-03	-3.139-07	-1.124-16	-8.293-03	-3.139-07	-1.129-16
	3	-8.293-03	-5.077-04	0.0	-8.293-03	-4.616-04	0.0
	4	-3.154-08	4.310-10	0.0	-2.628-08	4.492-10	0.0
	5	2.044-08	0.0	-1.817-10	2.061-08	0.0	-1.774-10
	6	8.783-08	1.610-10	0.0	8.183-08	1.499-10	0.0
	7	3.112-07	-6.228-10	0.0	2.846-07	-6.398-10	0.0
	8	9.565-09	0.0	3.428-10	9.238-09	0.0	3.487-10
	9	-2.693-07	-2.389-10	0.0	-2.434-07	-2.281-10	0.0
M_{XN} (21.20)	1	0.0	0.0	8.331-03	0.0	0.0	8.331-03
	2	-2.994-09	-5.086-04	8.331-03	-2.721-09	-4.624-04	8.331-03
	3	0.0	0.0	8.331-03	0.0	0.0	8.331-03
	4	0.0	0.0	4.548-07	0.0	0.0	4.135-07
	5	-2.208-09	-4.548-07	0.0	-2.016-09	-4.135-07	0.0
	6	0.0	0.0	-4.548-07	0.0	0.0	-4.134-07
	7	0.0	0.0	0.0	0.0	0.0	0.0
	8	0.0	0.0	0.0	0.0	0.0	0.0
	9	0.0	0.0	0.0	0.0	0.0	0.0

Table A.20. End cap displacements (in.)
for parameter study model *S1N*

Loading (in.-lb)	Reference point	Outside			Inside		
		Δ_x	Δ_y	Δ_z	Δ_x	Δ_y	Δ_z
M_{ZN} (45)	1	-6.694-03	4.754-04	0.0	-6.694-03	3.961-04	0.0
	2	-6.694-03	-2.813-07	-1.806-17	-6.694-03	-2.813-04	-1.943-17
	3	-6.694-03	-4.759-04	0.0	-6.694-03	-3.967-04	0.0
	4	-3.928-08	2.238-10	0.0	-2.973-08	2.466-10	0.0
	5	1.336-08	0.0	-5.631-11	1.347-08	0.0	-5.315-11
	6	7.401-08	-2.713-12	0.0	6.417-08	-9.996-12	0.0
	7	3.002-07	-3.493-10	0.0	2.524-07	-3.731-10	0.0
	8	5.899-09	0.0	1.670-10	5.373-09	0.0	1.710-10
	9	-2.756-07	1.229-11	0.0	-2.281-07	1.504-11	0.0
M_{XN} (45)	1	0.0	0.0	6.703-03	0.0	0.0	6.703-03
	2	-3.071-09	-4.760-04	6.703-03	-2.559-09	-3.966-04	6.703-03
	3	0.0	0.0	6.703-03	0.0	0.0	6.703-03
	4	0.0	0.0	4.505-07	0.0	0.0	3.754-07
	5	-1.617-09	-4.505-07	0.0	-1.352-09	-3.754-07	0.0
	6	0.0	0.0	-4.505-07	0.0	0.0	-3.754-07
	7	0.0	0.0	0.0	0.0	0.0	0.0
	8	0.0	0.0	0.0	0.0	0.0	0.0
	9	0.0	0.0	0.0	0.0	0.0	0.0

Table A.21. End cap displacements (in.)
for parameter study model *P30A*

Loading (in.-lb)	Reference point	Outside			Inside		
		Δ_x	Δ_y	Δ_z	Δ_x	Δ_y	Δ_z
M_{ZN} (260)	1	-3.993-03	6.639-04	0.0	-3.993-03	6.504-04	0.0
	2	-3.993-03	-2.291-05	-4.128-09	-3.993-03	-2.291-05	-4.128-09
	3	-3.993-03	-7.096-04	0.0	-3.993-03	-6.961-04	0.0
	4	-4.320-06	-1.998-07	0.0	-4.289-06	-1.990-07	0.0
	5	-2.279-06	0.0	1.292-07	-2.241-06	0.0	1.294-07
	6	3.417-06	1.694-07	0.0	3.300-06	1.692-07	0.0
	7	1.785-05	1.949-07	0.0	1.745-05	1.942-07	0.0
	8	-2.154-06	0.0	-1.212-07	-2.118-06	0.0	-1.213-07
	9	-1.808-05	-1.829-07	0.0	-1.777-05	-1.826-07	0.0
M_{XN} (260)	1	0.0	0.0	8.643-03	0.0	0.0	8.643-03
	2	-1.507-06	-1.240-03	8.642-03	-1.478-06	-1.216-03	8.642-03
	3	0.0	0.0	8.640-03	0.0	0.0	8.640-03
	4	0.0	0.0	2.882-05	0.0	0.0	2.825-05
	5	1.738-07	-2.881-05	0.0	1.703-07	-2.825-05	0.0
	6	0.0	0.0	-2.881-05	0.0	0.0	-2.825-05
	7	0.0	0.0	0.0	0.0	0.0	0.0
	8	0.0	0.0	0.0	0.0	0.0	0.0
	9	0.0	0.0	0.0	0.0	0.0	0.0

Table A.22. End cap displacements (in.)
for parameter study model *P30B*

Loading (in.-lb)	Reference point	Outside			Inside		
		Δ_x	Δ_y	Δ_z	Δ_x	Δ_y	Δ_z
M_{ZN} (660)	1	-3.051-03	5.733-04	0.0	-3.051-03	5.450-04	0.0
	2	-3.051-03	-2.211-05	1.645-10	-3.051-03	-2.211-05	1.618-10
	3	-3.051-03	-6.175-04	0.0	-3.051-03	-5.892-04	0.0
	4	-3.195-06	-5.608-08	0.0	-3.060-06	-5.516-08	0.0
	5	-4.051-07	0.0	5.120-08	-3.704-07	0.0	5.065-08
	6	4.871-06	8.773-08	0.0	4.605-06	8.720-08	0.0
	7	1.901-05	5.281-08	0.0	1.808-05	5.191-08	0.0
	8	-4.690-07	0.0	-4.769-08	-4.399-07	0.0	-4.693-08
	9	-1.711-05	-9.638-08	0.0	-1.633-05	-9.582-08	0.0
M_{XN} (660)	1	0.0	0.0	5.020-03	0.0	0.0	5.020-03
	2	-1.398-06	-8.419-04	5.018-03	-1.332-06	-8.018-04	5.018-03
	3	0.0	0.0	5.017-03	0.0	0.0	5.017-03
	4	0.0	0.0	2.891-05	0.0	0.0	2.754-05
	5	1.032-07	-2.891-05	0.0	9.820-08	-2.754-05	0.0
	6	0.0	0.0	-2.891-05	0.0	0.0	-2.753-05
	7	0.0	0.0	0.0	0.0	0.0	0.0
	8	0.0	0.0	0.0	0.0	0.0	0.0
	9	0.0	0.0	0.0	0.0	0.0	0.0

Table A.23. End cap displacements (in.)
for parameter study model P3C3

Loading (in.-lb)	Reference point	Outside			Inside		
		Δ_x	Δ_y	Δ_z	Δ_x	Δ_y	Δ_z
M_{ZN} (1357)	1	-2.359-03	5.102-04	0.0	-2.359-03	4.620-04	0.0
	2	-2.359-03	-2.037-05	3.741-11	-2.359-03	-2.037-05	3.555-11
	3	-2.359-03	-5.569-04	0.0	-2.359-03	-5.027-04	0.0
	4	-2.520-06	8.009-09	0.0	-2.206-06	9.283-09	0.0
	5	7.393-07	0.0	7.990-10	7.578-07	0.0	3.165-10
	6	5.432-06	3.165-08	0.0	4.989-06	3.106-08	0.0
	7	1.947-05	-1.264-08	0.0	1.778-05	-1.391-08	0.0
	8	6.193-07	0.0	2.888-09	6.279-07	0.0	3.600-09
	9	-1.658-05	-3.737-08	0.0	-1.503-05	-3.673-08	0.0
M_{XN} (1357)	1	0.0	0.0	2.993-03	0.0	0.0	2.993-03
	2	-1.154-06	-6.162-04	2.992-03	-1.049-06	-5.601-04	2.992-03
	3	0.0	0.0	2.991-03	0.0	0.0	2.991-03
	4	0.0	0.0	2.873-05	0.0	0.0	2.612-05
	5	4.761-08	-2.873-05	0.0	4.328-08	-2.612-05	0.0
	6	0.0	0.0	-2.873-05	0.0	0.0	-2.611-05
	7	0.0	0.0	0.0	0.0	0.0	0.0
	8	0.0	0.0	0.0	0.0	0.0	0.0
	9	0.0	0.0	0.0	0.0	0.0	0.0

Table A.24. End cap displacements (in.)
for parameter study model P' 0D

Loading (in.-lb)	Reference point	Outside			Inside		
		Δ_x	Δ_y	Δ_z	Δ_x	Δ_y	Δ_z
M_{ZN} (2878)	1	-1.731-03	4.551-04	0.0	-1.731-03	3.763-04	0.0
	2	-1.731-03	-1.779-05	-3.473-13	-1.731-03	-1.779-05	-1.540-12
	3	-1.731-03	-4.907-04	0.0	-1.731-03	-4.119-04	0.0
	4	-3.001-06	5.041-09	0.0	-2.407-06	6.827-09	0.0
	5	4.221-07	0.0	-2.958-09	4.422-07	0.0	-3.188-09
	6	4.502-06	7.126-09	0.0	3.817-06	6.572-09	0.0
	7	1.861-05	-7.446-09	0.0	1.559-05	-9.399-09	0.0
	8	2.777-07	0.0	3.490-09	2.902-07	0.0	3.821-09
	9	-1.730-05	-1.086-08	0.0	-1.438-05	-1.026-08	0.0
M_{XN} (2878)	1	0.0	0.0	1.932-03	0.0	0.0	1.932-03
	2	-9.425-07	-5.017-04	1.931-03	-7.854-07	-4.181-04	1.931-03
	3	0.0	0.0	1.930-03	0.0	0.0	1.930-03
	4	0.0	0.0	2.835-05	0.0	0.0	2.362-05
	5	-5.296-09	-2.835-05	0.0	-4.530-09	-2.362-05	0.0
	6	0.0	0.0	-2.835-05	0.0	0.0	-2.362-05
	7	0.0	0.0	0.0	0.0	0.0	0.0
	8	0.0	0.0	0.0	0.0	0.0	0.0
	9	0.0	0.0	0.0	0.0	0.0	0.0

Table A.25. End cap displacements (in.)
for parameter study model *P30E*

Loading (in.-lb)	Reference point	Outside			Inside		
		Δ_x	Δ_y	Δ_z	Δ_x	Δ_y	Δ_z
M_{ZN} (45)	1	-6.857-03	4.813-04	0.0	-6.857-03	4.011-04	0.0
	2	-6.857-03	-2.797-07	-1.365-17	-6.857-03	-2.797-07	-1.388-17
	3	-6.857-03	-4.819-04	0.0	-6.857-03	-4.016-04	0.0
	4	-3.898-08	2.062-10	0.0	-2.956-08	2.289-10	0.0
	5	1.307-08	0.0	-5.204-11	1.326-08	0.0	-4.942-11
	6	7.343-08	3.285-13	0.0	6.364-08	-8.475-12	0.0
	7	2.991-07	-3.117-10	0.0	2.514-07	-3.354-10	0.0
	8	6.786-09	0.0	1.497-10	6.472-09	0.0	1.534-10
	9	-2.734-07	8.855-12	0.0	-2.262-07	1.512-11	0.0
M_{XN} (45)	1	0.0	0.0	6.866-03	0.0	0.0	6.866-03
	2	-2.958-09	-4.819-04	6.866-03	-2.465-09	-4.016-04	6.866-03
	3	0.0	0.0	6.866-03	0.0	0.0	6.866-03
	4	0.0	0.0	4.483-07	0.0	0.0	3.736-07
	5	-1.381-09	-4.483-07	0.0	-1.155-09	-3.736-07	0.0
	6	0.0	0.0	-4.482-07	0.0	0.0	-3.735-07
	7	0.0	0.0	0.0	0.0	0.0	0.0
	8	0.0	0.0	0.0	0.0	0.0	0.0
	9	0.0	0.0	0.0	0.0	0.0	0.0

Appendix B

ISOMETRIC VIEWS OF FINITE-ELEMENT MESHES

Isometric views of the finite-element mesh for the outside surface of each of the parameter study models are shown here. These figures are helpful in identifying the locations of the stress values given in Tables 7 through 12, as well as the results printed on microfiche. Figures 3 and 4 of the text show the "pentagonal" identification scheme used. The control node for each of the figures shown here is readily identifiable, becuase it is the only node with five (rather than four) neighboring elements. The isometric views are also useful because they give the reader a feel for the relative fineness of the finite-element meshes used in the study. Reference 1 also gives cross-sectional views in the X-Y and Y-Z planes for each model. In each of the titles, the first number within the parentheses is the D/T ratio, while the second is the d/D ratio for that model.

ORNL-DWG 76-11336R

MODEL UA (100,0.5)

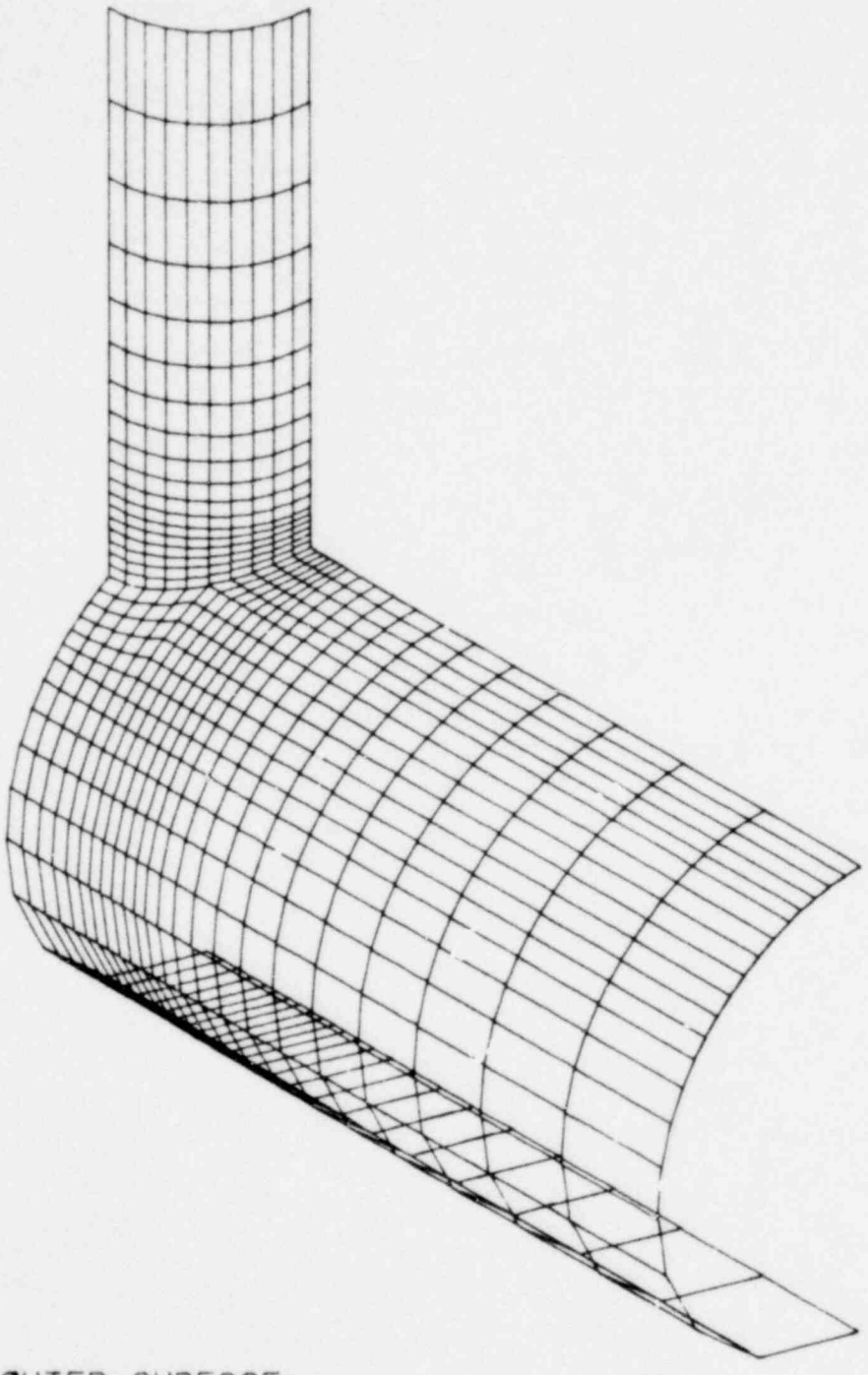

OUTER SURFACE

ORNL-DWG 76-11337R

MODEL UB (80,0.5)

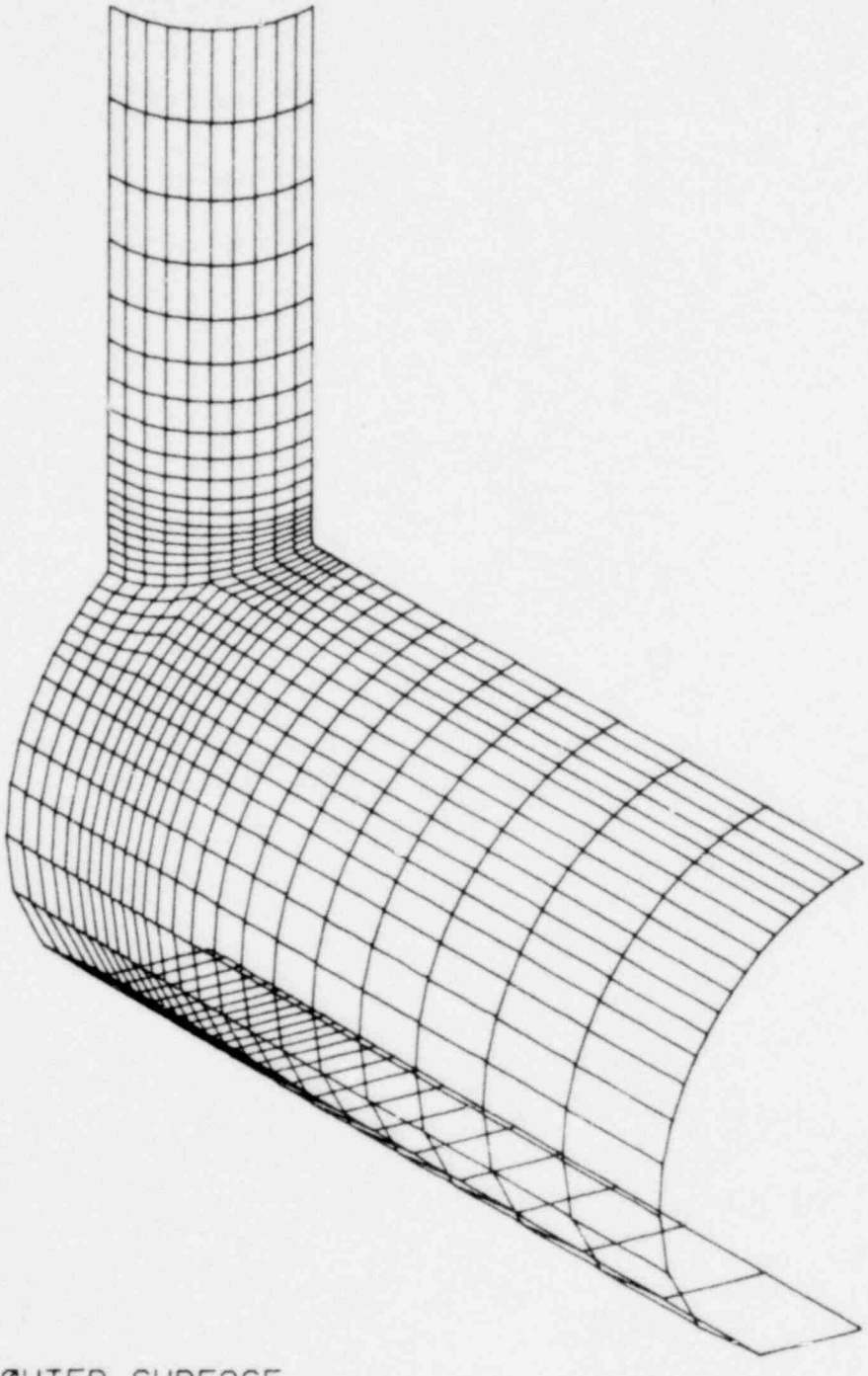

OUTER SURFACE

ORNL-DWG 76-11338R

MODEL UC (40,0.5)

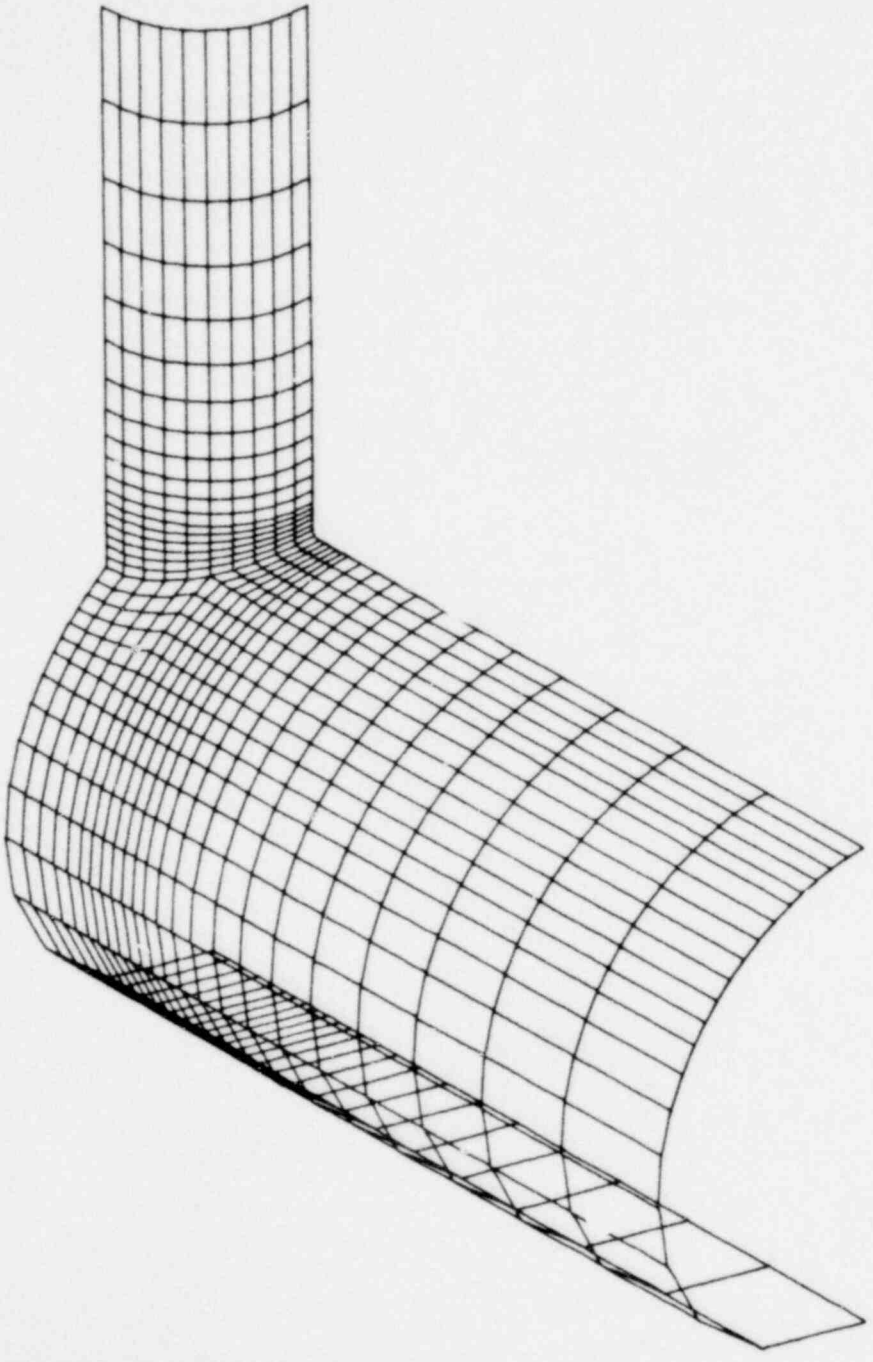

OUTER SURFACE

ORNL-DWG 76-11339R

MODEL UD (20,0.5)

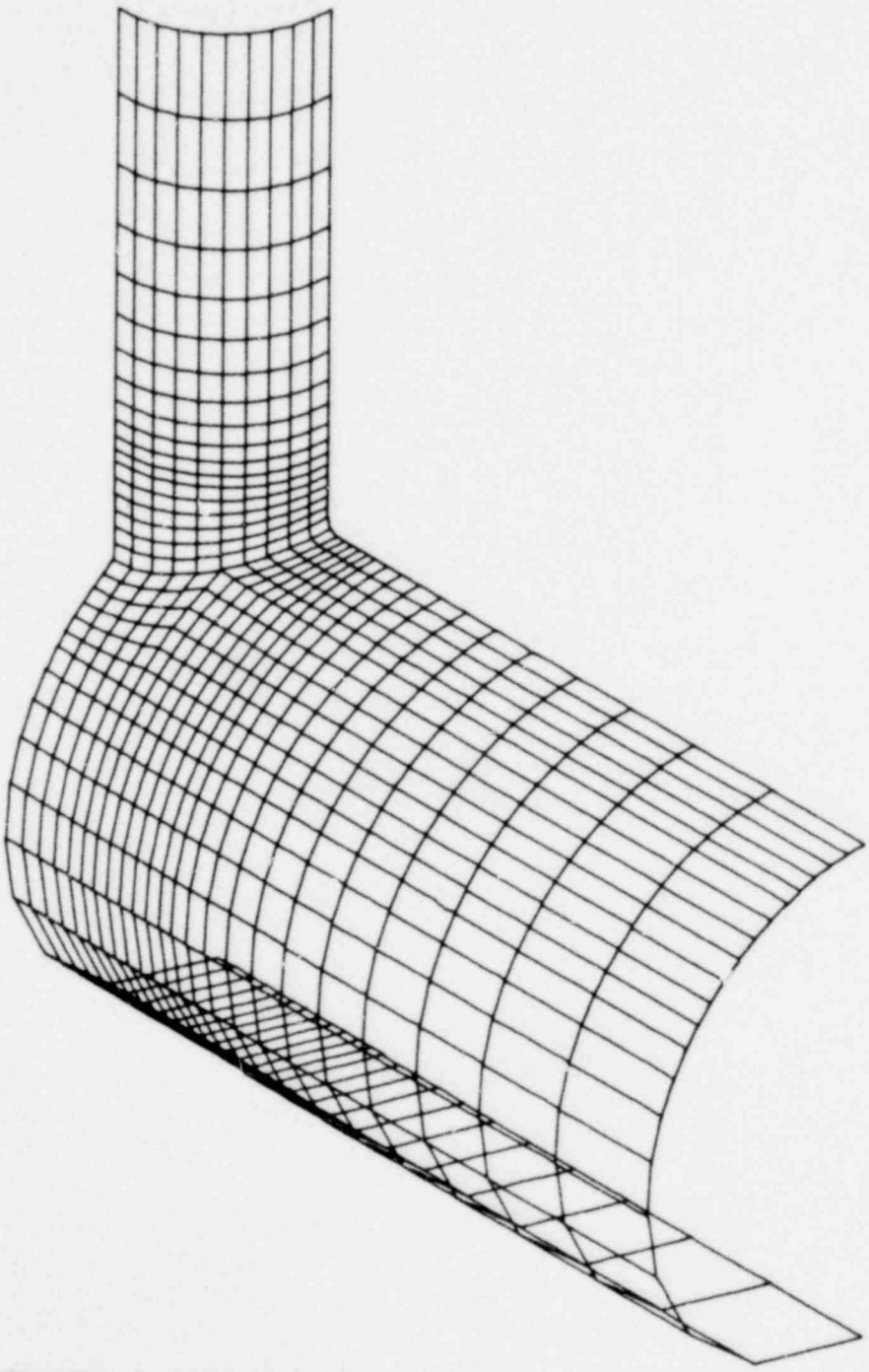

OUTER SURFACE

ORNL-DWG 76-11340R

MODEL UE (10,0.5)

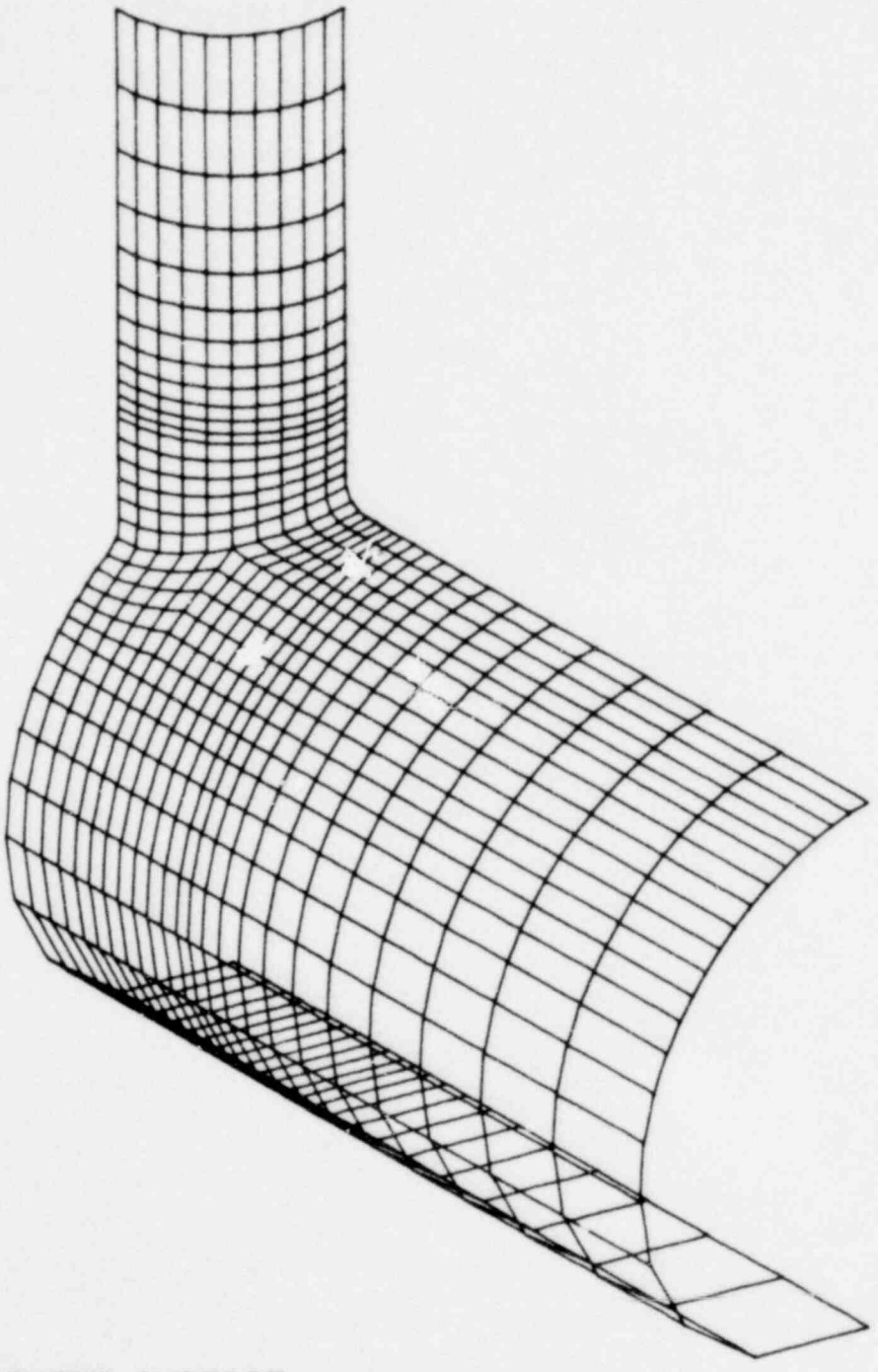

OUTER SURFACE

ORNL-DWG 76-11341R

MODEL UF (10,0.08)

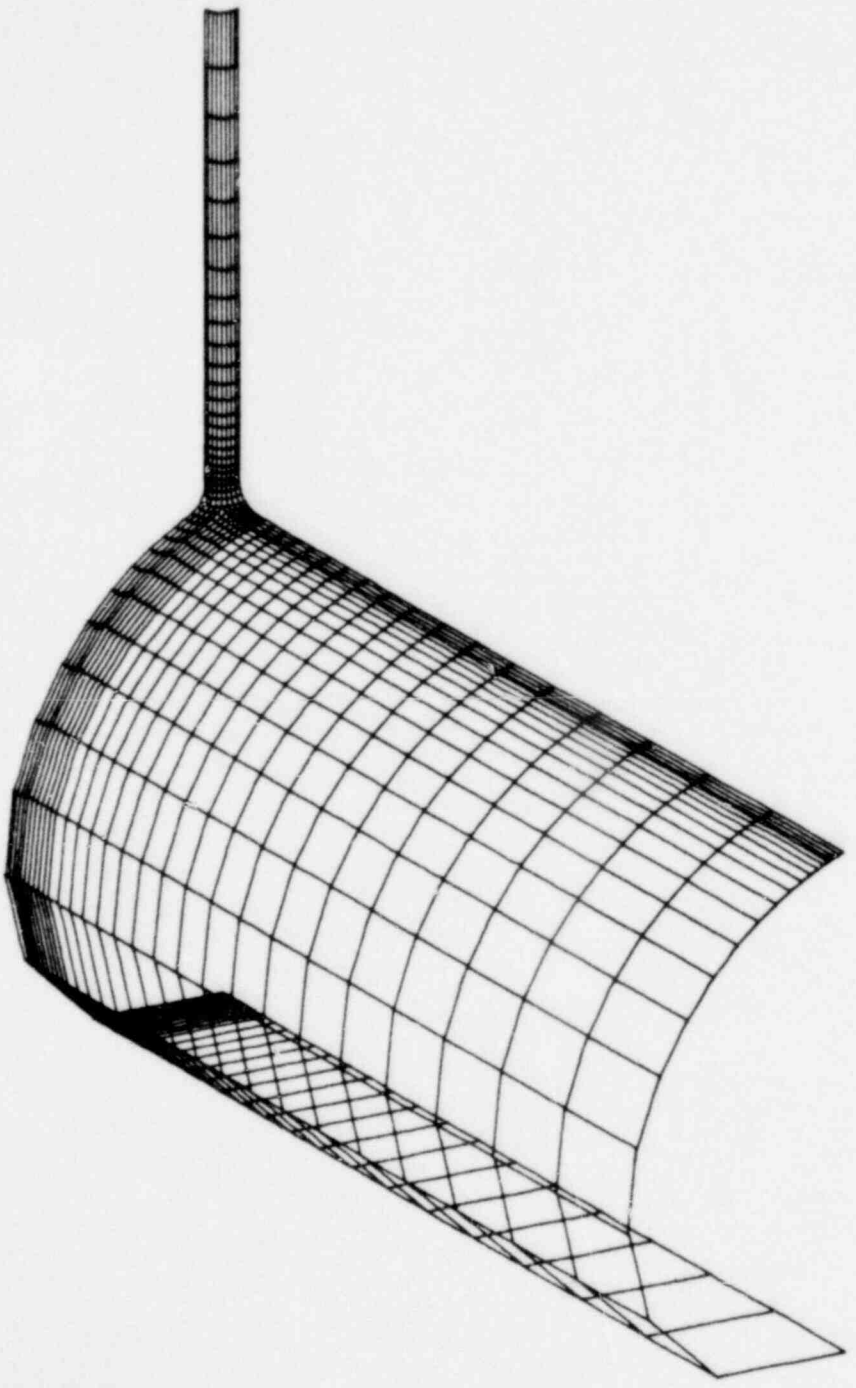

OUTER SURFACE

ORNL-DWG 76-11342R

MODEL S1A (100,0.5)

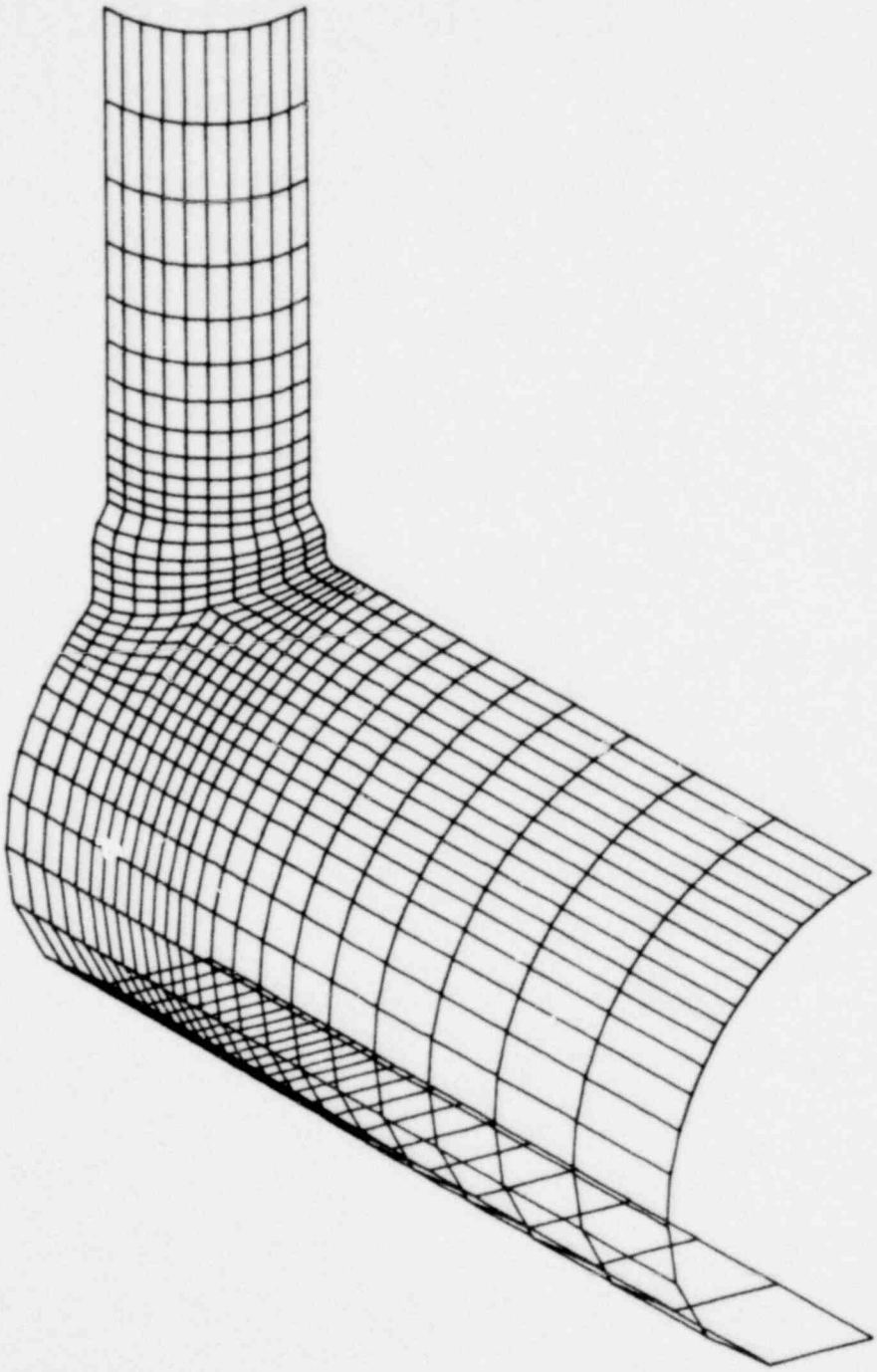

OUTER SURFACE

ORNL-DWG 76-11343R

MODEL S1B (80,0.5)

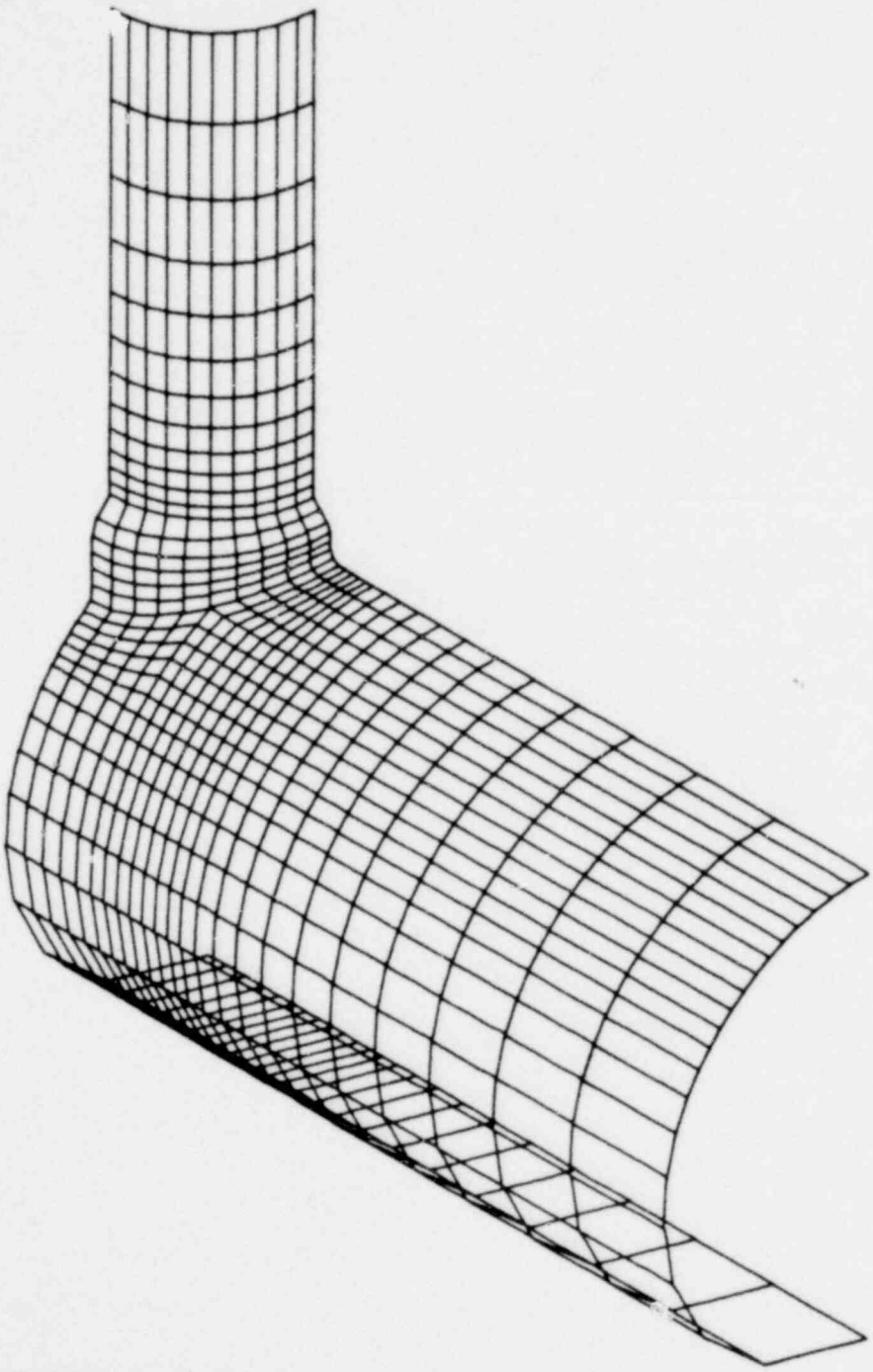

OUTER SURFACE

ORNL-DWG 76-11344R

MODEL S1C (40,0.5)

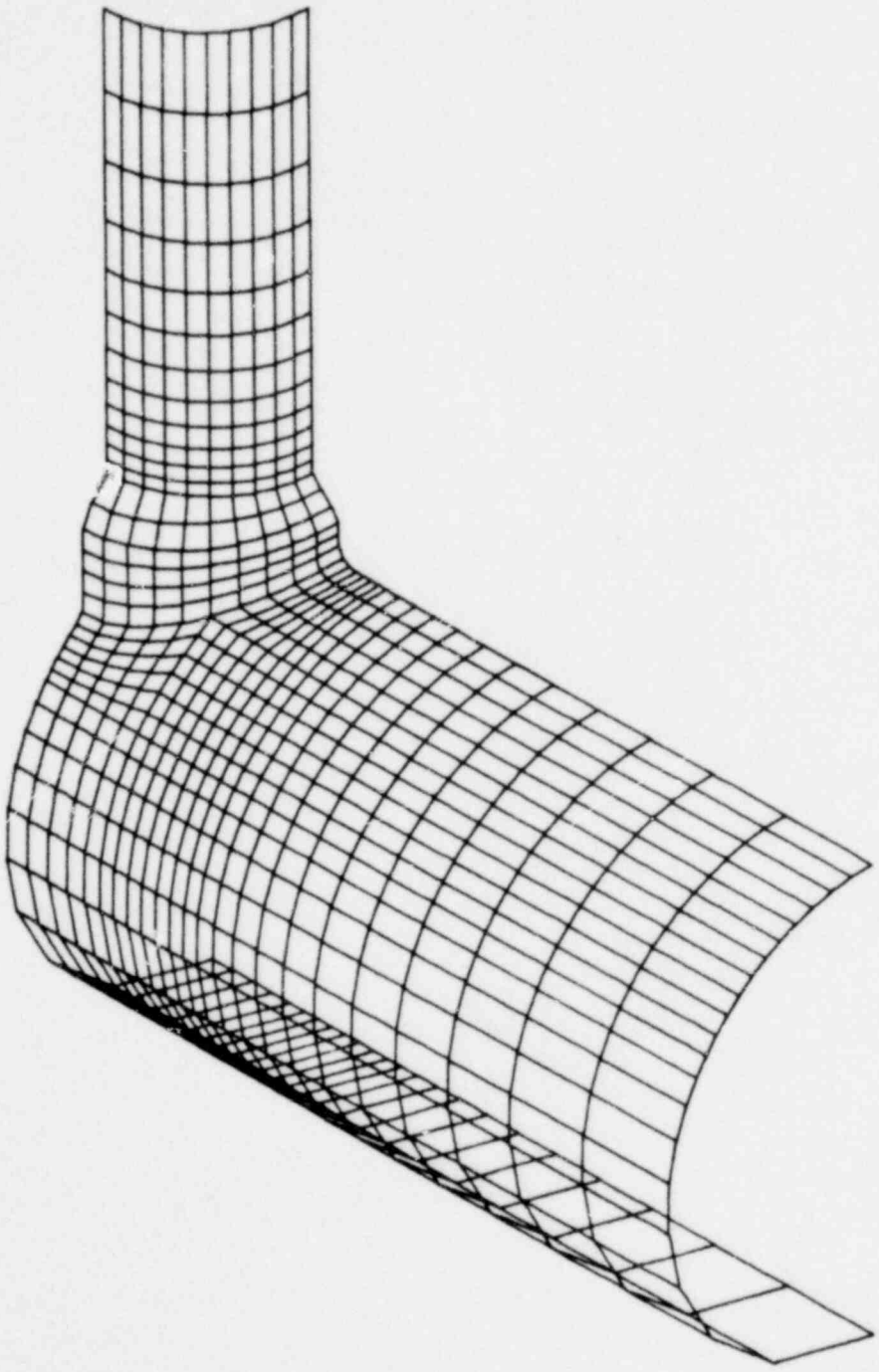

OUTER SURFACE

ORNL-DWG 76-11345R

MODEL S1D (20,0.5)

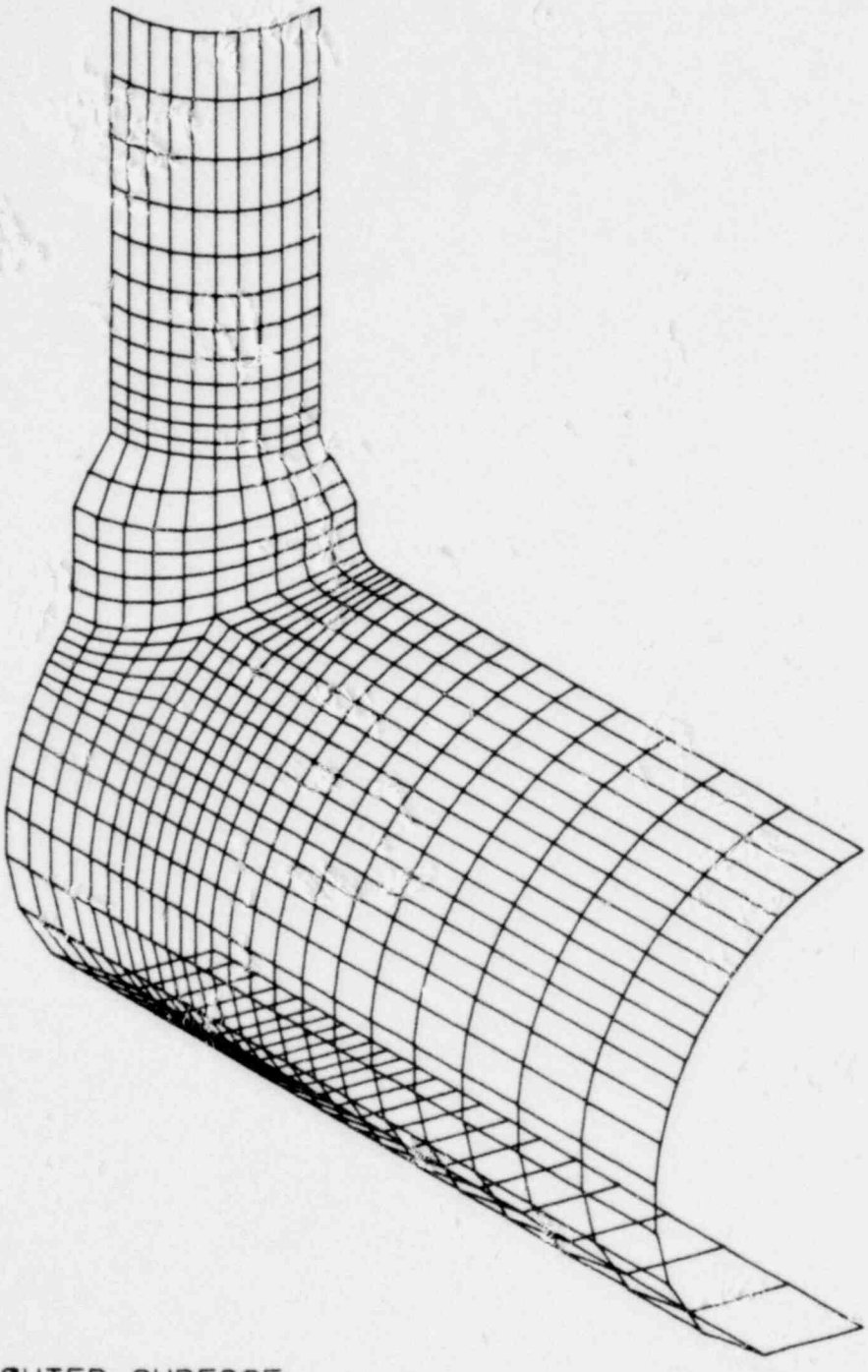

OUTER SURFACE

ORNL-DWG 76-11346R

MODEL S1E (10,0.5)

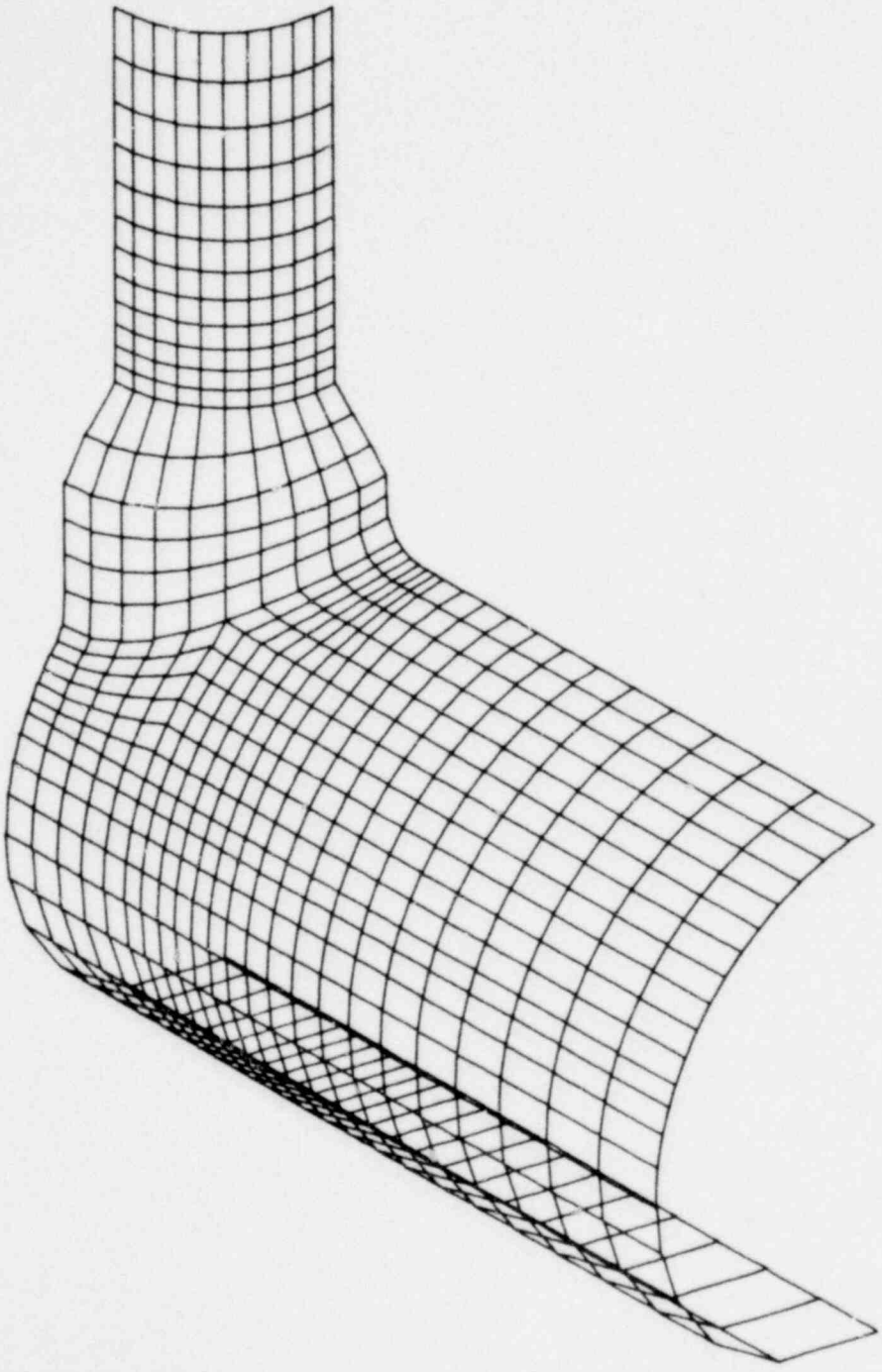

OUTER SURFACE

ORNL-DWG 76-11347R

MODEL S1F (40,0.32)

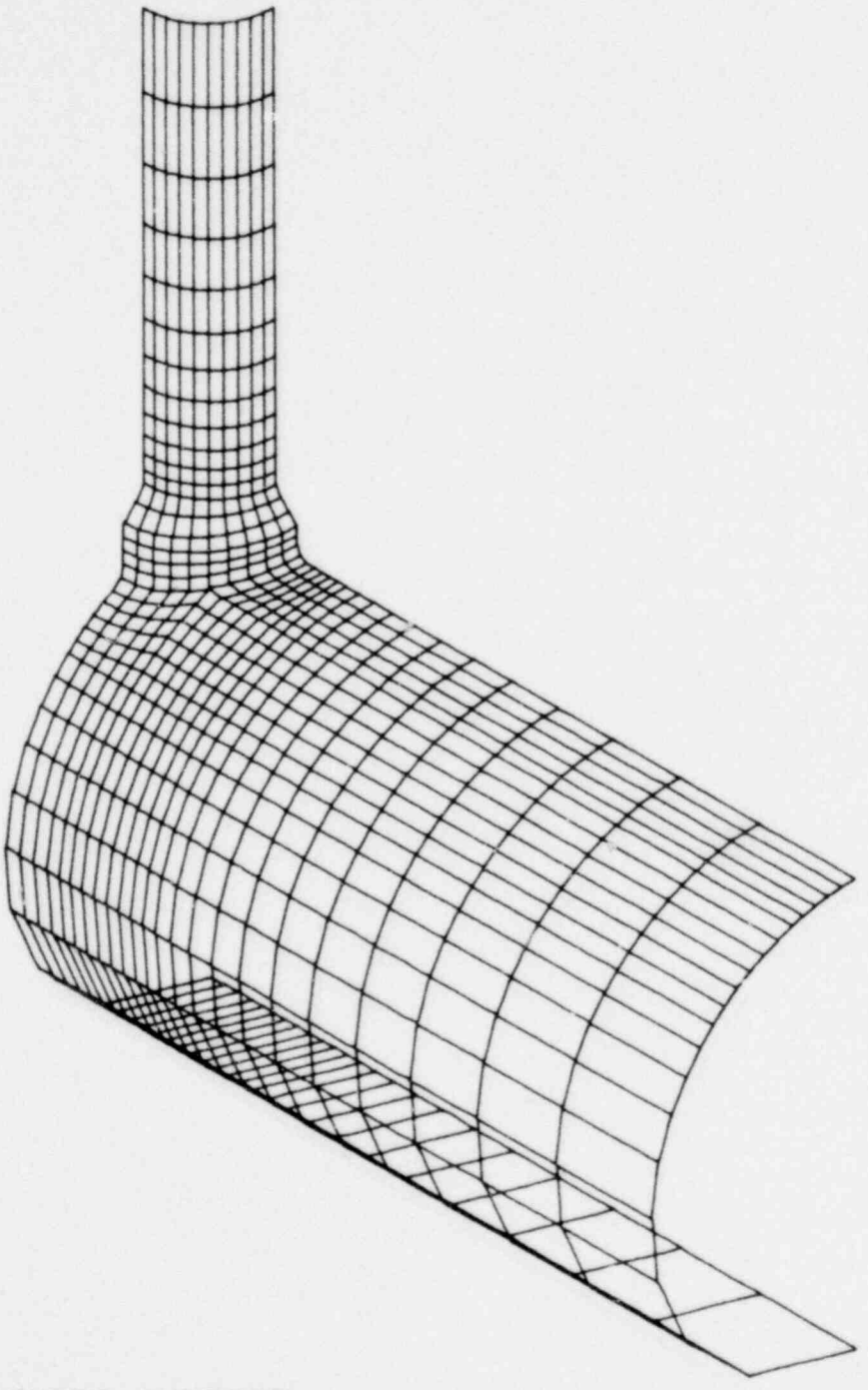

OUTER SURFACE

ORNL-DWG 76-11348R

MODEL S1G (20,0.32)

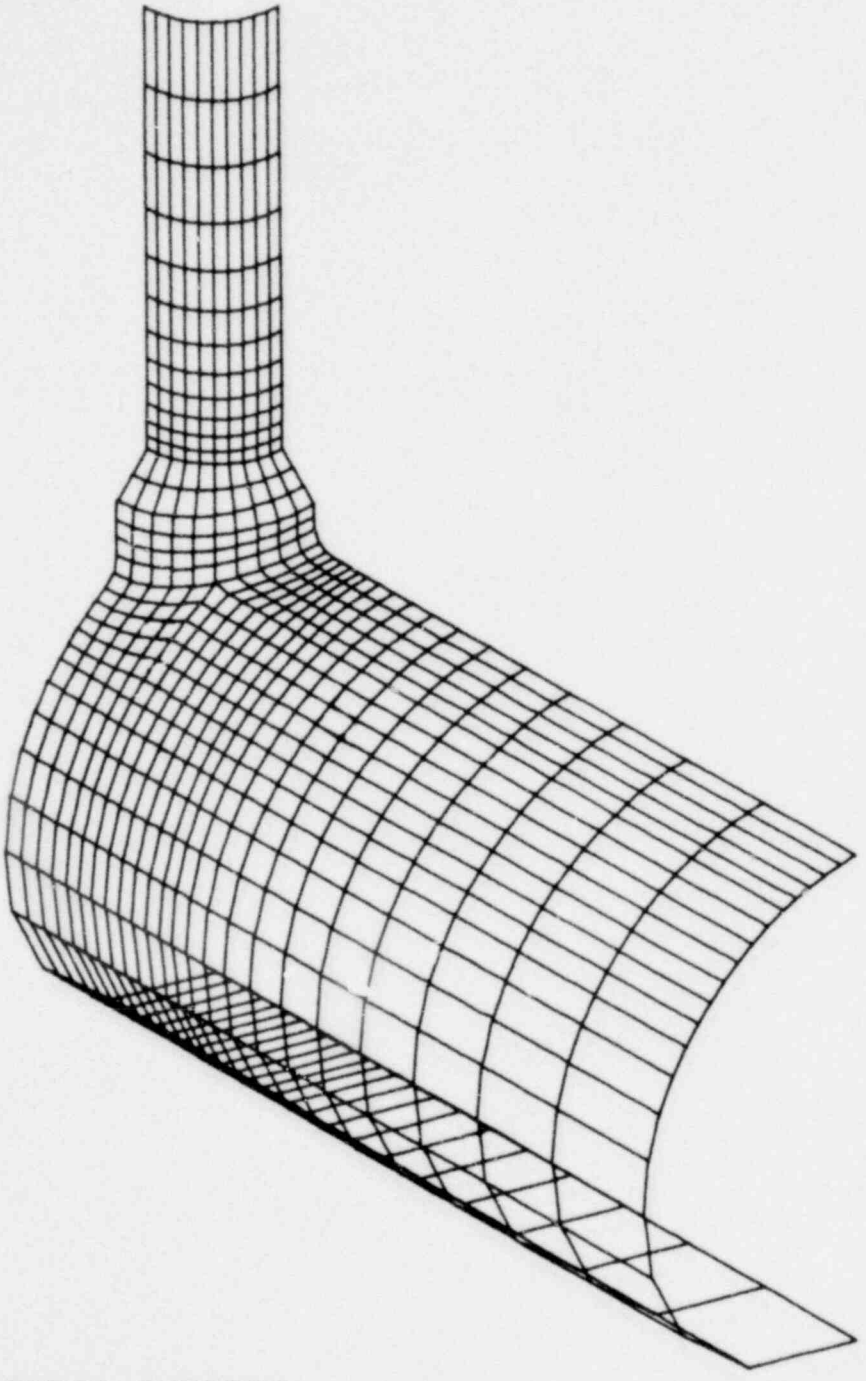

OUTER SURFACE

ORNL-DWG 76-11349R

MODEL S1H (10,0.32)

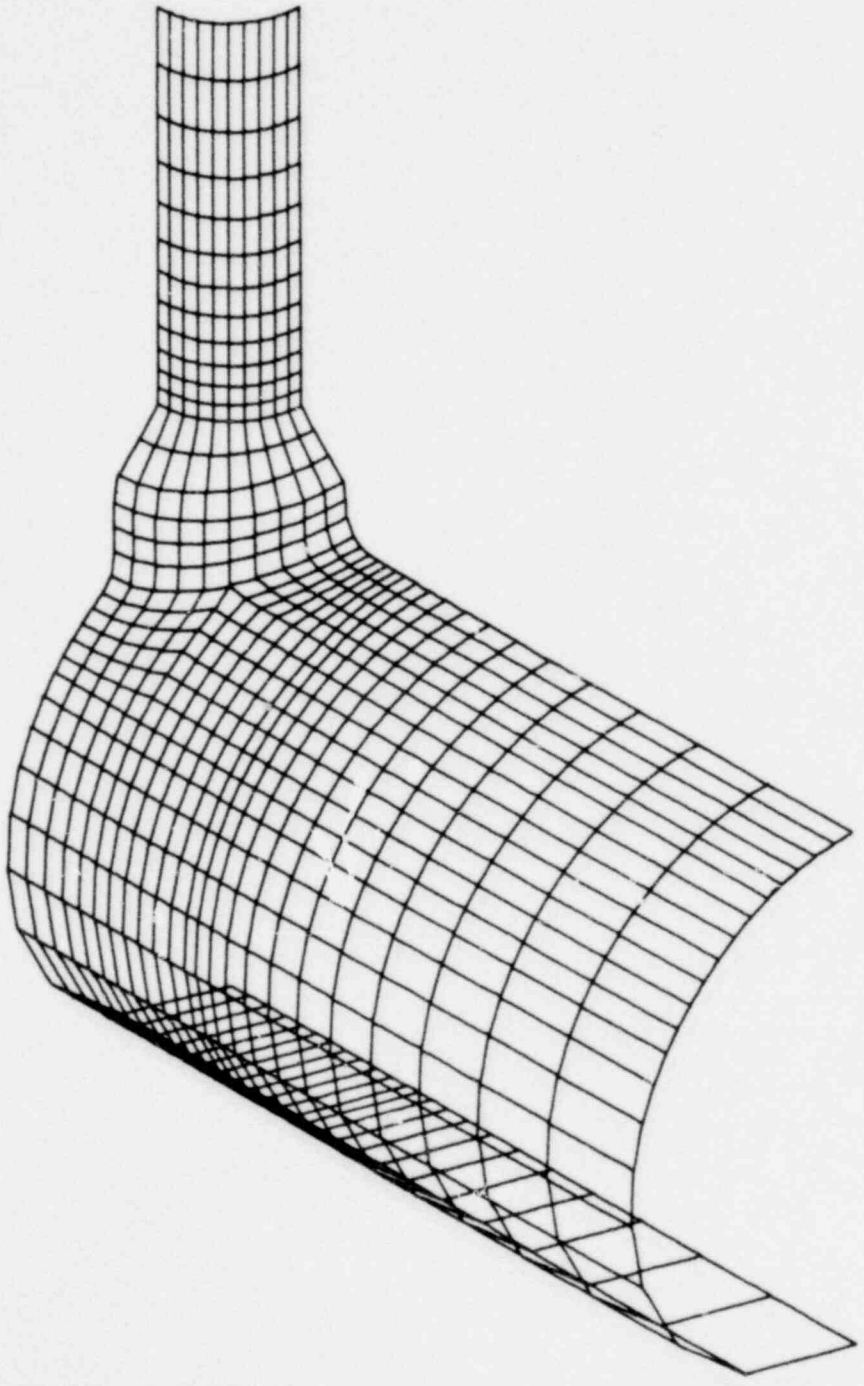

OUTER SURFACE

ORNL-DWG 76-11350R

MODEL S1I (40,0.16)

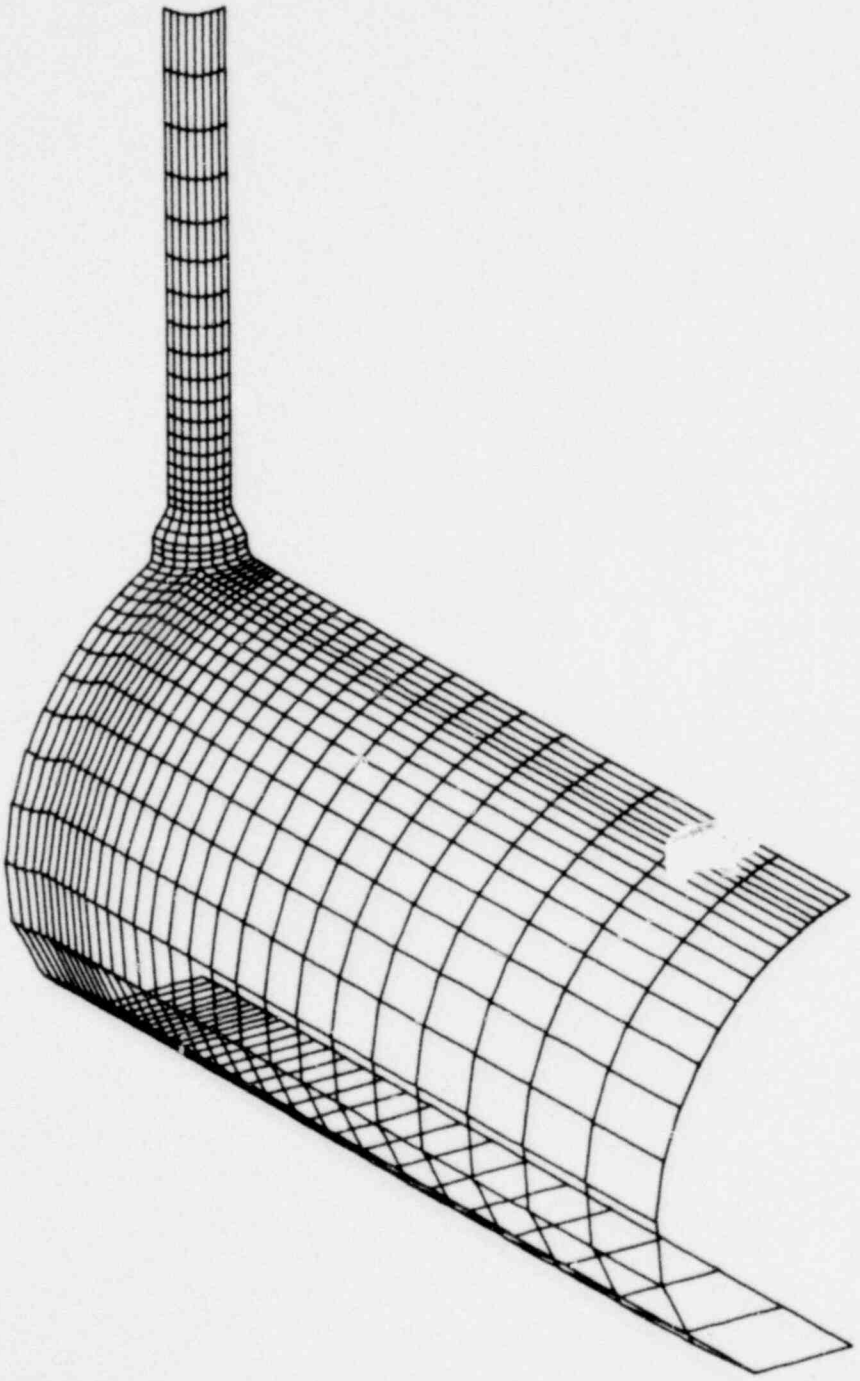

OUTER SURFACE

ORNL-DWG 76-11351R

MODEL S1J (20,0.16)

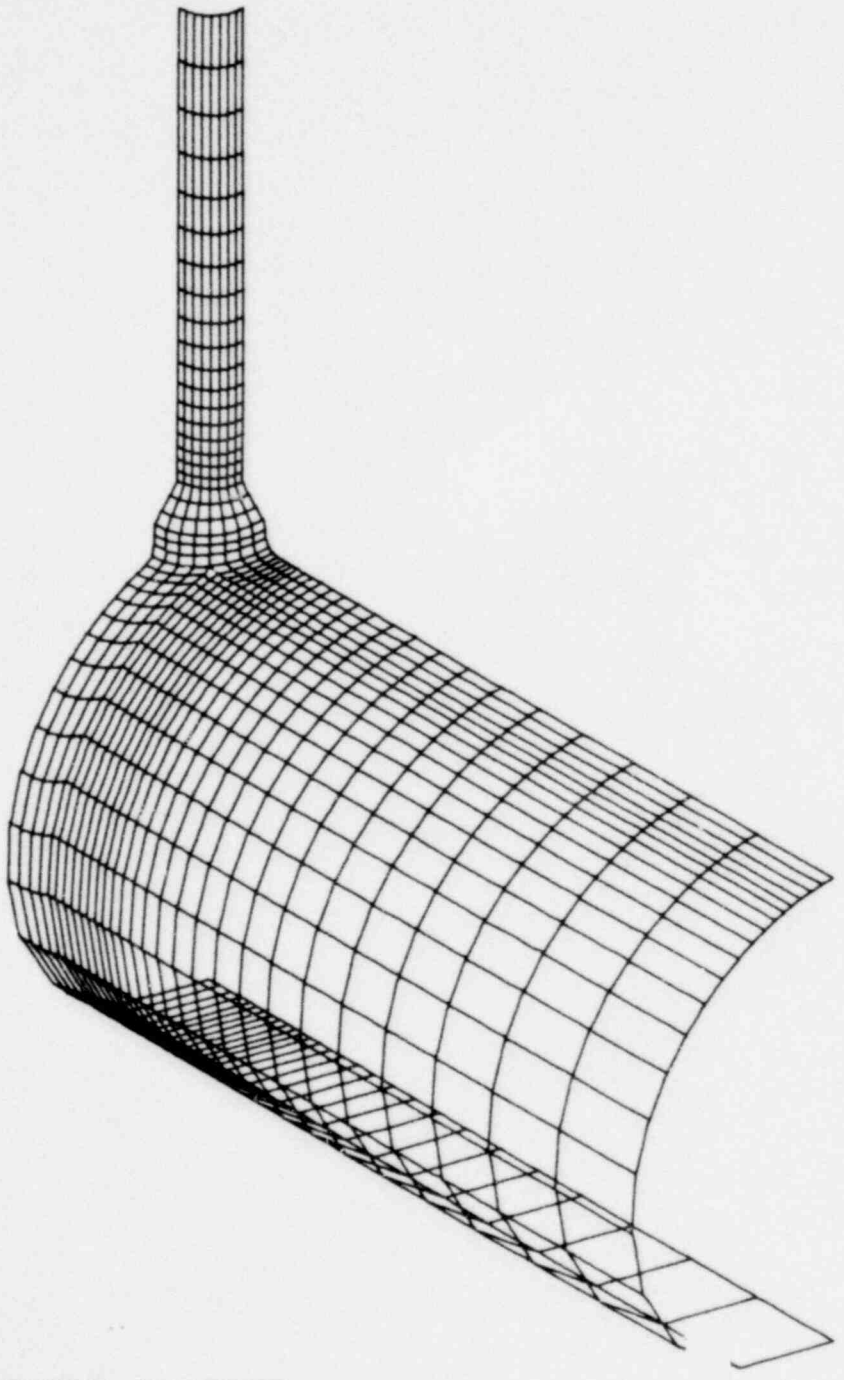

OUTER SURFACE

ORNL-DWG 76-11352R

MODEL S1K (10,0.16)

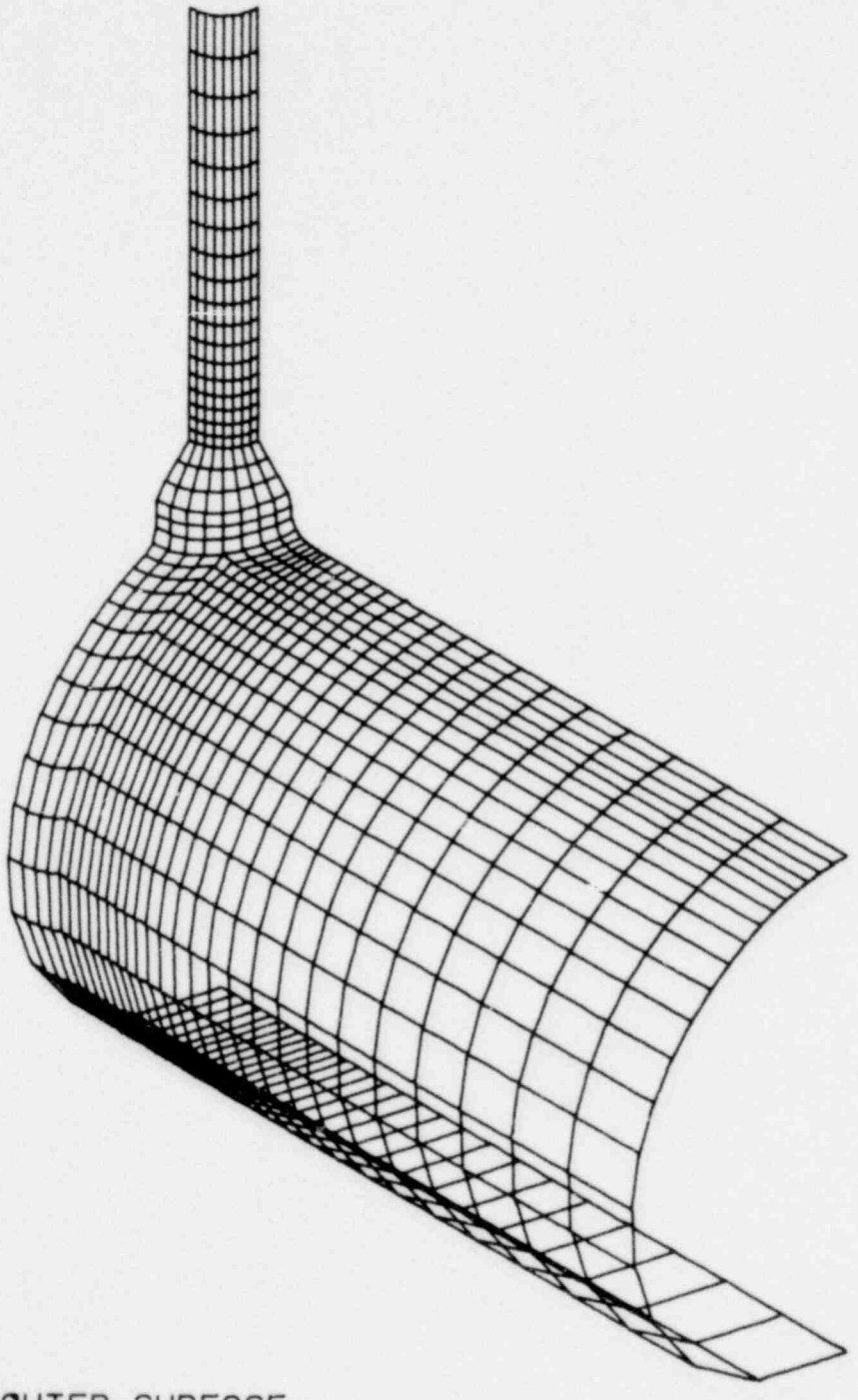

OUTER SURFACE

ORNL-DWG 76-11353R

MODEL S1L (40,0.08)

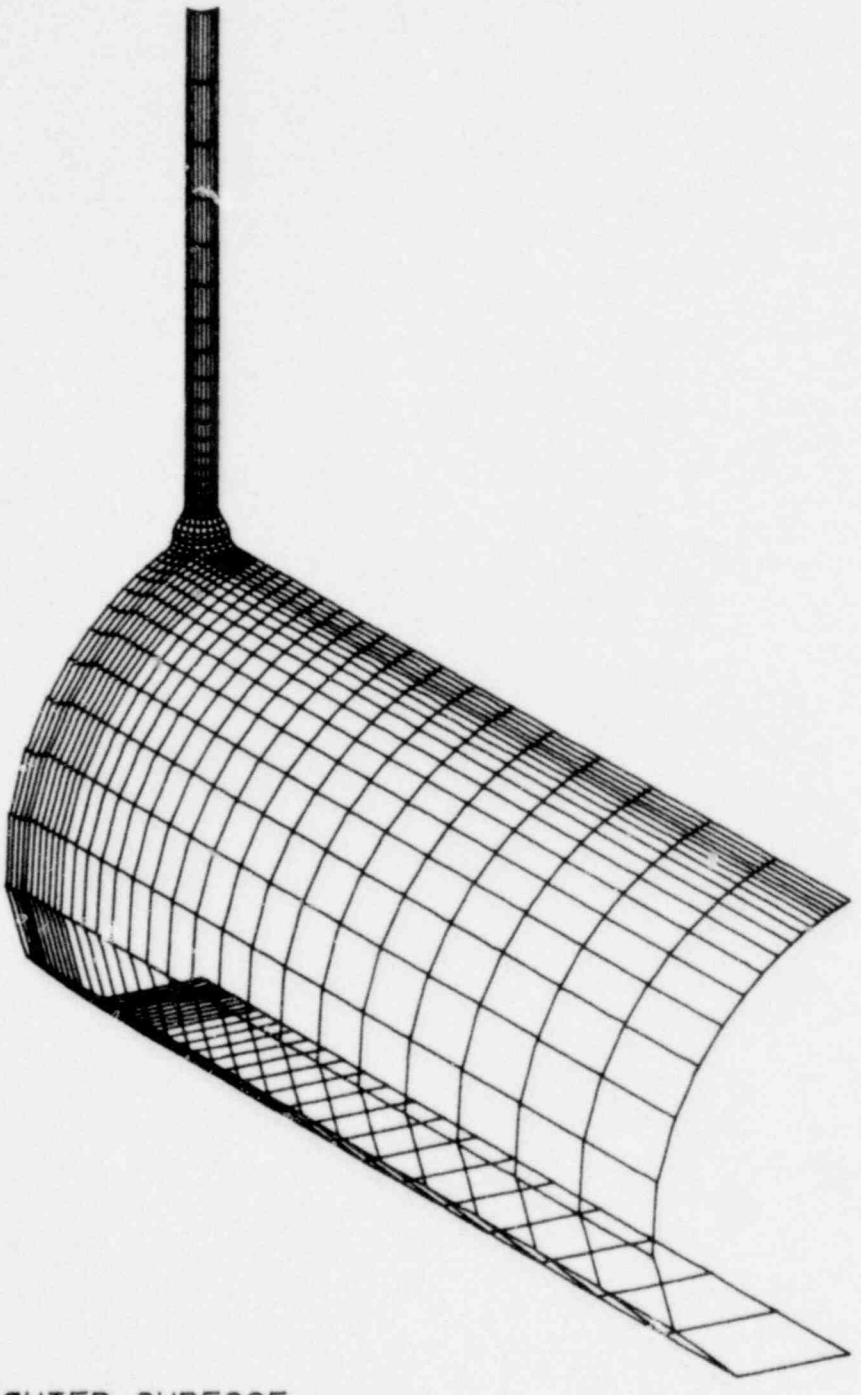

OUTER SURFACE

ORNL-DWG 76-11354R

MODEL S1M (20,0.08)

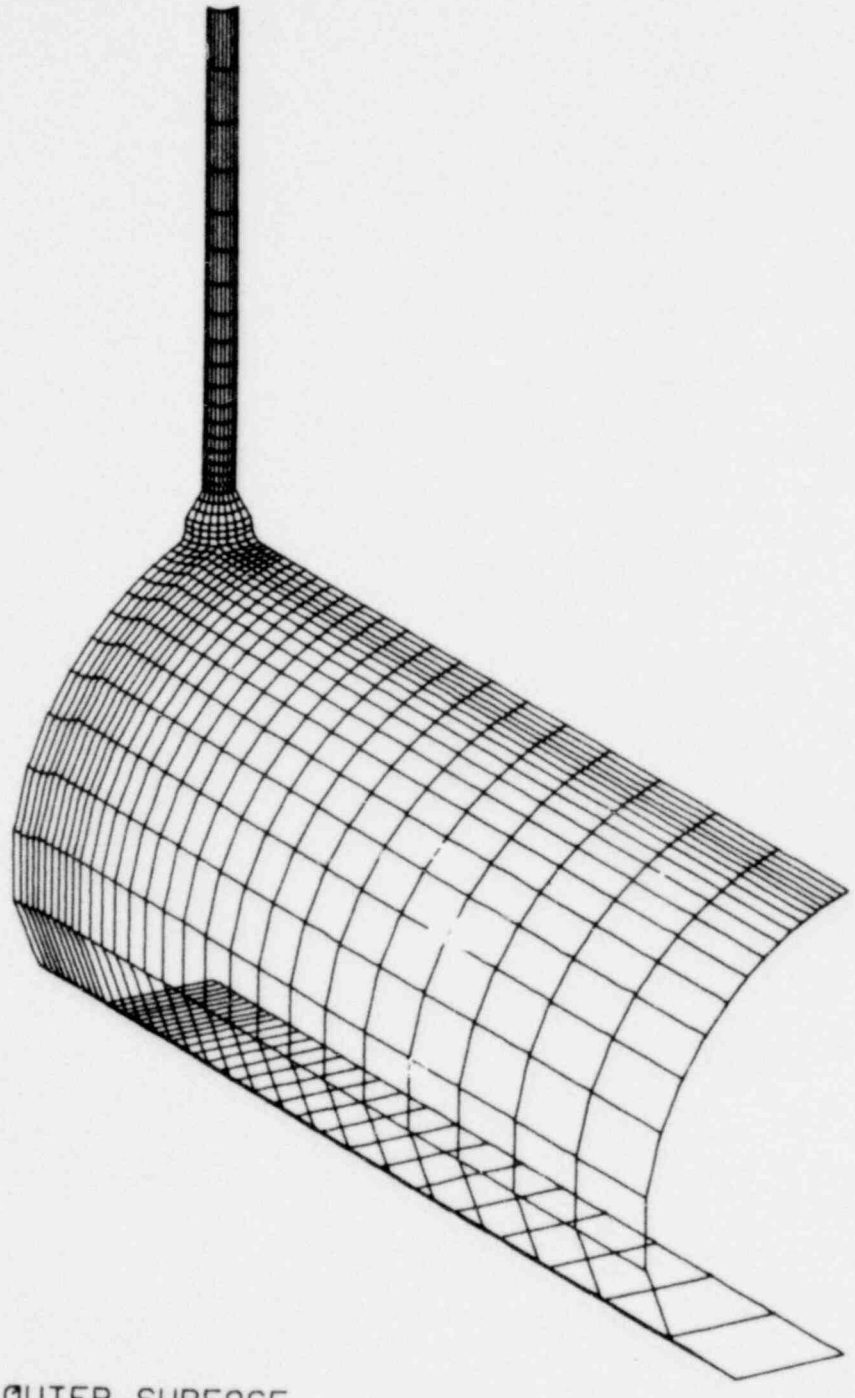

OUTER SURFACE

ORNL-DWG 76-11355R

MODEL S1N (10,0.08)

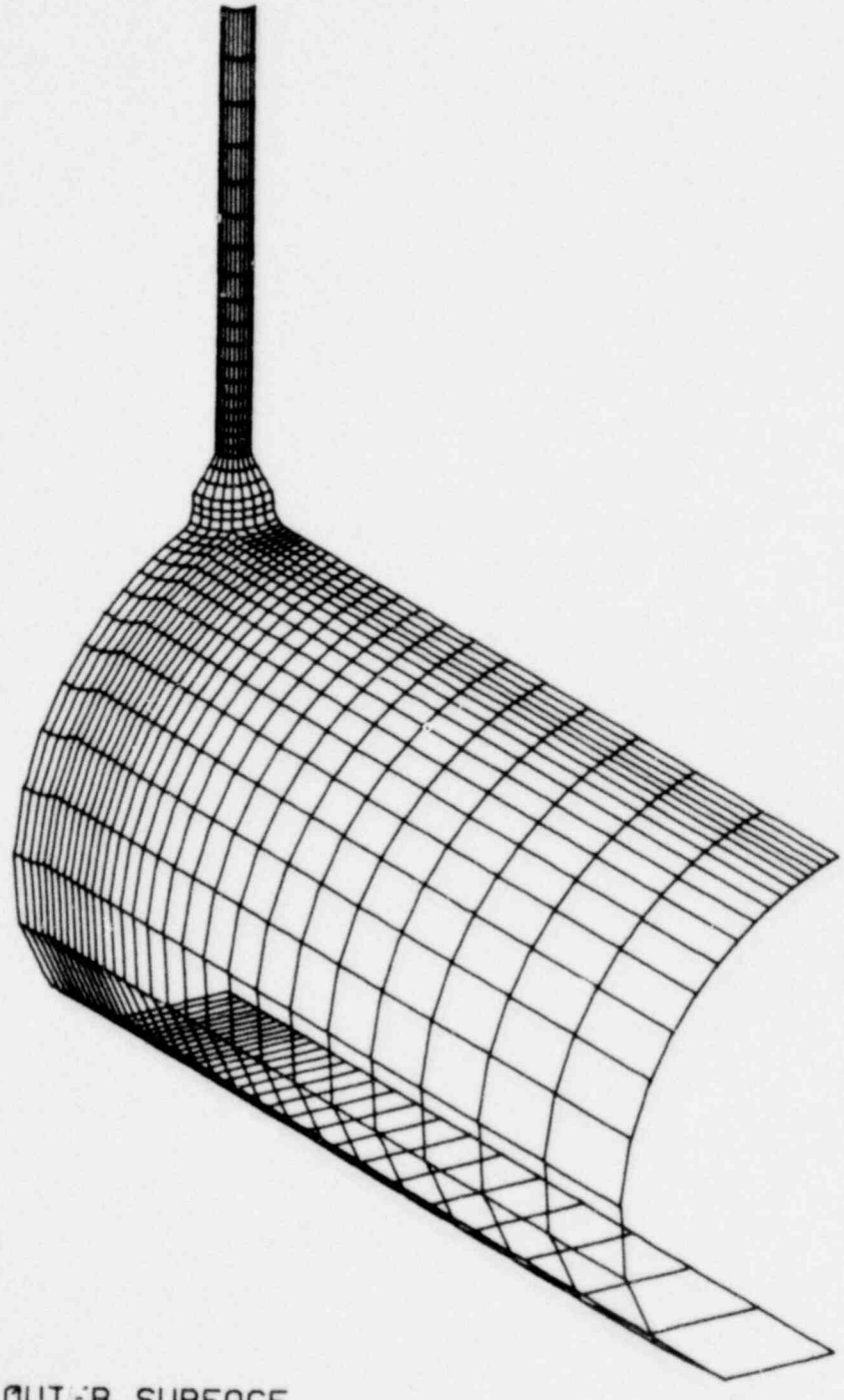

OUTER SURFACE

ORNL-DWG 76-11356R

MODEL P30A (100,0.32)

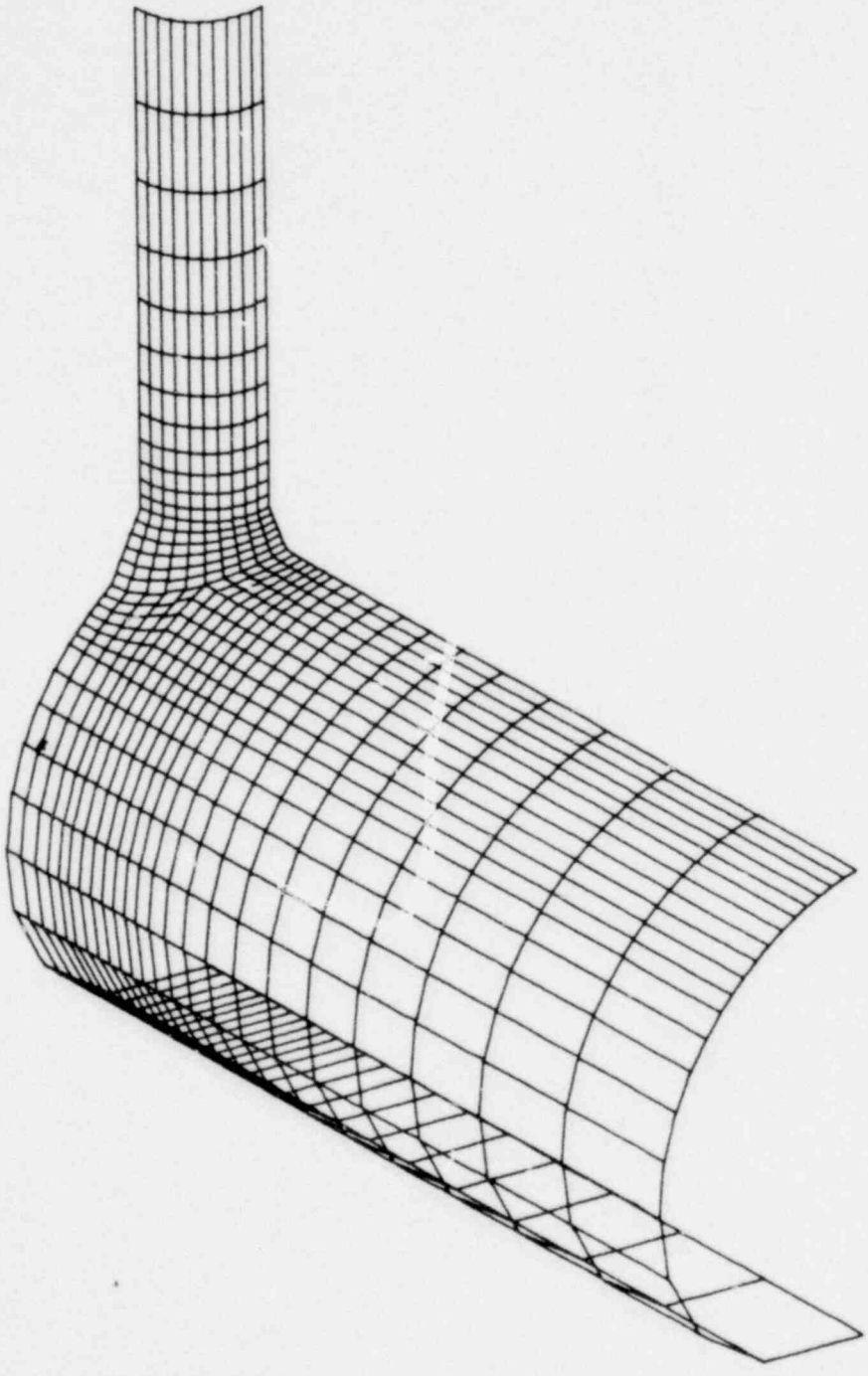

OUTER SURFACE

ORNL-DWG 76-11357R

MODEL P30B (40,0.32)

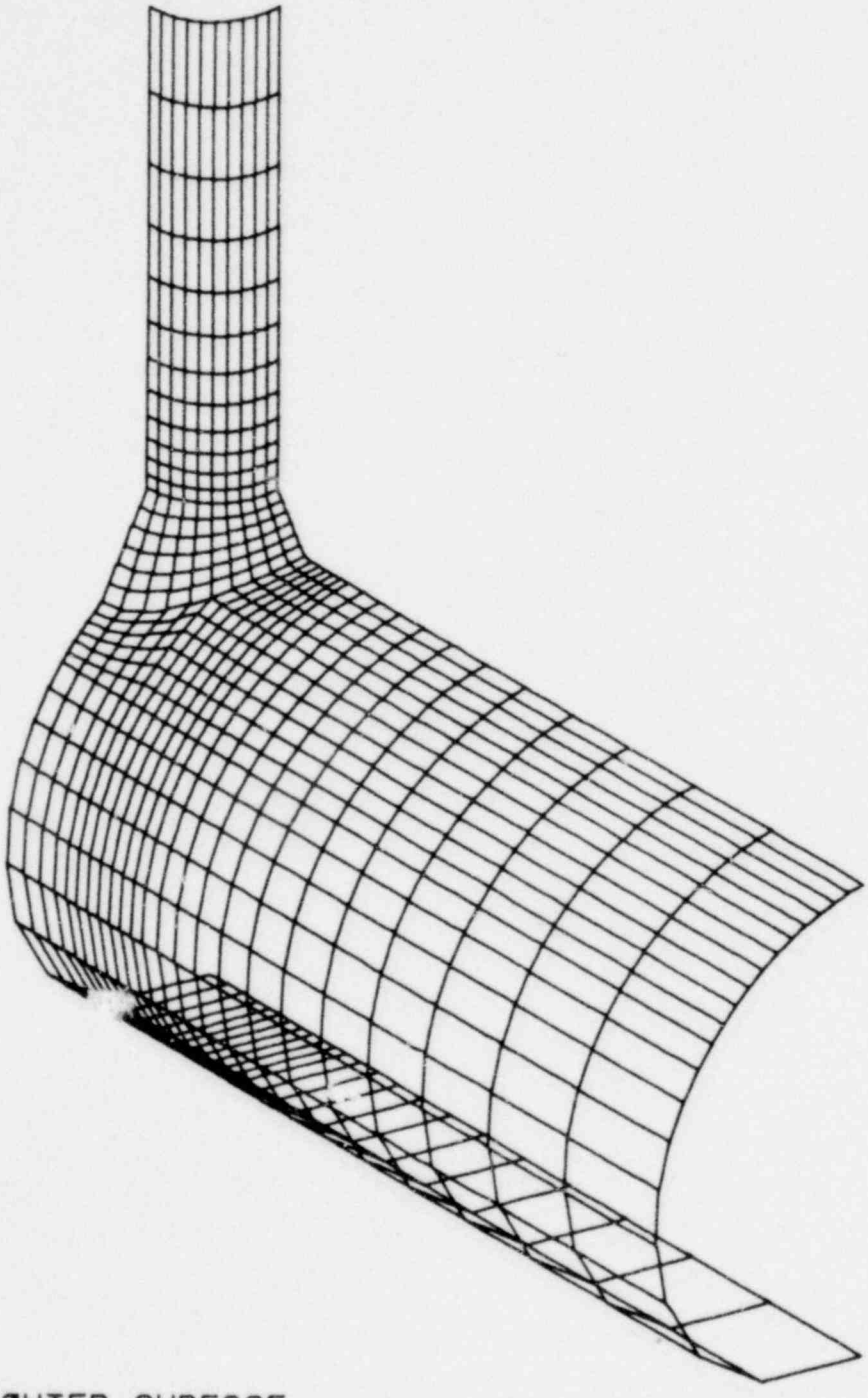

OUTER SURFACE

ORNL-DWG 76-11358R

MODEL P30C (20,0.32)

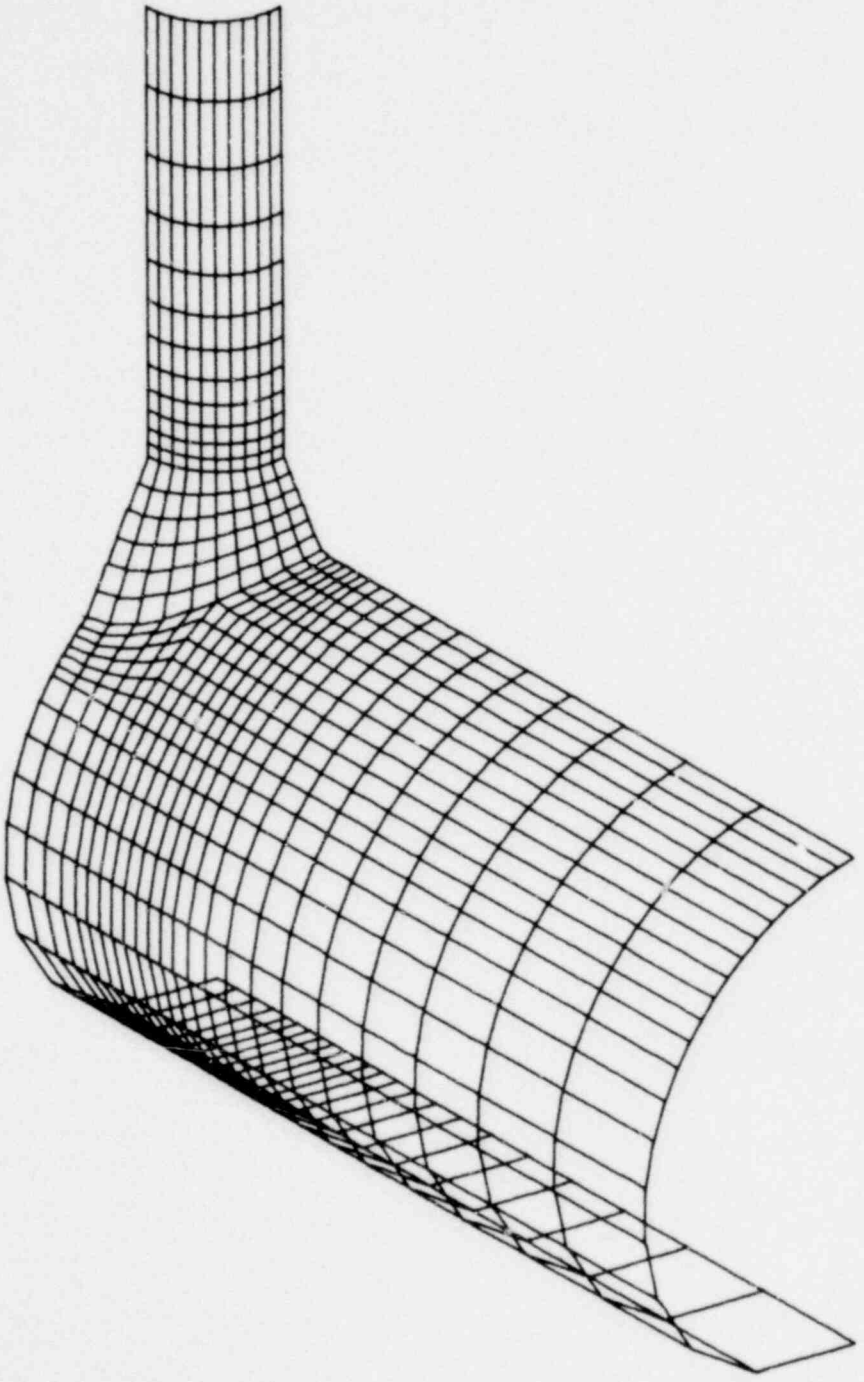

OUTER SURFACE

ORNL-DWG 76-11359R

MODEL P30D (10,0.32)

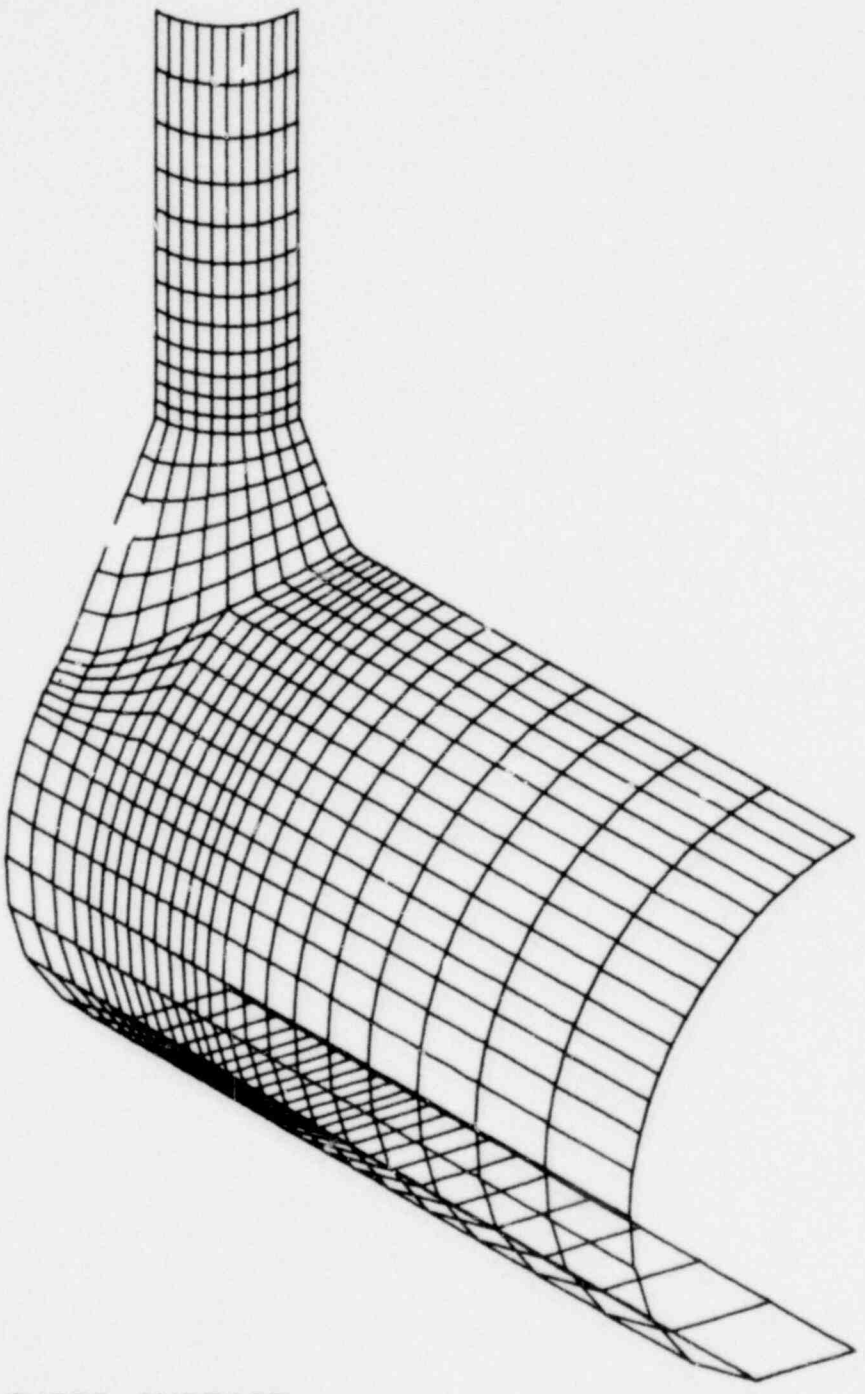

OUTER SURFACE

ORNL-DWG 76-11360R

MODEL P30E (10,0.08)

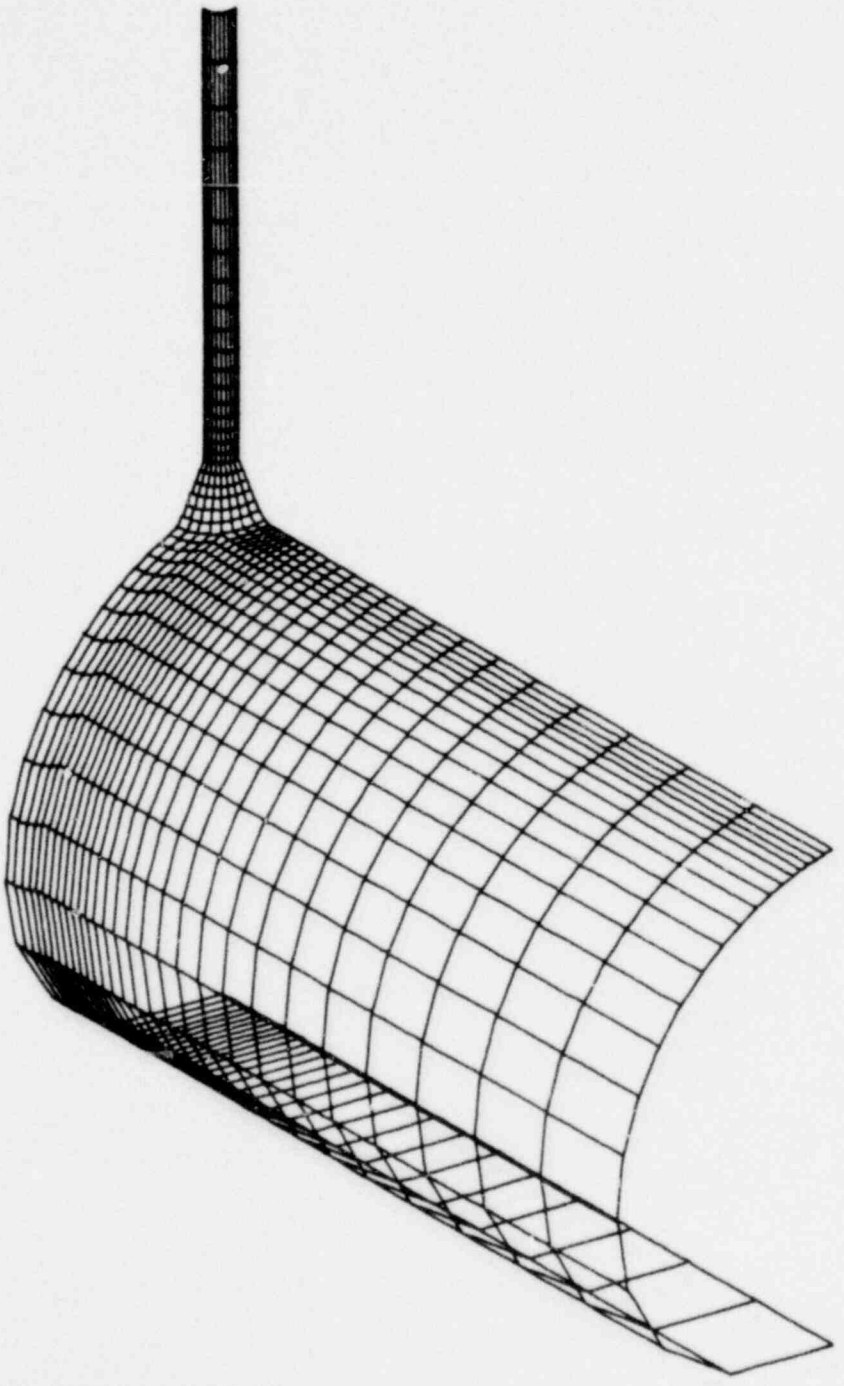

OUTER SURFACE

NUREG/CR-0506
ORNL/NUREG-52
Dist. Category R5

Internal Distribution

1-2.	B. R. Bass	31.	F. R. Mynatt
3.	R. H. Bryan	32.	T. W. Pickel
4-8.	J. W. Bryson	33.	H. Postma
9.	J. R. Buchanan	34.	C. E. Pugh
10.	J. A. Clinard	35.	J. L. Rich
11.	C. W. Collins	36.	J. E. Smith
12.	J. M. Corum	37.	W. C. T. Stoddard
13.	W. B. Cottrell	38.	R. E. Textor
14.	W. G. Dodge	39.	H. E. Trammell
15.	W. L. Greenstreet	40.	D. B. Trauger
16.	R. C. Gwaltney	41.	G. D. Whitman
17.	R. F. Hibbs	42.	G. T. Yahr
18-19.	W. G. Johnson	43.	ORNL Patent Office
20.	R. L. Huddleston	44-45.	Central Research Library
21.	P. R. Kasten	46.	Y-12 Document Reference Section
22.	J. G. Merkle	47-48.	Laboratory Records Department
23-30.	S. E. Moore	49.	Laboratory Records, ORNL RC

External Distribution

50. Office of Assistant Manager, Energy Research and Development, DOE, ORO
51-140. Special Design Criteria distribution (by NRC)
141-142. Technical Information Center, DOE
143-482. Given distribution under category R5 (10-NTIS)

☆U.S. GOVERNMENT PRINTING OFFICE: 1979-640-079-133

NUREG/CR-0506
ORNL/NUREG-52

STRESSES IN REINFORCED NOZZLE-CYLINDER ATTACHMENTS UNDER EXTERNAL MOMENT LOADINGS ANALYZED BY THE FINITE-ELEMENT METHOD – A PARAMETER STUDY

J. W. Bryson W. G. Johnson B. R. Bass

MICROFICHE ENCLOSED

ATTACHMENT NOT FILMED

ANO. 7910010551

NO. OF PAGES 35 microfiche

☐ DUPLICATE: ALREADY ENTERED INTO SYSTEM
UNDER ANO. _____

☐ ILLEGIBLE: HARD COPY AT:
- ☐ PDR
- ☐ CF
- ☐ OTHER _____

1059 13